Université de Montréal

La Visualisation *in vivo* des « espèces oxygénées radiculaires» au niveau des cellules ganglionnaires de la rétine.

par

Katrina Angela Mears

Département d'Ophtalmologie, École de Sciences Biomedicales

Faculté de Médécine

Thèse présentée à la Faculté des études supérieures

en vue de l'obtention du grade de mâitrise

en sciences biomedicales

Option generale

Avril 2009

Université de Montréal

Faculté des études supérieures

Cette thèse intitulée :

La Visualisation *in vivo* des « espèces oxygénées radiculaires» au niveau des cellules ganglionnaires de la rétine.

(Imaging Reactive Oxygen Species *in vivo)*

présentée par :

Katrina Angela Mears

a été évaluée par un jury composé des personnes suivantes :

Dr Adriana Di Polo PhD président-rapporteur

Dr Leonard A. Levin MD, PhD directeur de recherche

Dr Sylvain Chemtob MD, PhD membre du jury

Université de Montréal

Résumé Titre: La Visualisation *in vivo* des « espèces oxygénées radiculaires» au niveau des cellules ganglionnaires de la rétine.

Le But : Les espèces d'oxygène réactives sont non seulement produites à la suite de la blessure cellulaire, mais servent aussi des molécules faisantes des signes pour une variété de processus critiques, en incluant mitosis et de mort de cellule. Nous avons auparavant dit que la blessure à RGC axons incite un éclatement de superoxyde dans le corps de cellule, probablement de l'origine mitochondrial (*Lieven et al, 2006*). Nous décrivons maintenant une méthode pour refléter des espèces d'oxygène réactives dans la rétine de l'animal vivant en utilisant un confocal le lisant rapidement du laser ophthalmoscope a appelé la Rétine de Heidelberg Angiograph 2 (HRA2) équipé avec les lasers doubles.

La méthodolologie : Après les études préliminaires en utilisant d'autres indicateurs (hydroethidium; HEt) pour les espèces d'oxygène réactives, nous avons essayé de refléter des espèces d'oxygène réactives dans le dans le modèle de vivo l'utilisation 5-(et 6)-chloromethyl-2', 7 '-dichlorodihydrofluorescein diacetate, l'acétyle ester (le CM-H_2DCFDA). Un nerf optique de Longs-Evans rats a été écrasé intraorbitalement, en épargnant la circulation retinal. Dans certains rats colliculi supérieur de Longs rats Evans avait été auparavant exposé via craniotomy et surposé avec Gelfoam saturé avec le vert indocyanine (ICG). Aux points de temps variables les animaux ont été injectés intraveineusement ou intravitreally avec HEt ou le CM-H_2DCFDA et reflétés avec fluorescein et-ou les filtres d'ICG en utilisant le HRA2.

Les résultats: Nous avons démontré le foyer brillant multiple de fluorescence dans la couche de cellule de ganglion quand nous avons rétrogradement étiqueté d'ICG bilatéralement, en indiquant qu'ICG était un colorant rétrogradement transporté qui pourrait être découvert avec le HRA2. Après axotomy et l'injection intravitreal de CM-H_2DCFDA, il y avait la fluorescence brillante dans le canal fluorescein dans quelques cellules dans la couche de cellule de ganglion, en accord avec la production d'une ou plusieurs espèces d'oxygène réactives.

Les conclusions : RGCs peut être identifié et les niveaux d'espèces d'oxygène réactives mesurés en utilisant une fréquence double confocal **Mots-clés** : cellules ganglionnaires de la rétine; especes oxygenique radiculaire; la visualisation;

Abstract

Title: Imaging Reactive Oxygen Species in RGCs *In vivo*

Purpose: Reactive oxygen species not only are generated as a result of cellular injury, but also serve as signaling molecules for a variety of critical processes, including mitosis and cell death. We previously reported that injury to RGC axons induces a burst of superoxide within the cell body, probably of mitochondrial origin (*Lieven et al, 2006*). We now describe a method for imaging of reactive oxygen species within the retina of the living animal using a confocal scanning laser ophthalmoscope called the Heidelberg Retina Angiograph 2 (HRA2) equipped with dual lasers.

Methods: Following preliminary studies using other indicators (hydroethidium; HEt) for reactive oxygen species, we attempted to image reactive oxygen species in the in vivo model using 5-(and-6)-chloromethyl-2',7'-dichlorodihydrofluorescein diacetate, acetyl ester (CM-H_2DCFDA). The resultant images were quantified using ImageJ. One optic nerve of Long-Evans rats was crushed intraorbitally, sparing the retinal circulation. In some rats the superior colliculi of Long-Evans rats had been previously exposed via craniotomy and overlaid with Gelfoam saturated with indocyanine green (ICG). At varying time points the animals were injected intravenously or intravitreally with HEt or CM-H_2DCFDA and imaged with fluorescein and/or ICG filters using the HRA2.

Results: We demonstrated multiple bright foci of fluorescence in the ganglion cell layer when we retrogradely labeled with ICG bilaterally, indicating that ICG was a retrogradely transported dye that could be detected with the HRA2. Following axotomy and intravitreal injection of CM-H_2DCFDA, there was bright fluorescence in the fluorescein channel in a few cells in the ganglion cell layer, consistent with production of one or more reactive oxygen species. There was no cross-talk between the fluorescein and ICG channels when detecting ICG or CM-H_2DCFDA, respectively.

Conclusions: Retrograde labeled RGCs can be identified and levels of reactive oxygen species measured using a dual frequency confocal scanning laser ophthalmoscope.

Keywords RGCs, oxidative radical, imaging

Table des matières

Liste des tableaux

Liste des figures

Figure 1.1f Annotated layers of the retina in a retinal cross section.

Image courtesy of Dr David Van Essen, Department of anatomy and neurobiology, Washington University in St Louis School of Medicine.

Source:

http://thalamus.wustl.edu/course/eyeret.html

Figure 1.1 g

Image showing layers of the retina.

Image courtesy of Dr Thomas Caceci, The Virgina-Maryland Regional college of Vetrinary Medicine.

Source :

http://www.csulb.edu/~cwallis/482/visualsystem/eye.html

Figure 1.1 h

Image showing layers of the retina.

Image courtesy of Dr Thomas Caceci, The Virgina-Maryland Regional college of Vetrinary Medicine.

Source: http://education.vetmed.vt.edu/Curriculum/VM8054/EYE/RETINA.HTM

Figure 1.5 A

Image showing structure of CMH_2DCFDA and its products.

Figure 1.5B

Ethidium and its related products

Figure 1.5 C

DAF-FM 4-amino-5-methylamino-2',7'-difluorofluorescein

Figure 1.5 D

Peroxynitrate

Figure 1.6 A Optics fundus camera. Image courtesy of Fundus Fluorescein and Indocyanine Green Angiography: A Textbook and Atlas. Amar Agarwal. 2008 ISBN 10 1-55642-787-5

Figure 1.6 B Optics of confocal scanning laser ophthalmoscope. Image courtesy of Fundus Fluorescein and Indocyanine Green Angiography: A Textbook and Atlas. Amar Agarwal. 2008 ISBN 10 1-55642-787-5

Figure 3.1 A

Image showing operating table setup in rodent surgery

Figure 3.1 B

Diagram showing rat skull and suture markings

Figure 3.1 C

Diagram showing the markings and areas of interest on the rat skull

Figure 3.1 D

Diagram showing the markings and areas of interest on the rat for superior colliculus labeling.

Figure 4.15 A to L Examination of optic nerve crush on retinal ganglion cells labelled with ICG.

Figure 4.16 A to D

Imaging superoxide following optic nerve crush using CMH_2DCFDA.

Figure 4.17 A to G

Labeling retinal ganglion cells with ICG and using CMH_2DCFDA to examine for reactive oxygen species following optic nerve crush.

La liste des sigles et la liste des abreviations

Age related macular degeneration = AMD

4-amino-5methylamino-2,7'-difluorescein = DAF-FM

5-(and-6)-carboxy-2',7'-dichlorodihydrofluorescein diacetate = CM-H_2DCFDA

Brain derived neurotrophic factor = BDNF

Carbonate = $CO3^-$

Confoal laser scanning ophthalmoscope = cSLO

4',6-diamidino-2-phenylindole = DAPI

4, 5,-diaminofluorescein diacetate = DAF-2-acetate

Dihydroethidium = HEt

Dimethyl sulfoxide = DMSO

4-(4-(dihexadecylamino)styryl)-N-methylpyridinium iodide = DiA

1,1'-dioctadecyl-3,3,3,3'-tetramethylindocarbocyanine = DiI

C18 3,3'-dioctadecyloxacarbocyanine perchlorate = DiO

1,1'-dioctadecyl-3,3,3',3'-tetramethylindotricarbocyanine iodide = DiR

Endoplasmic reticulum = ER

5-(and-6)-chloromethyl-2'7'-dichlorodihydrofluorescein diacetate acetyl ester (CM-H2DCFDA) = H_2DCFDA

2'7'-dichlorodihydrofluorescein diacetate acetyl ester = DCFDA

4 hydroxy-2-nonenal = HNE

Heidelberg Retinal Angiography 2 = HRA2

Heme oxygenase-1 = HO-1

Hydroxyl radical = OH^-

Indocyanine green = ICG

Inner limiting membrane = ILM

Inner plexiform layer = IPL

Intraocular pressure = IOP

Long term depression = LTD

Long term potentiation = LTP

Lucigenin = LC ●-

Mattrix metalloproteinase -2 = MMP-2

Millivolts = mV

Mitochondrial DNA = MnDNA

Mitochondrial Superoxide Dismutase = MnSOD

3-(4, 5-dimethylthiazol-2yl)-2, 5-diphenyl tetrazolium bromide = MTT

N-methyl-D-aspartic acid = NMDA

Neurotrophic growth factor = NGF

Neurotrophin 3 = NT3

Nitrate = NO_2

Outer limiting membrane = OLM

Outer plexiform layer = OPL

Poly(ADP ribose) polymerase = PARP

Reactive oxygn species = ROS

RGC = RGC

RGC 5 cell line = RGC-5

Retinal pigment epithelium = RPE

Retinal nerve fiber layer = RNFL

Retinitis Pigmentosa= RP

Royal College of Surgeons = RCS

Tropomyosin-Related Kinase A = TrkA

Tropomyosin-Related Kinase B = TrkB

Tropomyosin-Related Kinase C = TrkC

Yttrium aluminium garnet laser = YAG

Les Remerciements

Je voudrais remercier Dr Leonard Levin de sa direction exaltée et conseils exceptionnels et conseil partout dans mon projet de maîtrise et dans l'écriture de ce mémoire. Sans son aide cela n'aurait pas été possible. Je voudrais aussi admettre les membres du jury qui a lu et a évalué mon manuscrit et pour leur conseil utile. Je voudrais aussi admettre l'aide de Dr Adriana Di Polo en apprenant certaines des techniques étiquetantes.

Finalement je suis pour toujours redevable à ma famille, mes parents et Andrea, Elaine et Caoimhín pour leur encouragement et soutien constant pour aussi longtemps qu'ils m'ont connu.

Introduction 1.1 Ocular anatomy

The human eyeball is composed of the segments of two spheres of different sizes placed in front of the other called the anterior and the posterior poles (figure 1.1a).

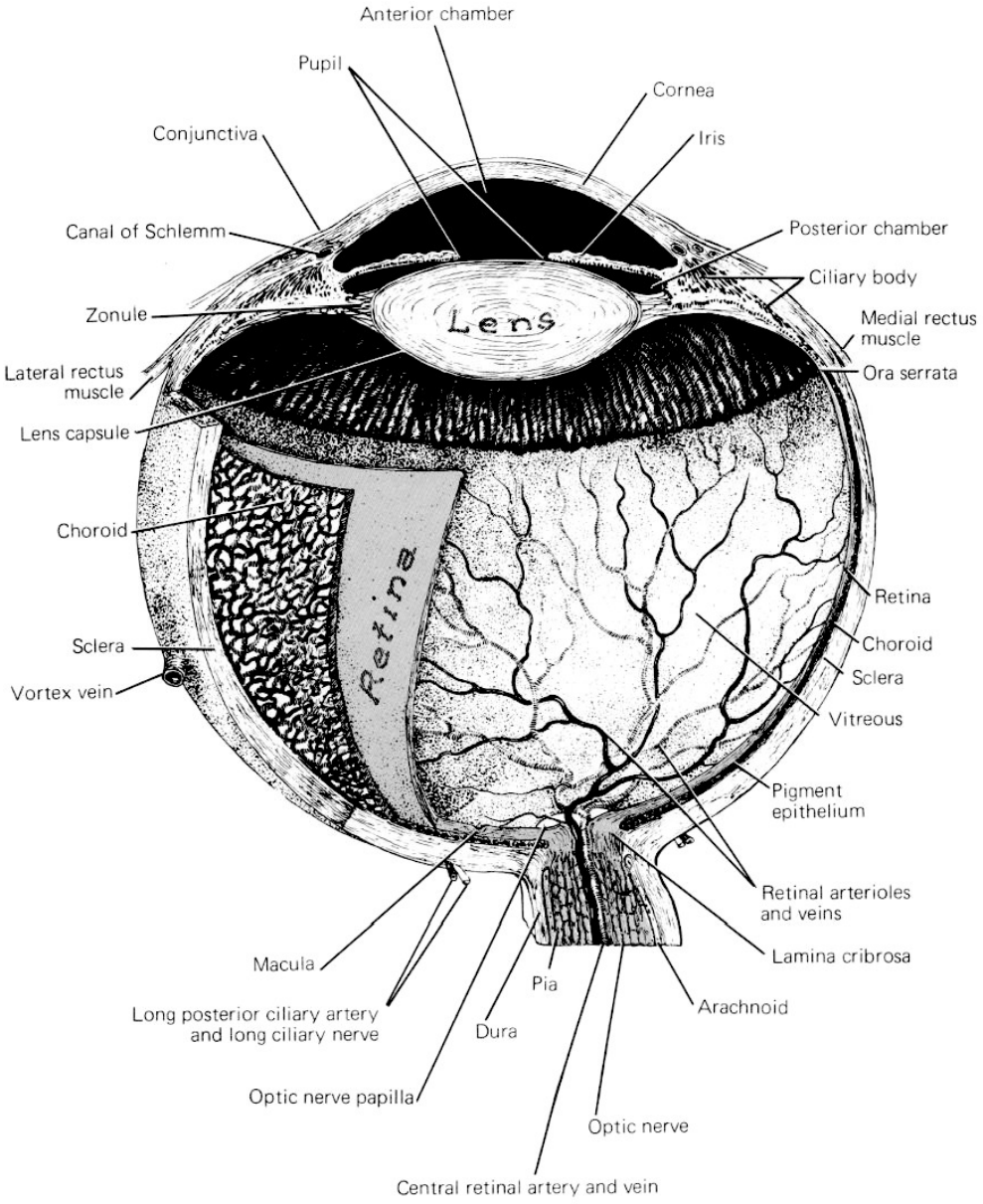

Figure 1.1a Diagram showing some of the structures in the mammalian eye. Courtesy of Dr Thomas Caceci, Virginia/Maryland Regional College of Veterinary Medicine, Virginia Polytechnic Institute and State University, Blackburg, Virginia, USA.

While we will outline the structure of the human eye, there are some subtle differences between this and other mammalian models which have been investigated by previous work, some of which we will outline during the introduction (*Morrison et al 1995*).

The anterior pole of the eye is the center of curvature of the transparent segment or cornea, which is involved in refracting or directing light rays through the anterior portion of the eye before light travels back through the lens and is focused on the retina. The posterior pole is the center of the posterior curvature of the eyeball and this is located slightly temporal to the optic nerve.

The sclera forms the posterior five-sixths of the eyeball and appears white to opaque in color. This fibrocollagenous structure gives the eyeball its shape and deformability and provides a degree of protection for the less robust, delicate structures located within the eyeball.

As the cornea is a structure which will be important to the study, we will briefly outline its anatomy in more detail. The cornea is a transparent multilayered transparent structure forming the anterior one-sixth of the eyeball. The layers from inside to out are as follows: the epithelial layer, Bowmans membrane, substantia propria, descements membrane and endothelium. The epithelial layer is stratified and consists of five layers of cells, ranging from the superficial flattened, nucleated, nonkeratinized squamous cells to the deeper cells which are more columnar in shape. The deepest columnar cells form a single layer and rest on a basement membrane. The columnar cells lateral borders interdigitate with each other and are attached by desmosomes and gap junctions while hemidesmosomes attach to the underlying Bowmans layer. Bowmans layer lies immediately beneath the basement membrane of the corneal epithelium and is acellular, consisting of interwoven collagen

fibrils embedded in intercellular substances. The stroma forms approximately 90% of the corneal thickness and is composed of lamellae of collagen fibrils that run in parallel with the surface which are embedded in glycosaminoglycans with occasional macrophages, lymphocytes and polymorphonuclear leukocytes. Descements membrane lies on the posterior surface of the stroma and is the basement membrane of the endothelium. It consists of collagen fibrils arranged in a hexagonal pattern and embedded in matrix. At the corneal margin the membrane terminates abruptly and becomes continuous with the trabecular tissue. The anterior border of the trabecular meshwork is known as the line of Schwalbe. The corneal endothelium consists of a single layer of flattened cells which are polygonal in shape and whose plasma membrane interdigitate with each other and are connected via tight junctions.

The limbus (corneoscleral junction) is an important landmark in our study and we will briefly outline its structure and importance (figure 1.1b).

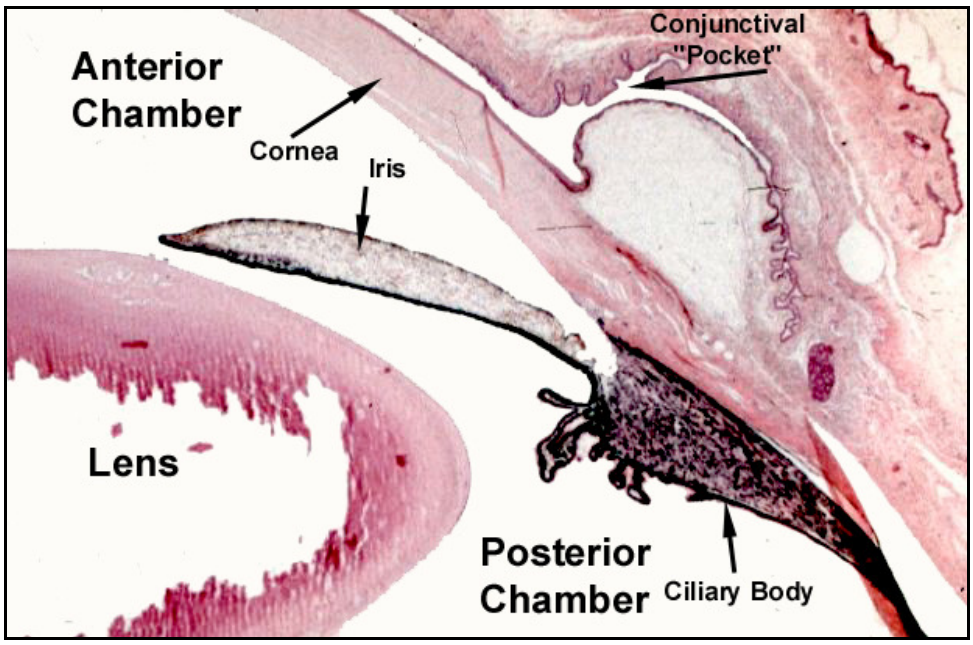

Figure 1.1b Section through anterior portion of eye showing limbal structures.

Courtesy of Dr Thomas Caceci, Virginia/Maryland Regional College of Veterinary Medicine, Virginia Polytechnic Institute and State University, Blackburg, Virginia, USA.

Previous studies in humans have demonstrated the limbus to be approximately 1.5 to 2.0 mm wide in the human model (*Patel et al 2006*) although there is a dearth in the literature of similar anatomical studies in the rat model or other mammalian models regarding its exact size and dimensions. The inner surface of this structure contains the trabecular meshwork and the canal of Schlemm. The aqueous fluid of the eye is produced in the trabecular meshwork while the canal of Schlemm serves to transport this fluid from the anterior chamber. Increased resistance to outflow of the aqueous fluid through the trabecular meshwork into the canal of Schlemm causes the condition known as glaucoma in which the intraocular pressure is often raised and atrophy of the optic nerve occurs. The limbus is an important landmark, particularly in our future experiments. It is the site where

the cornea and sclera merge with each other. The anatomic limbus is defined by Schwalbes line while the surgical limbus id defined by the beginning of the bluish area marking the transition zone between the cornea and the sclera. The surgical limbus is located slightly anterior to the anatomic limbus and is the entry point for virtually all types of anterior segment surgery and intravitreal injections in the human and mammalian models.

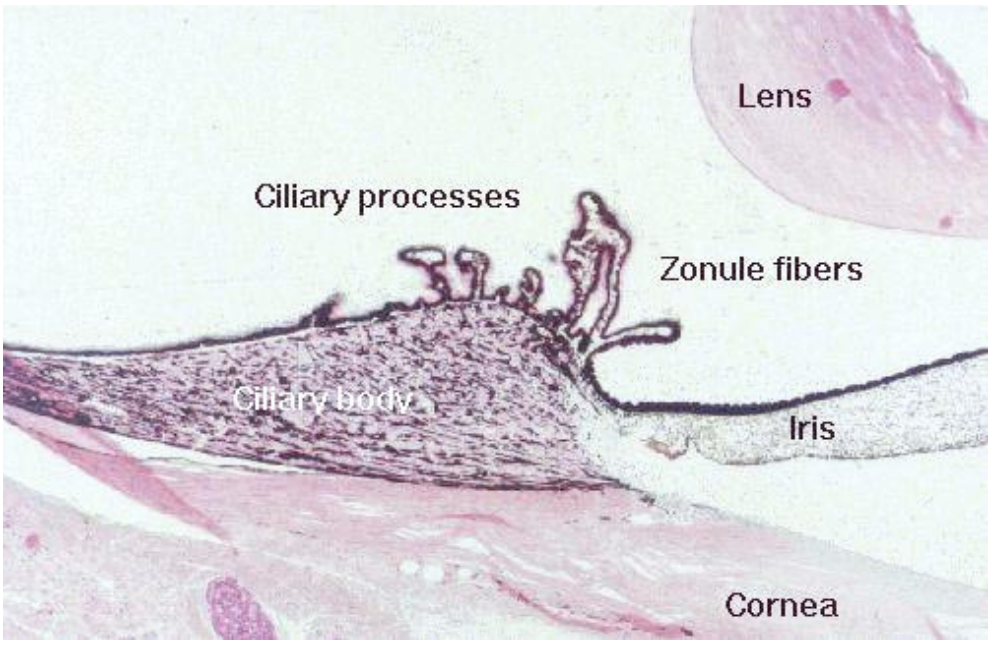

Figure 1.1c Diagram showing structures in the region of the corneoscleral junction.

Image courtesy of Dr Thomas Caceci, Virginia/Maryland Regional College of Veterinary Medicine, Virginia Polytechnic Institute and State University, Blackburg, Virginia, USA.

Posteriorly, the optic nerve exits the eye at the optic disc whose anatomical course will be discussed in greater detail in the next section.

Physiological concerns in rodents were also pertinent to this project. Previous studies had examined methods used to calculate the intravascular volume in adult rats (*Belcher et al 1957).* There have been few publications with regard to this in the literature with Belcher et al providing the most comprehensive review of this topic. Using this as a guide we were able to calculate the most appropriate volumes to inject intravascularly and intravitreally.

Histology of the retinal ganglion and retina

RGC bodies represent the output of the retina (see figure 1.1a). Their soma (bodies) are located in the retina while their axons extend as far as the lateral geniculate body where they synapse. Ganglion cells fire action potentials and have a negative resting potential of approximately – 70 mV. At this resting potential there is a tension between the concentrations and charges of sodium and potassium inside and outside the neuron. When ganglion cells receieve a suprathreshold level of input from the bipolar cells, voltage-gated sodium channels open and Na+ ions rush in along the concentration gradient. This causes a sudden reversal of the charge from negative to positive and this propogates down the body (axon) of the neuron. Finally the potassium channels open, which restores the cell to its negative resting potential. The refractory period of the RGC is defined as the time after a neuron has fired an action potential during which it cannot fire another. The firing rate of the neuron (e.g., spikes per second) is what represents information about stimulus intensity within each neuron.

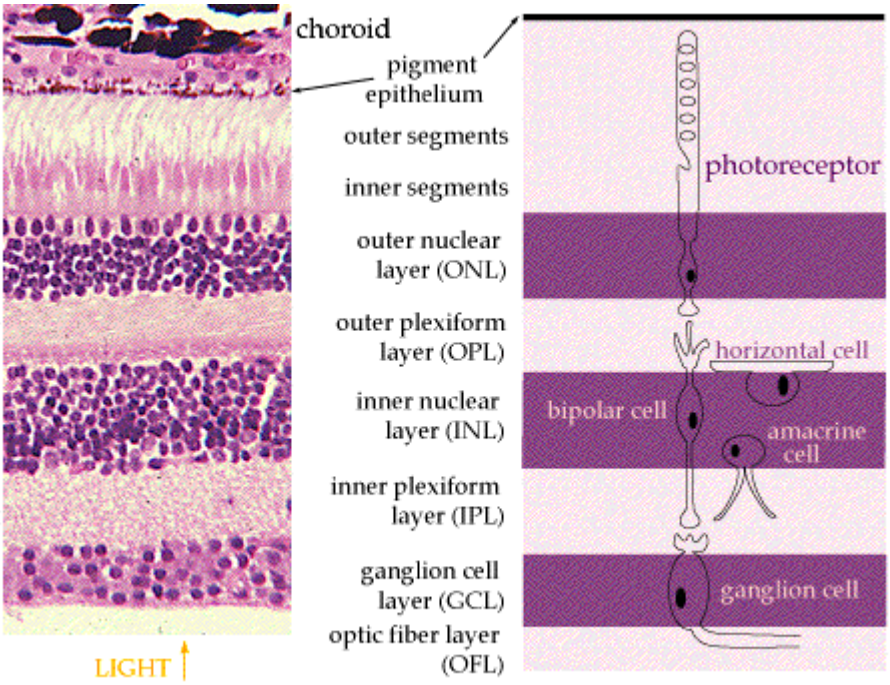

Figure 1.1f above shows the annotated layers of the retina in a retinal cross section with the actual cells in the schematic on the right. Courtesy of Dr David Van Essen, Department of Anatomy and Neurobiology, Washington University in St Louis School of Medicine.

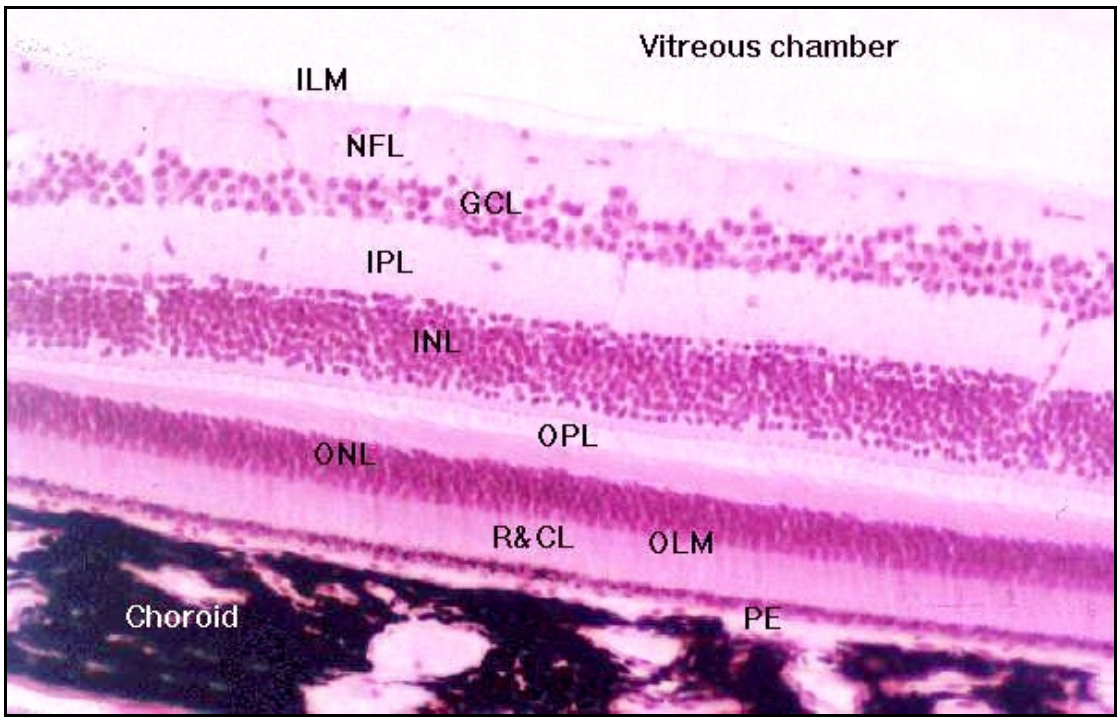

Figure 1.1g below shows retinal layers in a mouse model

Image showing layers of the retina. Image courtesy of Dr Thomas Caceci, The Virigina-Maryland Regional college of Vetrinary Medicine.

RGCs fire action potentials in response to certain types of retinal stimulation. The pioneering work by Hubel and Weisel marked the earliest attempted by researchers to characterize their receptive fields (*Hubel et al 1977*). The receptive field is defined as the part of the retina that needs to be stimulated in order to elicit a spike.It is the part of the visual world that the neuron is responsive to (that it "sees") or what the visual stimulus needs to be in order to elicit spikes.

Most RGCs have concentric (or center-surround) receptive fields. These receptive fields are divided into 2 parts (center/surround), one of which is excitatory ("ON"), the other inhibitory ("OFF"). For an ON/OFF center/surround cell, a spot of light shown on the

inside (center) of the receptive field will elicit spikes, while light falling on the outside ring (surround) will suppress firing below the baseline rate.

Visual neurons do not simply "pipe" the output of the retina through the visual pathways. Instead, the activity of a given neuron is affected by the activity of nearby neurons. Lateral inhibition in the RGCs is a prime example. When a RGC fires action potentials, it also inhibits the firing of nearby (lateral) ganglion cells. Lateral inhibition performs edge (contrast) enhancement.

RGCs are located in the inner portion of the retina (figure 1.1f) and these cells are concerned with conveying visual information from the retina along the visual pathway. The human retina is approximately 0.2 mm thick with an area of approximately 1100 mm^2. As the below diagram of the retina shows, it is composed of 10 layers. In order to better understand the background to our project, it is necessary to have a knowledge of the anatomy and histology of the retina. The inner limiting membrane (ILM) marks the boundary between the vitreous humor in the posterior chamber and the retina itself. Which is the most anterior portion of the retinal layers.

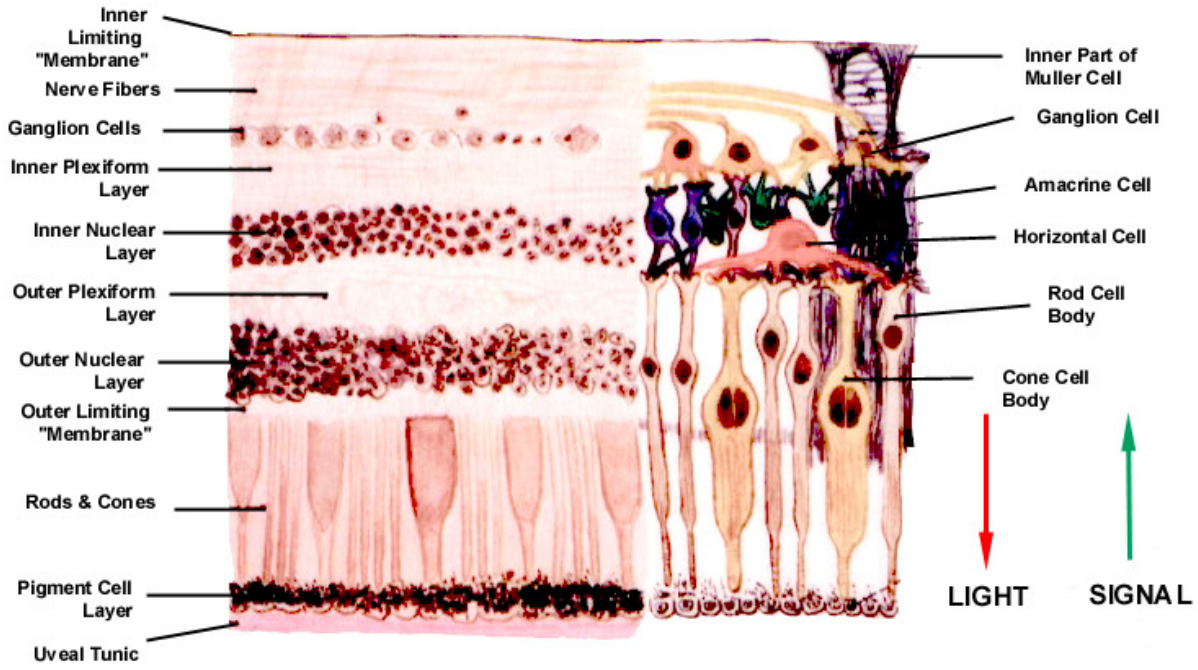

Figure 1.1 H Image showing the layers of the retina.

Image courtesy of Dr Thomas Caceci, The Virgina-Maryland Regional college of Vetrinary Medicine.

The ganglion cell layer is comprised of the cell bodies and the axons of the ganglion cells as well as displaced amacrine cells. The inner plexiform later (IPL) contains synapses made between bipolar, amacrine and ganglion cells, its thickness varying depending on the animal concerned with higher order primates having thinker retina and consequently more developed peripheral and specialized image processing.

The inner nuclear layer (INL) contains bipolar cells, horizontal and amacrine cell bodies.

The outer plexiform layer (OPL) contains a network of synapses between the dendrites of horizontal cells from the inner nuclear layer and the photoreceptor cell inner segments from the outer nuclear layer. The outer limiting membrane coincides with the base of the inner segments of photoreceptors. The photoreceptor layer contains inner and outer segments of

rod and cone photoreceptors.

Pigment epithelium contains darkly pigmented cells responsible for absorbing light not captured by photoreceptors and therefore reducing scattering. In our project we are primarily concerned with RGCs.

Anatomy of the visual pathway

In the human model, the optic nerve is divided into intraocular (1 mm), intraorbital (25 mm), intracanalicaular (5 mm) and intracranial (10 mm) segments.

The intraocular portion includes the optic disc and the portion of the optic nerve that lies within the sclera. The optic disc is generally approximately 1.5 mm in diameter and marks the point at which the axons of the RGCs converge before exiting. It has a pink colour and is paler than the surrounding retina with a flat or slightly raised edge and a central slight depression. The axons of the RGCs located in the peripheral retina take up a peripheral position and those from the central retina take up a more central position in the optic nerve. As the RGCs axons bend sharply posteriorly at the disc, they are unmyelinated and supported by astrocytes and at the periphery of the disc are covered by the internal limiting membrane of the retina.

The orbital portion of the optic nerve crosses the lamina cribrose which the portion of the bone resembling a sieve and acquire a myelin sheath which are formed by oligodendrocytes. Outside this is a dense sheath of dura mater, a middle delicate sheath of arachnoid and an innermost vascular sheath of pia mater. Posteriorly the sclera and sheaths

blend together and the sheaths are continuous through the optic canal with the meningeal coverings of the brain.

The optic nerve is surrounded by orbital fat and within this are the ciliary vessels and nerves. The ciliary ganglion lies between the lateral border of the nerve and the lateral rectus muscle. Posteriorly the nasociliary nerve and the ophthalmic artery run forward and pass medially to cross the optic nerve. At about the same position, the nerve to the medical rectus muscle from the inferior division of the oculomotor nerve crosses below the optic nerve. At about the same position the nerve to the medial rectus muscle from the inferior division of the oculomotor nerve crosses below the optic nerve. At approximately 12 mm behind the eyeball, the inferomedical dural sheath surface is pierced by the central retinal artery and vein of the retina. The artery crosses the subarachnoid space obliquely before entering the optic nerve. The vein has a more prolonged course in the subarachnoid space and lies posterior to the artery. The central vessels assume an axial position and pass forward to emerge on the optic disc. At the apex of the orbital cavity, the optic nerve lies within the muscular cone formed by the four recti and is surrounded by their tendinous origins. The optic nerve axons are grouped together into bundles separated by fine septa derived from the inner surface of the pial sheath.

In the intracanalicular portion of the optic nerve, the optic canal lies within the lesser wing of the sphenoid bone and is about 5 mm long. The optic nerve passes through the optic canal surrounded by its three meningeal coverings (dura mater, pia mater, arachnoid mater). The subarachnoid space is filled with cerebrospinal fluid around the optic nerve, communicates and is discontinuous with the intracranial subarachnoid space. Also passing through the optic canal are the ophthalmic artery on the infero-lateral border of the optic

nerve and the postganglionic sympathetic nerves accompanying the artery.

The intracranial portion is 10 mm in length and begins as the optic nerve leaves the canal and passes backward, upward and medially within the subarachnoid space and reaches the optic chiasm which is located in the floor of the third ventricle. The optic nerve is ocomposed of 1,200,000 myelinated axons and about 90% of these are of small diameter (1 µm) and the remainder measure from 2 to 10 µm in diameter.

The optic chiasm is situated at the junction of the anterior wall and floor of the third ventricle. It is composed of a flattened bundle of nerve fibers with dimensions of 12 mm wide and 8 mm from anterior to posterior. The chiasm is covered with pia mater and projects downward into subarachnoid space. In the human chiasm the nerve fibers from the nasal half of the retina cross the midline and enter the optic tract of the opposite side ; the nerve fibers from the inferior nasal retina cross at the anterior part of the chiasm, whereas the nerve fibers from the superior nasal retina cross at the posterior part of the chiasm. The nerve fibers from the temporal half of the retina pass backward into the optic tract of the same side. The partial crossing of the optic nerve fibers in the optic chiasm is essential for binocular vision.

The optic tracts emerge from the posterolateral angles of the optic chiasma as a cylindrical band. Each passes posterolaterally between the tuber cinereum medically and the anterior perforated substance laterally. The tract becomes flattened and and winds around the lateral margin of the upper part of the cerebral peduncle, adherent to midbrain and overlapped by the uncus and the parahippocampal gyrus. In the human most of the nerve fibers in the

optic tract terminate in the lateral geniculate body and are concerned with conscious visual sensations; these fibers constitute the lateral root of the optic tract. The smaller medial root contains fibers which are of unknown function. Priot to its entry into the lateral geniculate nucleus, about 10% of fibers pass medially in the superior brachium below the pulvinar of the thalamus to enter the superior colliculus and the pretectal nucleus. These fibers are involved in visual body reflexes and light reflexes respectively (*Shernab et al 1982*).

Lateral geniculate body

The lateral geniculate body is a small ovoid swelling on the undersurface of the pulvinar of the thalamus which is connected by the superior brachium which is formed by the nerve fibers that do not terminate in the lateral geniculate body but pass to the superior colliculus and pretectal nucleus as described above. The dorsal or main lateral geniculate nucleus has a laminated structure and consists of six curved layers of cells oriented in a dome-shaped mound, often likened to a stack of hats on top of one another. These layers of cells are separated by white bands of optic nerve fibers and are numbered 1 to 6 beginning at the hilus and continuing dorsally to the crest of the geniculate body. The nerve fibers are the axons of the ganglion cell layer of the retina and come from the temporal half of ipsilateral eye and from the nasal half of the contralateral eye, the latter fibers crossing the midline in the optic chiasm. The nerve fibers that cross the midline terminate in layers 1, 4 and 6 while the optic nerve fibers that do not cross terminate in layers 2, 3 and 5. The peripheral retinal fibers end in the anterior part and the upper retinal quadrants end medially and the lower ones laterally. The macular fibers end in the center and posterior part of the nucleus. Each

lateral geniculate body receives information from both retina.

Optic radiations

The optic radiations or geniculocalcarine tracts are formed of nerve fibers that originate from the nerve cells in the laminae of the lateral geniculate bodies. Fibers originating from the lateral portions of the lateral geniculate body receive fibers from the inferior retinal quadrants (superior visual field) fan out laterally and inferiorly around the anterior tip of the inferior (temporal) horn of the lateral ventricle, before swinging posteriorly. The fibers associated with the peripheral part of the retina swing farthest forward and those related to the macula loop very little. These forward looping fibers form the loop of Meyer. The fibers continue posteriorly in the retrolentiform part of the internal capsule, lying lateral to the inferior (temporal) and posterior (occipital) horns of the lateral ventricle. They terminate by turning medially to enter the occipital cortex. Here, the fibers end on the inferior lip of the calcarine fissure.

Fibers originating from the medial portions of the lateral geniculate body receive impulses from the superior retinal quadrants (inferior visual field) and turn directly posteriorly and accompany the other fibers in the retrolentiform part of the internal capsule. On entering the occipital cortex, the fibers terminate in the superior lip of the calcarine fissure.

Visual cortical areas

The primary visual area (area 17) occupies the walls of the deep calcarine sulcus on the medial surface of the hemisphere and extends onto the cortex superior and inferior to sulcus. Posteriorly it extends as far as the occipital pole and a small portion of variable size extends forward above the calcarine sulcus as far as the parieto-occipito sulcus; below the calcarine sulcus, it extends forwards a little further.

Grossly on sections, the primary visual cortex can be recognized by its thinness and the characteristic presence of a white line or stria (of Gennari) in the gray matter . This white line is formed by the fourth layer of the cortex by the presence of myelinated fibers emanating from the optic radiation and association fibers.

Histologically the visual cortex is of the granular type with only a few pyramidal cells being present. Although the cortex is thinner (1.5 mm) than other cortical regions, the cell population is greater and the intercellular spaces are reduced compared with other cortical regions. The primary visual cortex has six layers. The cells in laminae II and III project to the secondary visual area (areas 18 and 19). The cells of laminae V project to the superior colliculus; those of lamina VI to the lateral geniculate body. The cortex receives fibers from the temporal half of the ipsilateral retina and the nasal half of the contralateral retina. The right half of the field of vision is represented in the visual cortex of the left cerebral hemisphere and vice versa. The superior retinal quadrants (inferior field of vision) pass to the superior wall of the calcarine sulcus, while the inferior retinal quadrants (superior field of vision) pass to the inferior wall of the calcarine sulcus. The macula lutea which is the central part of the retina and the area for most acute vision is represented on the cortex in the posterior part of the area 17 and accounts for one third of the visual cortex. The

peripheral parts of the retina are represented more anteriorly *(Alexander et al 1986).*

The secondary visual areas are also known as areas 18 and 19 and surround the primary visual areas on the medial and lateral surfaces of the hemisphere. These areas are nonstriate and histologically show the usual six layers. The secondary association areas receive afferent fibers from the primary visual cortex and other cortical areas as well as the thalamus. The secondary visual areas have a role to play in relating the visual information received by the primary visual area to past visual experience, thus enabling the individual to recognize and appreciate what one is doing. In addition to this, area 18 also integrates the two halves of the visual fields by means of commisural fibers that cross the midline in the splenium of the corpus callosum. It is possible that area 18 is involved in sensory motor eye coordination and is linked to the frontal eye field. The frontal eye field is the area anterior to the facial area of the precentral gyrus extending into the middle frontal gyrus (Brodmann areas 6, 8 and 9). Area 18 may also be linked by descending pathways to the cranial nerve nuclei controlling the extraocular muscles and thought to be involved in smooth pursuit of visual targets *(Ts'o et al 1988, Bosking et al 1997, Van Essen et al 1992, LeVay et al 1980, Livingstone et al 1988, Halder et al 1995).*

1.2 Retinal ganglion cell death

Our study focuses primarily on the imaging of reactive oxygen species in RGCs undergoing axonal injury. Therefore a brief introduction is included on the mechanisms of retinal ganglion cell death. There are a myriad of proposed mechanisms involved in retinal ganglion cell death, however the focus here will be on a small number of these.

All optic neuropathies cause retinal ganglion cell death. The initial site of injury in one type of optic neuropathy i.e. glaucoma, is in the RGC axons within the optic nerve. RGC axons are vulnerable as they pass through the sieve-like lamina cribrosa and elevated IOP as in glaucoma can cause distortion and compression of RGC axons leading to ischemia, hypoxia and deprivation of neurotrophic factors. In other diseases of the optic nerve, the intraocular pressure is normal and RGC death and subsequent loss of vision continues to occur. Although there are many proposed mechanisms, the exact etiology behind RGC death in these circumstances remains unknown.

During development neurons are eliminated by the intrinsic process of apoptosis and only those which secrete neurotropic factors escape death. It is proposed that in developing RGCs, deprivation of BDNF and NGF leads to cell death. It is not yet established whether this occurs in the adult RGC maintenance and could perhaps be a factor in disease where axonal transport is disrupted (Pease et al 2000). The actions of neurotrophins are mediated by two principal transmembrane-receptor signaling systems. Each neurotrophin receptor — TrkA, TrkB, TrkC and the p75 neurotrophin receptor (p75NTR) — is characterized by specific affinities for the neurotrophins nerve growth factor (NGF), brain-derived

neurotrophic factor (BDNF), neurotrophin 3 (NT3) and NT4. An emerging concept is that the two distinct receptor classes, Trk and p75NTR, preferentially bind mature and proneurotrophins (neurotrophin precursors), respectively, to elicit opposing biological responses. LTD, long-term depression; LTP, long-term potentiation.

We know from previous work that apoptosis plays a central role in optic neuropathies (*Murphy et al 2006*). Although there are many proposed mechanisms this brief discussion will focus on three main parts to this pathway: the BCL-2 protein family (whose expression has already been shown in the retina by Levin et al), the caspase pathway and the calcium - dependent pathways.

The BCL-2 protein family is especially important in glaucoma. Several BCL-2 pathways in mammals and many inhibit apoptosis(bcl-2 bcl-x) and others promote it (Bad, Bax, Bid). One mechanism of action involves either promoting or preventing cytochrome c release from mitochondria.

Recent Bax deficient mice showed preserved RGCs indicating that is required for survival. The caspase pathway is also proposed to be involved in executing RGC death, broadly speaking caspases 1, 2, 4, 5, 8, 9, 10 are inhibitors and 3, 6, 7, and 14 are effectors.

Calcium dependant pathways are very important in the apoptotic process. High intraaxonal or intracellular levels of calcium are toxic and calcium enters the cell in three ways: the voltage-gated calcium channels, store-operated channels, receptor-gated channels. Within the cell, calcium is sequestered by mitochondria, ER and calcium-binding proteins.

Calcium-induced apoptosis depends on calcineurin, a calcium-dependant phosphatase. Calcicneurin can dephosphorylate the proapoptotic BAD protein. BAD can then translocate

from cytoplasm to mitochondria where it can bind BCL2 or BCL-X_L . Formation of these protein complexes leads to increased permeability of the mitochondrial cell membrane, cytochrome C release and neuronal apoptosis.

1.3 Retinal ganglion cell death models

Despite its unique location described previously, the optic nerve is a central nervous system white matter tract. Therefore, injury to the mammalian RGC axon results in death of the cell body, and an inability of the axon to regenerate. The precise timing of this process remains unknown. Understanding how to prevent this irreversible loss of RGCs is important in finding new therapies for optic neuropathies.

There are several models used for the study of RGC death in the live (in vivo) animal model including mouse, murine, bovine, feline, canine, rat and monkey. Each of these has varying similarity to the human model. Although we cannot directly extrapolate findings from animal models to the human model, they allow us to study RGC death in a relatively similar environment. Previous studies have shown that the morphological changes at the primate optic nerve head are similar to that seen in human patients with glaucoma, although the course of the disease is much more rapid, taking place over months. Primates can be difficult to study in large numbers and in order to overcome this obstacle, models have been devised for rodent models. In the rat, the limbal and episcleral veins can be occluded by cautery (*Garcia-Valenzuela et al 1995*), sclerosis with hypertonic saline (*Morrison et al 1997*), or argon laser (*Schori et al 2001*). In view of the applicability and robustness of the rodent model, we choose the rat as our model to study the generation of reactive oxygen species following RGC damage (*Shen et al 1999*).

A well-established method for causing axonal damage and enabling study of the resultant effects on the RGC is directly damaging the optic nerve. The injury used is typically acute, although graded injuries have been designed to more closely mimic the chronic nature of some diseases. Most of these models are done with rodents, more commonly rats because of difficulty in surgical exposure and a tendency to bleed in the mouse or rat. The most common model for optic nerve injury is in rodents, either rats or mice, and uses either optic nerve transection (e.g. crush) or experimental glaucoma (raising the eye pressure). Rodents allow us to study RGCs, which closely resemble those in the human eye. These models are universally used in virtually every laboratory in the world studying optic nerve disease (*Berkelaar et al 1994, Bertrand et al 2007, Freeman et al 2000, Lebrun-Julien et al 2009, Li et al 1999, Lieven et al 2006, Schlamp et al 2001, Swanson et al 2005*). There has been extensive use of rats in ophthalmology research in this and other facilities with the techniques which we will use already well established in the literature (*Berkelaar et al 1994, Freeman et al 2000, Li et al 1999, Schlamp et al 2001, Swanson et al 2005, Lieven et al 2006*).

The actual injury can be obtained by either crushing or transecting the optic nerve (*Morrison et al 1997*). Crushing the optic nerve, if done carefully, can preserve circulation to the retina, but careful post-operative ophthalmoscopy using either a direct or indirect ophthalmoscope is necessary to exclude infarction.

To eliminate the potential for disturbing the retinal blood supply, the optic nerve can be transected via an intracranial approach. This approach avoids the blood vessels that supply the retina directly. However, this technique also involves aspiration of part of the overlying cortex to gain access to the intracranial optic nerve, which might have other effects on the

animal. Other techniques described in the literature have used a lateral approach from the temporal aspect of the orbit and in this way result in less damage to the surrounding orbital structures and cortex. It is for this reason that the technique we will use in our study will involve the lateral approach to the optic nerve.

Partial crush injuries of the optic nerve have been used to produce graded optic nerve loss. This technique results in the continuous loss of fibers when studied at time points days or even weeks after the initial injury (*Yoles et al 1997*). This further loss after the primary insult has been named secondary degeneration, similar to what is seen with other injuries within the central nervous system. The mechanism by which this occurs has been hypothesized to be due to excitotoxicity within the retina. Another technique described in the literature has described using an inflatable balloon against the optic nerve within the orbit in feline models to induce chronic optic nerve compression *(Lu et al 2006, Clifford-Jones et al 1985*). However, this primarily induces demyelination and relatively less axonal injury (*Gellrich et al 2002*).

Optic nerve head ischemia can be used to model the potential role of blood flow reduction in glaucoma. This spans several models already established in the literature. The blood supply to the optic nerve head can be interrupted by occluding the posterior ciliary circulation originally described in the 1970s (*Levy et al 1976*). In the monkey this can be done under direct observation. In the rat model, the meninges can be separated from the nerve and compressed with a ligature, interrupting the blood supply to the optic nerve head. However, this will also interrupt the blood supply to the central retinal artery. Infusion of

endothelin-1, a potent vasoconstrictor, into the subarachnoid space around the optic nerve of rabbits or primates can be used to induce optic nerve head ischemia, and therefore also injure optic nerve axons indirectly (*Tezel et al 2000*). This has the advantage that the injury is relatively chronic (weeks), unlike the acute injuries associated with ligating blood vessels. Acutely elevating the intraocular pressure above the systolic blood pressure will cause retinal hypoperfusion, and if sustained, will infarct RGCs, indirectly causing an optic neuropathy. Several novel mechanisms have also been more recently described in the literature including the photoembolic technique used in primates (*Chen et al 2008*)

RGC excitotoxicity has been extensively studied in the literature in various animal models (*Yucel et al 2005, Hare et al 2004, Schori et al 2001, Woldemussie et al 2002*). It has already been established from these and other studies that RGCs are very susceptible to the toxic effects of the excitatory amino acid transmitter glutamate. This *excitotoxicity* is mediated by N-methyl-D-aspartate (NMDA) receptors. There also is a role for non-NMDA receptors in glutamate excitotoxicity of RGCs. Glutamate, NMDA, or other excitotoxic compounds can be injected intravitreally in the experimental animal and have been shown to cause loss of RGCs. Some animal studies have even examined the potential use of a vaccine in mice which mitigates against the excitotoxic effects of glutamate (*Schori et al 2001*). In the neonatal animal these agents can be given systemically. Systemic glutamate does not have a significant effect in the adult animal as it does not cross the blood-retinal barrier.

Methanol is clinically associated with a toxic optic neuropathy, and has been used in animal models to induce an experimental optic neuropathy. In the rat model there are potent

mechanisms for the prevention of methanol toxicity via the oxidation of its toxic metabolite formate. This can be blocked by the co-administration of nitrous oxide, allowing the formate levels to increase to toxic levels, inhibit mitochondrial cytochrome oxidase, and induce an optic neuropathy and a retinal injury, i.e. a mixed neural injury *(Murray et al 1991*).

1.4 RGC Labeling

Techniques available for labeling RGCs

Currently there are several available methods for labeling of RGCs in both the *in vitro* and the *in vivo* model. Currently there are several methods available for imaging mammalian neurons in a time-lapse fashion in the live animal in the peripheral nervous system (*Walsh et al 2003*) and in the brain (*Vercelli et al 2000, Grutzendler et al 2002, Trachtenberg et al 2002*). In the retina the periodic imaging of the retina and its dendritic processes has been possible in the living zebra fish (*Munn et al 2006, Zoloessi et al 2006*). In the mammalian model RGCs have been imaged in the live animal using various techniques (*Codeiro et al 2004, Engelmann et al 1999, Gray et al 2008, Higashide et al 2006, Sabel et al 1997, Schmitz-Valckenberg et al 2008, Seeliger et al 2005, Thanos et al 2002*). For technical reasons, in vivo imaging of individual RGCs and their dendric arbors which require even higher resolution to image, have not been previously possible in mammals (*Chalupa et al 2006, Morgan et al 2005*)

The retrograde labeling technique for RGCs has been cited extensively in the literature in

which a fluorescent dye is either injected into the superior colliculis or the area is overlaid with a piece of gelfoam soaked in the required fluorescent probe. Retrograde markers in which the dye is transported using the intrinsic retrograde transport mechanism of cells include dyes such as fluorogold, fast blue, cascade blue, latex nanospheres, cascade blue, lucifer yellow, diamidino yellow and hydroxystilbamidine methanesulfonate. Dynein, a motor protein responsible for retrograde axonal transport, carries vesicles and other cellular products toward the cell bodies of neurons. Its light chains bind the cargo and its globular head regions bind the microtubule, "inching" along it. Retrograde transport medicated by dynein sends chemical messages and endocytosis products traveling towards endolysosomes from the axon back to the cell. Fast retrograde transport can cover 100 to 200 millimeters per day *(Otas et al 2003, Sabry et al 1995, Karp et al 2005, Brown et al 2003, Roy et al 2007).*

Anterograde tracers perclude those which hitchhike on the axons intrinsic anterograde transportation mechanism include those such as dextran conjugates, Pha-L, Biocytin. Bidirectional transportation systems which utilise both antergrade and retrograde transportation mechanisms include markers such as DiI and DiO

Other groups have outlined the use of ICG, which is a tricarbocyanine dye and can be used as a a RGC marker in the rat model using the well-described retrograde labeling technique. This dye has an axonal transport rate of 2 mm per hour and persistence of this for between 7 to 14 day and its appearance in the RGCs seen within 4 hours of injection into the lateral geniculate nucleus (*Paques et al 2003*). These features make it an important novel method of marking RGCs.

The dialkylcarbocyanines have spectral properties that are largely independent of the length of the alkyl chains, and are instead determined by heteroatoms in the terminal ring systems and the length of the connecting bridge. They have extremely high extinction coefficients, moderate fluorescence quantum yieldsand short excited state lifetimes in lipid environments. Despite this, their fluorescence is easily detected when incorporated into membranes. There are several in existence including DiI, DiO, DiA and DiR.

In an attempt to seek a less invasive method of labeling RGCs, several researchers have published techniques using members of the fluorescent protein family to label RGCs. The family of fluorescent proteins encompasses several proteins having the distinctive B-pleated sheet structure of fluorescent proteins. The cell surface glycoprotein known as Thy-1 is expressed by projection neurons in many parts of the nervous system and in the retina is largely expressed in RGCs. In the transgenic mouse model developed by Feng (*Feng et al 2000*), the fluorescent protein is under the control of the Thy-1 promoter construct protein. One paper examined mice in which cyan fluorescent protein was expressed in RGCs and used DiI as the confirmatory marker for RGCs. This represented a less invasive mechanism for labeling RGCs in the live animal and utilised the confocal scanning laser ophthalmoscope to image the RGCs (*Leung et al 2008*). Another more recent paper utilized a similar technique except this time used mice which had yellow fluorescent protein expression (*Walsh et al 2008*).

1.5 Detecting reactive oxygen species

There are several labeling markers available on the market for indicating the presence of reactive oxygen species. These include the non-specific markers of reactive oxygen species as well as the more specific markers which label individual reactive oxygen species.

Non-specific markers of reactive oxygen species

5-(and-6)-carboxy-2',7'-dichlorodihydrofluorescein diacetate (CM -H_2DCFDA)

Non specfic markers of reative oxygen species include CM-H_2DCFDA, known by its chemical name as 2,7-dichlorodihydrofluorescein diacetate. Upon passive entry into the RGC, CM-H_2DCFDA undergoes deacetylation by non-specific cell esterases forming the product 2,7–dichlorodihydrofluorescein. Following reaction with certain intracellular reactive oxygen species (peroxyl, alkoxyl,, carbonate and hydroxyl radicals and peroxynitrite) it forms an intermediate radical and then finally the fluorescent product called 2, 7- dichlorofluorescein (*Le Bel et al 1992, Ischiropoulos et al 1999, Bilski et al 2002, Ohashi et al 2002, Wardman et al 2002, Myhre et al 2003*). This final product of oxidation has an excitation maximum of 488 nm and an emission maximum of 525 nm.

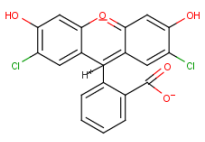

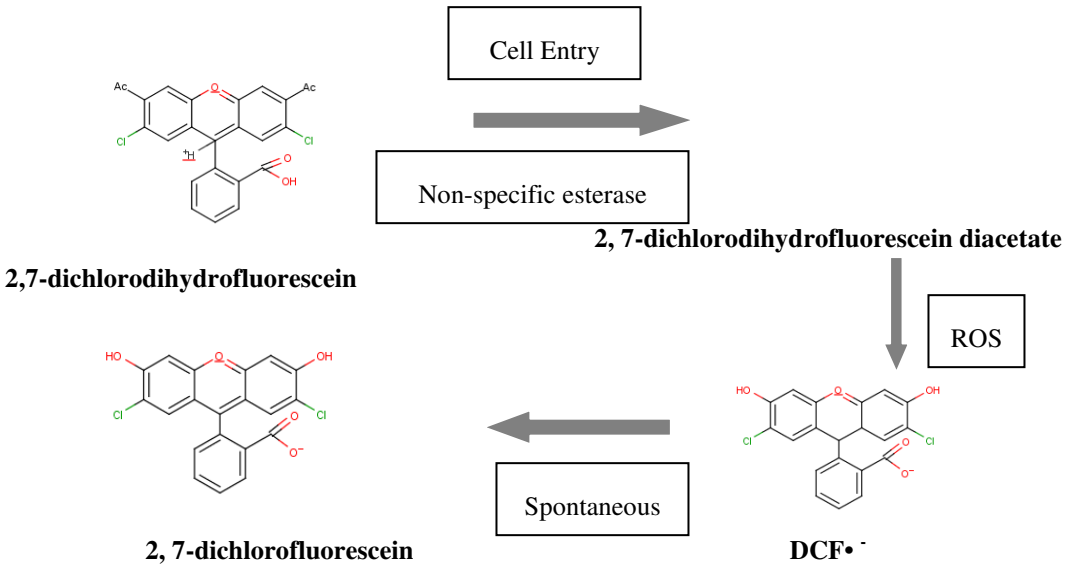

Figure 1.5 A showing the various products produced by 2, 7,-dichlorodihydrofluorescein.

CMH_2DCFDA has a very low reactivity towards some other reactive oxygen species such superoxide radicals or its dismutation product, hydrogen peroxide.

Superoxide anion

Dihydrorhodamine (RhH_2) forms fluorescent rhodamine in the presence of free $\cdot OH^-$ or $CO_3\cdot^-$ or $NO_2\cdot$ radicals, while similarly to $DCFH_2$ is unreactive with $O_2\cdot^-$ or H_2O_2 in the absence of catalyst (*Crow et al 1997, Wrona et al 2005*).

Dihydroethidium (also known as hydroethidine) can be used to analyze the presence of superoxide anion *(Fink et al 2004, Zhao et al 2003, Zhao et al 2005*). Although not specific, it is much more reactive than the dihydrofluoresceins or dihydrorhodamines. Dihydroethidium has an excitation and emission spectrum of 488 nm and 550 nm respectively. Once oxidized to ethidium, it can intercalate with the cells nuclear DNA to

form oxy-ethidium-DNA and undergo a shift in its excitation/absorption spectra. Although somewhat specific for the superoxide anion, dihydroethidium is readily oxidized and often gives a high background fluorescence (*Bruxer et al 1999, Zhao et al 2003*). It can also undergo a direct redox reaction with ferricytochrome c. It has been used to analyze respiratory burst in respiratory phagocytes as well as the generation of the superoxide anion in previous in-vitro studies using the RGC-5 cell line (*Lieven et al 2006*).

Figure 1.5 B Structures of ethidium bromide, dihydroethidium and related pathways of conversion to its byproducts are shown below.

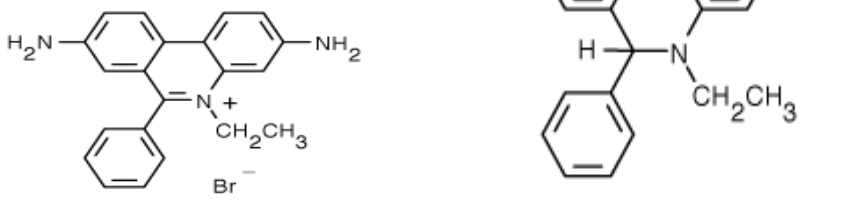

Ethidium Bromide ***Dihydroethidium***

Mitochondrial superoxide levels can be detected using MitoSOX Red mitochondrial superoxide indicator. This is a highly selective dye for the detection of superoxide in mitochondrial live cells. It is a live-cell permeant and is rapidly and selectively targeted to the mitochondria and once inside is oxidised and exhibits red fluorescence upon binding to nucleic acids (excitation/emission, 510/ 580 nm).

Lucigenin, bis-N-methylacridinium dinitrate has been widely studied as an indicator of superoxide anion production. Despite this there is little doubt that like CM-H_2DCFDA, it is

also capable of detecting superoxide anion. After the addition of superoxide to the free radical obtained on the reduction of lucigenin (LC·-), which forms an unstable product called dioxetane (*Faulkner et al 1993*). The dioxetane cleaves spontaneously to produce N-methylacridone in an excited state and it is this which emits light. Numerous nucleophiles and reducing agents can induce luminescence (*Maskiewicz et al 1978, Maskiewicz et al 1978*).

Hydrogen peroxide. Hydroperoxide, peroxyl radicals

The Amplex Red peroxide/peroxidase assay provides a one-step assay for detecting hydrogen peroxide or the activity of horseradish peroxidase by either measuring fluorescence with a fluorescence-based microplate reader or a fluorometer or by measuring absorption- based microplate reader or spectrophotometer. The Amplex Red peroxidase substrate can detect the presence of active peroxidases and the release of hydrogen peroxide produced as a product of enzyme-coupled reactions.

For the detection of peroxyl radicals an assay which utilizes BIODIPY dyes is available. This is based on the loss or shift of the dye's fluorescence as a result of its interaction with the peroxyl radicals and on the retention of the fluorescent signal in the presence of antioxidants that intercept these free radicals. The assay is suitable for a fluorescence microplate reader and radiometric measurements are made with either a fluorescence microplate reader or flow cytometer. Peroxyl radicals can also be detected in erythrocyte or red blood cell membranes using a water-soluble BIODIPY dye or BIODIPY FL hexadecanoic acid. This exhibits the red shift common to the fluorescence of lipophilic BIODIPY dyes when they are concentrated, permitting the radiometric measurement of hydroxyl radical production as well as allowing the onset of lipid peroxidation in live cells

to be measured.

Hydroxyl radicals

Hydroxyl radicals can be detected following reaction with spin traps. An example of this is proxyl fluorescamine. This contains a nitroxide moiety that effectively quenches its fluorescence. Once it traps a hydroxyl radical, its fluorescence is restored and the radicals electron spin resonance signal is destroyed, making these probes useful for detecting radicals either by fluorescence or by electron spin resonance spectroscopy.

Singlet oxygen species

Singlet oxygen sensor green reagent is highly selective for singlet oxygen and while simultaneously showing no appreciable response to other ROS. Prior to its reaction with singlet oxygen, it exhibits weak fluorescence with excitation peaks at 372 and 393 nm and emission peaks at 395 and 416 nm. In the presence of singlet oxygen, it emits a green fluorescence similar to that of fluorescein. It has a peak excitation spectra of 504nm and a peak emission spectra of 525 nm.

Trans -1- (2'-methoxyvinyl) pyrene can be used for the detection of picomolar quantities of singlet oxygen in chemical and biological systems. While this is highly selective for singlet oxygen species, this probe also has the advantage of not reacting with activated oxygen species such as hydroxyl radical, superoxide or hydrogen peroxide.

Nitric oxide

The nitric oxide radical is very unstable and is readily oxidized to the nitrosium cation (NO+) which is moderately stable in aqueous solutions but highly reactive with nucleophiles or other nitrogen oxides.

The most successful indicator for nitric oxide is 4, 5-diaminofluorescein diacetate (DAF-2 acetate) developed by Kojima (*Kojima et al 1998*). As with other fluorescein diacetates, DAF-2 diacetate is membrane permeant and is deacetylated by intracellular esterases to 4, 5-diaminofluorescein (DAF-2). DAF-2 remains nonfluorescent until it reacts with the nitrosonium cation produced by spontaneous oxidation of nitric oxide to form a fluorescent heterocycle which becomes trapped in the cells cytoplasm. DAF-2 has been used to identify individual nitric oxide-producing neurons in brain slices in both living plant cells and in mitochondria (*Brown et al 1999, Foissner et al 2000, López-Figueroa et al 2000*).

DAF-FM (4-amino-5-methylamino-2',7'-difluorofluorescein) and its diacetate derivative (DAF-FM diacetate) have significant utility for measuring nitic oxide production in living cells or solutions.

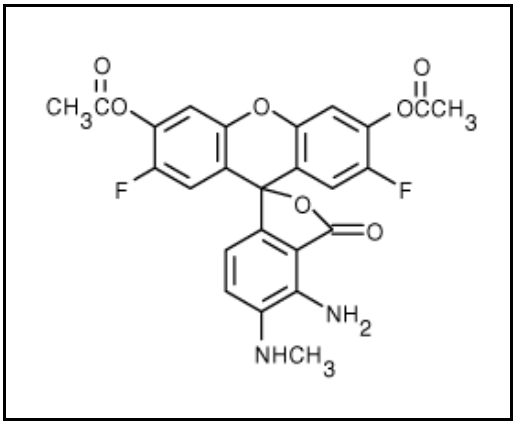

Figure DAF-FM

There are several other reagents available including anti-nitrotyrosine antibody capable of detecting nitrotyrosine. Nitrotyrosine is associated with a large number of diseases including Multiple sclerosis, Alzheimers disease, Parkinsons as well as being indicative of vascular and tissue injury from ischemia-reperfusion injury. There are several pathways suggested for the formation of tyrosine nitrotyrosine. Nitric oxide (NO) can interact rapidly with superoxide ($\cdot O2^-$) to form peroxynitrite ($OONO^-$) which is a potent oxidant of aromatic, aliphatic and sulfhydryl residues (*MacMillan-Crow et al 1996*). Heme peroxidases, such as myeloperoxidase and eosinophilperoxidase have been shown to utilize hydrogen peroxide (H_20_2) to oxidize nitrite ($NO2^-$) and catalyze tyrosine nitration (*Kilinc et al 2001*). Additionally other heme proteins such as hemoglobin and catalase may contribute to tyrosine nitration using NO as a substrate (*Grzelak et al 2001*). Tryptophan resides can also be oxidized by peroxynitrite (*Kato et al 1997*).

Peroxynitrate

There are a number of assays available for the detection of peroxynitrite including the probe hydroxyphenyl fluorescein developed by Nagano et al (*Nagano et al 2003*). Although this particular assay is not specific for peroxynitrite, it also detects hydroxyl and peroxynitrite radicals ($ONOO^-$), Under oxygen, ●NO is converted to No-derived nitrogen oxides (ONOO● and H_20_3).

1.6 Optical and technical aspects of the Heidelberg Confocal Scanning Laser Ophthalmoscope.

For our project, we sought to acquire live images of RGCs in adult Long-Evans rats. Because of the challenges of imaging such a small area with high resolution, we chose a confocal scanning laser ophthalmoscope, Heidelberg engineering. We will refer to this as cSLO in the following text which explains the rationale behind our choice of this apparatus. We chose this particular model as it had dual lasers.

According to recent studies, confocal scanning systems have at least 15 dB better signal-to-background ratio than any fundus camera based digital imaging system for imaging the retina (*Bellman et al 2005, O Connor et al 1999*). Indeed some studies even demonstrated the risk of misdiagnosis when a fundus camera image is used instead of a cSLO (*Flower et al 1999*).

The confocal scanning laser ophthalmoscope from Heidelberg engineering has three laser sources, namely the indocyanine green excitation diode laser (excitation wavelength of 785 nm, absorption spectra from 800-900 nm), infrared reflectance diode laser (excitation of 820 nm) and finally the solid state saphire laser (excitation at 488 nm and absorption spectra of 500 – 650 nm). This apparatus is already used in clinical ophthalmology for examining the retinal vasculature and structural features and abnormalities of the retina in humans. In our project the fact that there were a number of different lasers, each with unique excitative and emissive wavelengths means we could use different labeling dyes and examine their fluorescence simultaneously by simply changing the laser used to view the retina at that particular timepoint.

Resolution provided by the HRA2 is 5 μm/pixel resolution, while a fundus cameras produces 15 to 18 μm/pixel. The HRA2 produces 1536 X 1536 pixels with 30-degree field of view in high resolution mode or 768 X 768 in standard mode. There are three fields of view available on the HRA2 , namely 30 X 30 degrees, 20 X 20 degrees and 15 X 15 degrees.

The term 'confocal' means that the imaging system uses both a point source as well as a point detector, which have a common focal point. As a result of this, the scattered light does not fall on the detector. This improves signal/background ratio significantly. In addition to this, the use of a point source and a point detector somewhat simplifies the lens requirements as light travels along a principal ray. The ideal optical system should be *diffraction limited*, a goal that can be closer to realisation with in a confocal imager than a fundus camera system (*Barttsch DU et a 1994, Barttsch DU et al 1995*).

As we use a point source in the confocal imaging system, the retina must be therefore scanned horizontally and vertically in order to create a two-dimensional image. This is called a *flying-spot scanner*. Lasers are used as light souces as they produce a highly collimated beam that is easily scanned and produces a small spot on the retina.

The fact that the confocal retinal imaging system uses laser light sources also contributes to image quality because the highly collimated beam travels through the central, highest quality region of the optical system. The narrow plane of focus increases image quality and allows the photographer to select the optimal plane to view the pathology.

Confocal retinal imaging systems utilize laser light sources and this contributes to image quality because the highly collimated beam travels through the central, highest quality

region of the optical system. The narrow plane of focus increases the image quality. The broadband white Xenon flash tube used in fundus camera based systems, the narrow-band nature of laser illumination as more efficient in exciting the fluorescein and indocyanine green.

In addition to the above features, the HRA also has the ability to acquire images in the z – plane creating a 3-dimensional view of retinal ganglion cells to a depth of 8 mm using serial slices in the z-plane. Potentially this could enable us to detect fluorescence present at a deeper level of the retina, not present on the surface. Confocal scanning laser microscopy has a range of existing and potential clinical applications varying from quantitative asssessment of optic disc size in conditions such as papilledema (optic disc swelling) and serial assessments of optic disc in glaucoma *(Mulholland et al 1998, Chen et al 2007, Greenfield et al 2008, Lin et al 2007, Weinreb et al 2004).*

1.7 Applications of the heidelberg confocal scanning laser ophthalmoscope to live *in vivo* imaging

From its initial conception over the last 25 years, the ability to image cells in a time-lapse or even in a real-time fashion using fluorescent probes has permitted a greater understanding of the dynamics of cellular processes *(Lichtman et al 2003, Lichtman et al 2001, Kortuem et al 2000, Wigston et al 1990, Herrera et al 1990, Lichtmamn et al 1987).* Recent studies have demonstrated that the confocal scanning ophthalmoscope (cSLO) can be utilised for real-time in vivo imaging of RGCs in adult rats. Using the prototype Zeiss confocal laser scanning ophthalmoscope (cLSO), the pioneering studies by Cordeiro et al demonstrated apoptosis could indeed be imaged live in rats and used immunohistochemical identifcation of apoptotic cells in the retinas subsequently to confirm this *(Cordeiro et al 2004).* In her methodology she labeled RGCs undergoing apoptosis using intravitreal injections of Alexa Fluor 488-labeled annexin 5. This is a protein which has a strong affinity for phosphatidylserine when in the presence of Ca^{2+}. Phosphatidyl serine is an anionic phospholipid that is enriched in the inner leaflet of plasma membranes. In the early stages of apoptosis, Annexin 5 is externalised from the inner to the outer cell membrane, before DNA fragmentation and nuclear condensation occur. Previous studies have confirmed its ability to act as a marker for apoptosis both in vivo and in vitro *(Hendrikus H et al, Laxman et al 2002, Zhou et al 2008).* As the excitation and emission wavelengths of Alexa Fluor (excitation maximum 495 nm, emission maximum 519 nm) coincide with the respective excitation and emision wavelengths of the laser on the HRA2 (excites at 488 nm , emission peak 500– 650 nm), it is possible to directly image the apoptotic cells which

fluoresce when excited by the diode laser. However the process of cell labeling is not without its difficulties. Potential drawbacks of this labeling technique include its invasivesness and also the risk of damaging the RGC body or axons during the labeling process.

Higashide et al also demonstrated the successful retrograde labeling technique using DiA and imaging using the solid state saphire laser (excitation at 488 nm and absorption spectra of 500 – 650 nm) to excite the unique spectra of DiA (Max excite 450 nm, Max Emit 600 nm) *(Higashide et al 2006).* Furthermore more recent studies demonstrated the ability of the cSLO to image dendrite and axonal detail in RGCs of the macque monkey *(Gray et al 2008).*

Other studies have opened the window further on the massive potential of live *in vivo* imaging using the HRA2. This repertoire includes the observation of apoptosis *in vivo* following insults such as laser burns induced by the Neodymium-Yttium Aluminium Garnet (YAG) laser *(Schmitz-Valckenberg 2008)* and correlation of laser induced burns In another more recent paper Eter et al used CX3CR1GFP/+ knockin mice, in which macrophages, dendritic cells and microglia cells are constitutively fluorescent and then examined the distribution of these cells following argon laser treatment to the retina *(Eter et al 2008).* With further technical development, this technique has a myriad of potential applications in the human model including the monitoring of inflammatory responses to various treatments, adjusting treatments and titrating based on response. Apoptosis has also been observed in vivo following intravitreal injections of the apoptosis-inducing agent staurosporine *(Maass et al 2008).* More recent novel applications of the potential imaging capacity of the HRA2 have focused on a less invasive technique involving modification of

the cSLO. This was done by incorporating a laser to image cyan fluorescent protein (excitation 460 nm, 490 nm detection filter) in transgenic mice *(Feng et al 2000)* in which the Thy-1 promoter sequences drive the expression of the enhanced cyan fluorescent protein, designated Thy1-CFP *(Feng et al 2000)*. Superior colliculus labeling and subsequent imaging of RGCs using the HRA2 was also performed with DiI (Max excitation 553 nm, Max emission 570 nm) *(Leung CK et al 2008)*. Retinal flat mounts were once again used as a confirmatory test. Other recent studies have used similar transgenic mice but with upregulated yellow fluorescent protein and imaged in a similar fashion using the confocal laser scanning ophthalmoscope and the argon laser incorporated into the system (Max excitation 514 nm, 530-600 nm band pass filter) *(Walsh et al 2008)*.

Examination of the retinal nerve fiber layer can also be a good measure of the severity and distribution of RGC death and in another recent paper from Japan *(Kawaguchi et al 2006)* it was shown to be possible to quantitatively measure RNFL thickness and note the progressive decrease over a four week period following optic nerve crush.

1.8 Presence of oxidative stress in retinal disease

Retinal ganglion cells undergo apoptosis after axonal injury. There are many retinal diseases such as retinal artery occlusion and retinal vein occlusion which involve a compromise in the circulation to the retina with resultant production of oxidative species and death of retinal ganglion cells. The optic neuropathies include glaucoma, traumatic optic neuropathy have also been proposed to involve a similar mechanism.

Several other retinal diseases are proposed to involve the induction of oxidative stress using

the amino acid glutamate. These include glaucoma, diabetic retinopathy and various forms of retinal ischemia (*Osborne et al 1999*). Glutamate has been implicated in retinal ganglion cell death after acute insult and although it is present in synaptic nerve terminals in millmolar concentrations, the extracellular concentrations are normally high only during short periods of synaptic transmission. However certain forms of injury result in extended periods of elevated extracellular glutamate levels. High levels of extracellular glutamate have been shown to be toxic to nerve cells via two distinct processes. The first of these is known as excitotoxicity, which occurs through the activation of ionotropic glutamate receptors (*Rothman et al 1985, Rothman et al 1986).* The second process involves a programmed cell death pathway called oxidative glutamate toxicity or oxytosis and is mediated by a series of disturbances to the intracellular redox system (*Tan et al 2001, Murphy et al 1989*).

After axotomy there are several proposed mechanisms for death in the apoptotic cascade. Reactive oxygen species play important roles in gene expression and intracellular signaling and are made primarily during the production of mitochondrial energy. However high levels of ROS play important roles in the signaling of cell death in several neuronal systems including RGCs. Conversely studies which have demonstrated that with ROS scavengers, small reductions in cellular redox state and hypoxic conditions all contribute to the survival of RGCS after axotomy. Studies have demonstrated that axotomy of retinal ganglion cells leads to an increased production of superoxide anion in the hours following the injury (*Levin et al 2006*). Interestingly in sympathetic neurons, scavenging of superoxide anion has been shown to slow apoptosis after nerve growth factor deprivation.

Other oxidants in retinal disease such as the sulfhydryl radical have been shown to have an

important effect on RGC survival. The sulfhydryl reductant TCEP (tris(2-carboxyethyl) phosphine (TCEP) can protect RGCs in the optic nerve crush model and therefore increase RGC survival (*Swanson et al 2005*).

The peroxide radical, another molecule involved in retinal ganglion cell death. Inhibition of lipid peroxidation with tirilazad mesylate blocks RGC death in a culture model simulating axotomy (*Levin et al 1996*).

Retinitis pigmentosa (RP) refers to a heterogeneous group of inherited human diseases that cause primary degeneration of rod and cone photoreceptors. The Royal College of Surgeons (RCS) rat is a commonly used animal model of photoreceptor degeneration of relevance to RP (*Deshpande et al., 1992; LaVail, 1981*). There are several lines of evidence implying a role for oxygen in the RCS rat model of retinal degeneration. Manipulation of environmental oxygen conditions at key stages in the dystrophic RCS rat has reportedly been able to modulate the rate of photoreceptor cell death (*Maslim et al., 1997; Valter et al., 1998; Stone et al., 1999*).

Oxidative stress plays an important role in diabetic complications (*Baynes et al 1991, Kiwluru et al 1991, Kowluru et al 2001, Kowluru et al 2003, Feldmen et al 2003, Brownlee et al 2005, Caldwell et al 2005*) and reactive oxygen species (ROS) are considered a causal link between elevated glucose and metabolic abnormalities important in the development of diabetic complications. Retina and capillary cells experience increased oxidative damage in the diabetic milieu, and the antioxidant defense mechanism is impaired (*Kiwluru et al 1991, Kowluru et al 2001, Kowluru et al 2003, Caldwell et al 2005, Kanwar et al 2007*). Administration of antioxidants to diabetic rats protects the retina from oxidative damage

and also from the development of retinopathy. Furthermore, retinal mitochondria become dysfunctional and start to leak cytochrome *c* into the cytosol, and superoxide levels are elevated (*Kowluru et al 2003*).

Overexpression of the enzyme responsible for scavenging mitochondrial superoxide (MnSOD) prevents these diabetes-induced mitochondrial alterations and histopathology characteristic of diabetic retinopathy (*Kanwar et al 2007, Kowluru et al 2007*), thus suggesting a major role for mitochondrial superoxide in the development of diabetic retinopathy.

MMP-2 (Matriz Metalloproteinase 2) has been proposed to result in the apoptosis of retinal capillary cells (Renu et al 2009). The mechanism by which this occurs is not clear but could include damage to the mitochondria resulting in leakage of cytochrome *c* and activation of apoptosis. Studies have shown that the activation of MMP-2 cleaves the nuclear poly(ADP ribose) polymerase (PARP), which induces apoptosis via a mitochondrial pathway releasing apoptosis-inducing factor from the mitochondria *(Kwan et al 2004).* In the development of diabetic retinopathy, mitochondrial dysfunction and PARP activation are considered important in the accelerated apoptosis of retinal capillary cells (*Kowluru et al 2003, Kanwar et al 2007, Kowluru et al 2006, Kwan et al 2004),* thus further supporting the role of MMP-2 in the apoptosis of capillary cells.

Oxidative stress is believed to contribute to the pathogenesis of many diseases, including age-related macular degeneration (AMD). Although the vision loss of AMD results from

photoreceptor damage in the central retina, the initial pathogenesis involves degeneration of RPE cells. Evidence from a variety of studies suggests that RPE cells are susceptible to oxidative damage. Mitochondrial DNA (mtDNA) is particularly prone to oxidative damage compared to nuclear DNA (nDNA). Using the quantitative PCR assay, a powerful tool to measure oxidative DNA damage and repair, we have shown that human RPE cells treated with H(2)O(2) or rod outer segments resulted in preferential damage to mtDNA, but not nDNA; and damaged mtDNA is not efficiently repaired, leading to compromised mitochondrial redox function as indicated by the MTT assay. Thus, the susceptibility of mtDNA to oxidative damage in human RPE cells, together with the age-related decrease of cellular anti-oxidant system, provides the rationale for a mitochondria-based model of AMD.

1.9 Biochemical assays in the past to demonstrate the presence of oxygen species in retinal disease.

There have been numerous methods in previous papers which have attempted to image reactive oxygen species (ROS) however these have primarily involved the *in vitro* or *ex vivo* models.

One such assay which was used to image reactive oxygen species was H_2DCF-dA. This is a non-fluorescent compound which accumulates within cells upon deacetylation. H_2DCF then reacts with ROS to form fluorescent dichlorofluorescein (DCF). This has been used to demonstrate the accumulation of ROS in the Retinal Ganglion Cell- 5 line (RGC-5) in studies which have utilized various inducers of oxidative stress including hydrogen

peroxide and tert-butyl peroxide (t-BOOH) (*Maher et al 2004*). This study also demonstrated that ROS are produced endogenously by mitochondria using the same reagent to image ROS.

Other oxidative species which have been examined include lipoxidation products such as 4-Hydroxy-2-nonenal (HNE) adducts (*Liu et al 2003, Sayre et al 1997, Uchida et al 2003*) and the expression of heme oxygenase-1 (HO-1), a common oxidative stress-induced protein (*Elbirt et al 1999, Schipper et al 2004, Smith et al 1994*). In one study (*Liu et al 2007*) the RGC-5 cell line was again used with western blotting used as the technique to ascertain the total amount of HNE protein adducts formed, the calcein AM live/Dead viability assay was used to calculate cell survival. In this assay, polyanionic calcein is retained within live cells producing an intense uniform green fluorescence (excitation/emission, 495/515 nm). Ethidium homodimer which normally is excluded, enters cells with damaged membranes and undergoes a 40-fold enhancement of fluorescence on binding to nucleic acids (excitation/emission 495/635 nm). Cell number and viability was also measured in the RGC-5 cells using 3-(4, 5-dimethylthiazol-2yl)-2, 5-diphenyl tetrazolium bromide (MTT).

Finally RGC superoxide levels in situ have also used HEt (*Lieven et al 2006*). As decribed later in this work, HEt exhibits weak fluorescence and is oxidized by the superoxide anion to ethidium (excitation 480 nm, emission 586 nm). HEt enters the cell and after oxidation accumulates in the nucleus where it binds DNA and thereby undergoes a small shift in its emission spectrum to 567 nm. In this study RGC cells from Long-Evans rats were used (ex vivo model) and the RGCs were then identified in mixed retinal cultures using DAPI (excitation 330 nm, dichroic 400 nm, emission 450 nm).

Previous models have incorporated a model in which excitatory amino acids are injected intravitreally (NMDA, kinate, AMPA) to induce RGC damage. (*Vorwek et al 1996*). Intravitreal injection of NMDA led to the appearance of internucleosomal fragmentation of retinal DNA and of terminal transferase dUTP nick end labeling (TUNEL) positive nuclei in the inner retina. Ultrastructural features consistent with classis apoptotic changes were noted in degenerating cels in the RGC layer and the inner nuclear layer. Control retinas given vehicle or NMDA plus the glutamate receptor antagonist MK-80 1 did not show these changes. In this model simultaneous administration of NMDA and a caspase inhibitor also abolished or attenuated the loss of RGC in the retina. Therefore NMDA- induced excitotoxicity involoved apoptosis and caspases in their phometric analysis of retinal damage in NMDA- injected eyes also showed that BDNF, nipradiol, MK-801 or eliprodil could protect inner retinal cells. In other studies measurements of intravitreal glutamate levels indicated an increase in this excitatory amino acid in the vitreous after NMDA injection (*Kapin et al 1999, Kido et al 2000, Mizuno et al 2001, Morizane et al 1997*).

Chapter 2 Aims and hypothesis

Hypothesis

Reactive oxygen species not only are generated as a result of cellular injury, but also serve as signaling molecules for a variety of critical processes, including mitosis and cell death. We previously reported that injury to RGC axons induces a burst of superoxide within the cell body, probably of mitochondrial origin (*Lieven et al, 2006*). We now propose to describe a method for imaging of reactive oxygen species within the retina of the living animal using a confocal scanning laser ophthalmoscope called the Heidelberg Retina Angiograph 2 (HRA2) equipped with dual lasers.

Aims

We sought to examine whether we could detect ROS in RGCs in the live animals, by using chemical inducers. Our second aim was to determine whether crushing of the optic nerve could induce ROS.

As already outlined in the previous chapter, the majority of studies which examined oxidative stress in retinal ganglion cells have used either the in-vitro model (eg RGC-5 cell line) or the ex vivo model (*Liu et al 2007, Swanson et al 2005*). In our study we attempted to examine oxidative stress and retinal ganglion cells but take this one step further into the in vivo model and actually image oxidative species in real time in the live model. Although the monkey model is the closest experimental one to the human, it remains difficult in terms of economics, animal numbers and the animal housing space required for such a

study. For this reason the rat model was choosen.

The decision regarding the type of anesthezia to use took experimental times, preservation of corneal clarity as well as animal comfort into consideration. Initially consideration was given to intraperitoneal xylocaine and ketamine, however given the invasiveness as well as the duration of the surgery, deep anesthesia using inhaled isofluorane was used. This allowed better control of level of anesthesia and duration of the experiment.

In order to confirm the filters on the HRA2 were functional we performed a fluorescein angiogram in which fluorescein dye was injected intravenously into the rat and images were taken of the retina at time intervals. Fluorescein was used as the excitation/emission spectrum was the same as one of the lasers on the HRA2.

In order to correctly label the retinal ganglion cells, gelfoam soaked in the fluorescent dye (ICG) was placed adjacent to the superior colliculus (SC) so that the dye would permeate the SC and therefore travel retrogradely with the retrograde transport system in retinal ganglion cell nerve axons along the pathway already described in the introductary chapter and finally end in the retinal ganglion cell body in the retina. Again various retinal ganglion cell markers were given consideration, however because the excitation/emission specta parameters were of prime consideration, there were only a small number of markers which qualified for inclusion. In addition to this, consideration was given to the fact that another dye used to mark oxidative species would be used and therefore the excitation/emission spectra for this agent needed to be different and coincide with the second laser on the HRA2.

Corneal clarity and image optimisation were also considered in the planning stages for the study and various methods including balanced salt solution, 0.9% sodium chloride as well as saran wrap covering on the cornea were given consideration. In addition we also injected the diluents (0.9% sodium chloride) intravitreally alone and in combination in order to determine if they affected the clarity/fluorescence.

In order to induce oxidative stress various methods were used. This was done in order to verify if some of the compounds known to induce oxidative stress in the in-vitro and ex vivo models were also able to induce it in the in vivo model. Intravenous injections were considered as a delivery technique, however it was difficult to calculate the dose delivered to the retinal ganglion cells when administered systemically. In addition the systemic side effects of many of these compounds had not been investigated and using systemic methods of delivery risked introducing bias into the study. Intravitreal injection was an effective method of delivery in terms of its efficacy and ones ability to accurately calculate its concentration. It can be injected into the space directly adjacent to retinal ganglion cells and permeated them directly which added to its attractiveness as a method of delivery. Menadione (*Nguyen et al 2003*) has been used in ex vivo studies to generate intracellular superoxide anion by redox cycling by the addition of 1 mM to the cultures. Therefore it was appropriate to use a similar intravitreal concentration in this study and doses were calculated based on this.

HEt was used as this had already been used as a marker of oxidative radicals, it fluoresces at a different spectrum when oxidized and additionally the excitation/emission spectrum

matched those on the HRA2.

In order to induce oxidative stress on the optic nerve, optic nerve crush was performed using the already standard protocol (*Morrison et al 1997, Yoles et al 1997*). Currently there are no other models available in the literature

List of experiments which will be used to achieve our aims

Imaging of the retinal nerve fiber layer

4.1 Imaging of the retinal nerve fiber layer using the infra-red and red-free filters.

4.2 Imaging the retinal nerve fiber layer and determining the best method of preserving corneal clarity

4.3 Imaging the retinal nerve fiber layer following optic nerve transection

4.4 Examining the effect of intravitreal injection of 0.9% sodium chloride

HRA2 detection of fluorescent species

4.5 Quantifying the fluorescence of ICG, dihydroethidium and its derivatives using the HRA2

4.6A Detecting retinal ganglion cells using ICG

4.7 Examination of fluorescence pattern following injection of ICG into the optic nerve

4.8 Examination of fluorescence following injecting the optic nerve with DiO

4.9 Examination of fluorescence following intravenous injection of fluorescein

Markers of oxidative species : HEt

4.10 A Examination for background fluorescence of HEt in the absence of oxidative factors in the in vivo model and determining the optimum concentration

4.10 B Demonstrating that HEt does not react with hydrogen peroxide

4.10 C Examination of the fluorescence patten following intravenous injection of ethidium bromide

4.11 Examination of fluorescence pattern following intravitreal injection of menadione and intravenous injection

4.12A Examination of fluorescence patterns of a mixture of Menadione and HEt when both are injected intravitreally

4.12B Examination of fluorescence pattern following intravitreal injection of menadione and intravenous injection of HEt

4.13 Examination of fluorescence pattern following the injection of ferrous sulfate and dihydroethidium intravitreally

Markers of oxidative species : DCFDA

4.14A Determination of optimal intravitreal concentration of DCFDA

4.14B Fluorescence pattern following injection of DCFDA (intravenously) and hydrogen peroxide (intravitreally).

4.14C Demonstrate that DCFDA and hydrogen peroxide do not react when injected intravitreally

4.14D Examination of fluorescence following DCFDA intravenously and Menadione intravitreally.

Retinal ganglion cells after crush

4.15 Examining the effect of optic nerve crush on retinal ganglion cells labelled with ICG

4.16 Imaging superoxide following optic nerve crush using CMH_2DCFDA

4.17 Labeling retinal ganglion cells with ICG and using DCFDA to examine for reactive oxygen species following optic nerve crush.

Chapter 3 Materials and Methods

In the next few paragraphs the principles and rationale behind the procedures are explained and following this the steps in performing the specific experiments are detailed. The annotation of the experimental methods in this chapter correspond to the same ones in the next chapter with the results (eg experiment 3.10A corresponds to 4.10A).

Anesthesia

Optimizing animal comfort and minimizing pain during experiments was an important part of this study.

Anesthesia is administered at prescribed concentrations (see table 4.1 for dose). Check animal is asleep (response to pain, tail manipulation etc). Rodents are observed for signs of distress in the perioperative period (poor grooming, decreased appetite etc as outlined in standard animal handling protocols) and additional doses of analgesia and anesthetic will be administered as required. The choice between inhalational anesthesia (isofluorane) versus intraperitoneal injections (ketamine and xylocaine) was based on optimizing animal comfort whilst staying within the time constraints of the surgery. Some procedures took longer (eg superior colliculus labeling), particularly initially as there was a learning curve and therefore required the use of inhalational anesthesia. Both methods of anesthesia resulted in loss of corneal blink reflex during the procedure and therefore labrilube was place on the animals cornea at the start of each procedure in order to minimize this.

Figure 3.1 A

Fluorescein angiography

As already outlined in the previous chapter, fluorescein angiography is performed to verify that one of the HRA2 laser functions (excitation 488 nm/ emission 500-650 nm).

Fluorescein is made up at a concentration of 25g in 10 ml diluting medium. Place the anethetized Long-Evans rat (using standard protocol mentioned above already and mantaining corneal hydration as above) on the viewing platform of the HRA2.

The tail is warmed for about 10-15 minutes before starting using the infra-red heat lamp on with the animals in the cage for about 10-15 minutes. This causes vasodilatation and therefore facilitates visualization of the tail veins. Once the tail is warmed place the rat on the HRA2 platform ready to be imaged. A piece of cotton gauze is used to remove the scales from the tail by holding the tip of the tail and scraping the tail with the gauze in a direction towards the rats head. Again this process makes visualization of the tail veins easier. The tip of the tail is examined for a vein ideally (in adult rats) at about 3 cm from the end in the lateral position is optimal. The closer you go to the thicker part of the tail, the

more muscle so it gets more difficult, despite the fact that the veins are larger.

Work towards the head of the rat, making as few venepunctures a possible to avoid collapsing the venous system as all the veins are interconected. A butterfly needle of 30G is used with a 1 ml syringe attached to the butterfly, ideally with the syringe barrel fixed in a clamp so that there is no movement when you insert the needle. The area to be injected is cleaned with an alcohol swab to reduce infection. The needle is inserted in a parallel direction to the tail vein with the tip of the needle pointing towards the head of the rat. When a flashback is seen in the needle, try to avoid drawing the plunger as the vein may collapse. Once the flash is seen, inject material slowly.

Wait about 1 second after injecting before removing the needle to avoid the injected solution leaking out. After the needle is removed, a small amount of pressure is put on the tail with a gauze to prevent leakage. Imaging is done using the fluorescein filter at serial intervals of approximately 30 seconds.

Retrograde labeling of retinal ganglion cells with fluorescent markers

Inhalational anesthesia is set at oxygen flow rate of 2.5 L/minute, isofluorane of 5% for approximately 5 minutes until the animal is anesthetized in an anesthesia closed chamber.

The animal is fixed in the holding device. The animal is checked for depth of anesthesia Check animal is asleep (response to pain, tail manipulation etc). Lacrilube is placed in both corneas in order to maintain corneal hydration. The head area is shaved with an electric razor. Chlorhexidine is used to clean the area surrounding the planned incision.

Figure 3.1 A

A longitudinal incision is made in the centre of the head going from an imaginary line connecting both eyes to behind the midpoint of the ears. Skin retractors are placed and secured using tape. The fascia is cut and removed until the bony surface is exposed and suture lines are clearly delineated. See diagrams below for anatomical details.

Cotton wool is soaked in sterile saline to control bleeding. The bony surface is immersed in saline for a few minutes if necessary to control hemorrhage.

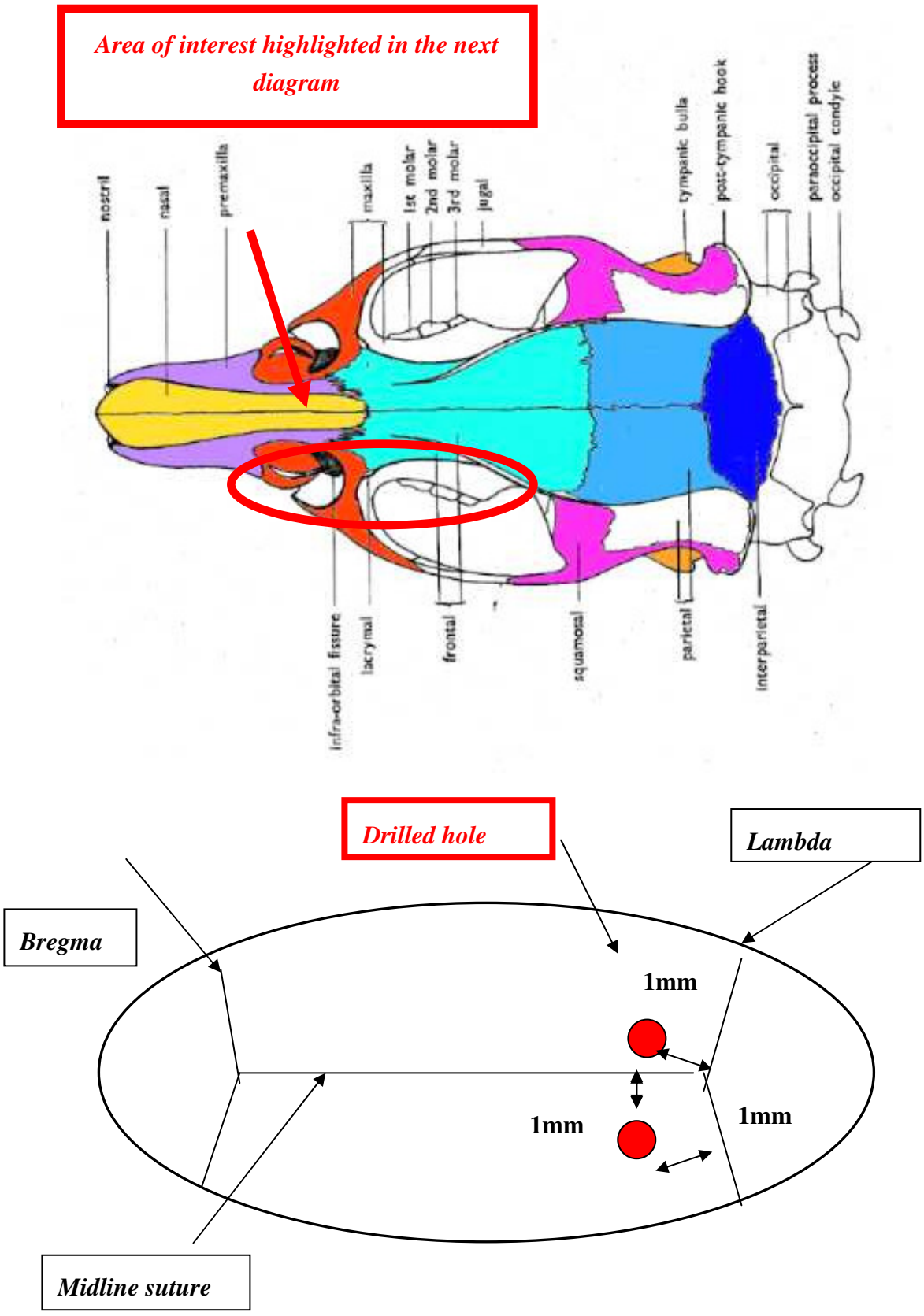

Figure 3.1 C Diagram showing markings and areas of interest on rat skull.

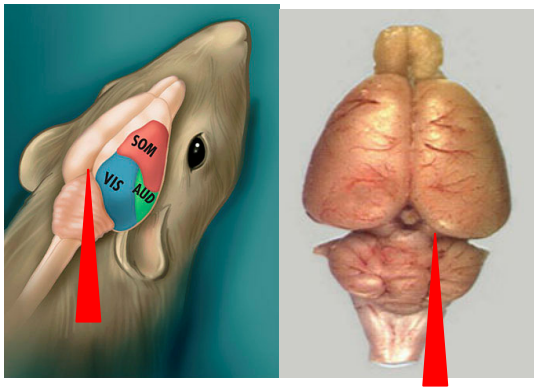

Figure 3.1 D Diagram showing markings and areas of interest on rat for superior colliculus labeling with superior colliculus highlighted with red arrow.

The area where the holes will be drilled is marked with marker pen. Two holes are drilled in the skull using anatomical markers to locate exact site. The hole is 1 mm from lambda suture and 1 mm from midline suture and approximately 3mm in diameter, although this will vary slightly depending on the age of the rat. Bleeding is controlled using normal saline. Dissect to the level of superior colliculus using gentle suction with a 20G needle White matter is encountered, then grey matter and then CSF. Caution is exercised at this point to avoid aspirating the superior colliculus. It appears as a yellow vascular structure amongst the adjacent grey matter. Cotton wool is soaked in normal saline to control hemorrhage. The superior colliculus is punctured gently with tip of a 25G needle. Hemorrhage is controlled using cotton soaked in saline. Gelfoam (dimensions 2 mm x 2 mm x 2 mm) soaked in desired dye is inserted into the area around the superior colliculus. Skin is closed using 5-0 vicryl. Polysporin is applied to the skin. Lacrilube is applied to both eyes again. Buphenorphine sc (see table 4.1A for dose) is given for analgesia. The rat is removed from the anesthetic apparatus and placed in the transportation cage. The rat is placed on a clean cotton napkin in the cage with rat food on the napkin beside it. This

minimizes the chances of contaminating its wound and eyes with sawdust and dust as it wakes up. The water bottle is filled. Mark the cage with the experiment details.

Intravitreal injections

Anesthetize the rat using intraperitoneal lidocaine and xylocaine as already outlined above. Inject 4 microliters of normal saline into right eye. Make an incision in lateral aspect of the conjuctiva of the right eye. Use the surgical limbus as your landmark and insert the hamilton 32 gauge syringe needle just posterior to this and inject 4 microliters of normal saline into the vitreal compartment of the eye. Following injection examine the fundus using the direct ophthalmoscope to ensure there is no damage to the retina of the animal. Left eye will be the control. Maintain corneal hydration using 0.9% sodium chloride topical drops applied to the cornea. Place the anethetized Long-Evans rat (using standard protocol mentioned above already and mantaining corneal hydration as above) on the viewing platform of the HRA2 and image at intervals.

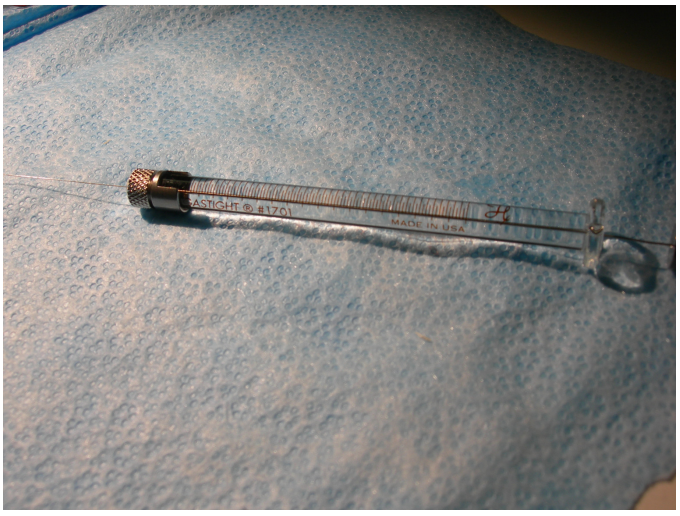

Figure 3.1 E Diagram showing Hamilton syringe

Intravenous tail injections

We performed intravenous delivery of some fluorescent agents in order to find the optimal method for administering these substances.

Place the anethetized Long-Evans rat (using standard protocol mentioned above already and mantaining corneal hydration as above) on the viewing platform of the HRA2.

The tail is warmed for about 10-15 minutes before starting using the infra-red heat lamp on with the animals in the cage for about 10-15 mins. The tail veins are seen more prominently towards the end of the 15 minutes. Once the tail is warmed place the rat on the HRA2 platform ready to be imaged. A piece of cotton gauze is used to remove the scales from the tail by holding the tip of the tail and scraping the tail with the gauze in a direction towards the rats head. This makes visualization of the tail veins easier.

The tip of the tail is examined for a vein ideally (in adult rats) at about 3 cm from the end in the lateral position is optimal. The closer you go to the thicker part of the tail, the more muscle so it gets more difficult, despite the fact that the veins are larger. Work towards the head of the rat, making as few venepunctures a possible to avoid collapsing the venous system. A butterfly needle of 30G is used with a 1 ml syringe attached to the butterfly, ideally with the syringe barrel fixed in a clamp so that there is no movement when you insert the needle. The area to be injected is cleaned with an alcohol swab to reduce infection. The needle is inserted in a parallel direction to the tail vein with the tip of the needle pointing towards the head of the rat. When a flashback is seen in the needle, try to avoid drawing the plunger as the vein may collapse. Once the flash is seen, inject material slowly. Wait about 1 second after you inject before removing the needle to avoid the injected solution leaking out. After the needle is removed, a small amount of pressure is put

on the tail with a gauze to prevent leakage. Imaging is done using the fluorescein filter at serial intervals of approximately 30 seconds.

Imaging the retina

Anesthetize the rat (see figure 3.1 A). Check animal is asleep (response to pain, tail manipulation etc). Rodents will be observed for signs of distress in the perioperative period (poor grooming, decreased appetite etc as outlined in standard animal handling protocols) and additional doses of analgesia and anesthetic will be administered as required. Animal is placed on the viewing platform on the HRA2. Cornea is frequently lubricated with balanced salt solution to maintain corneal clarity.

Optic Nerve Crush

As already outlined in the preceding chapters, optic nerve crush has been previously demonstrated to induce the production of oxidative species in the *in vivo* model.

Anesthetize the rat (see figure 3.1 A). Check animal is asleep (response to pain, tail manipulation etc). Rodents will be observed for signs of distress in the perioperative period (poor grooming, decreased appetite etc as outlined in standard animal handling protocols) and additional doses of analgesia and anesthetic will be administered as required.

Figure 3.1 A

Put lacrilube ointment in both of the rats eyes to maintain corneal hydration. Shave the lateral side of the right temporal area with electric razor to minimize contamination from animal hairs. Use chlorhexidine to clean the area surrounding the planned incision. The lateral canthus is clamped with a fine hemostat for 5 seconds and then incised. A lateral conjunctival incision is made using a microscissors (Fine Surgical Tools, Vancouver Canada) and using blunt dissection the lateral aspect of the orbit is exposed until finally the retrobulbar portion of the optic nerve is visualized.

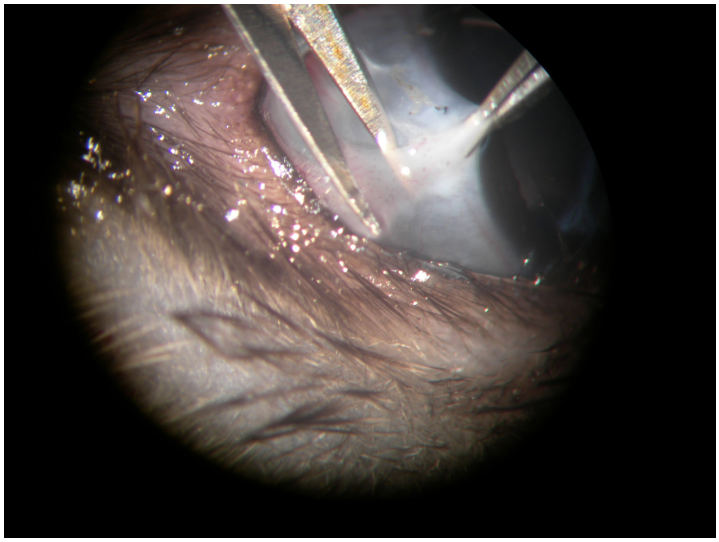

Figure 3.1 F

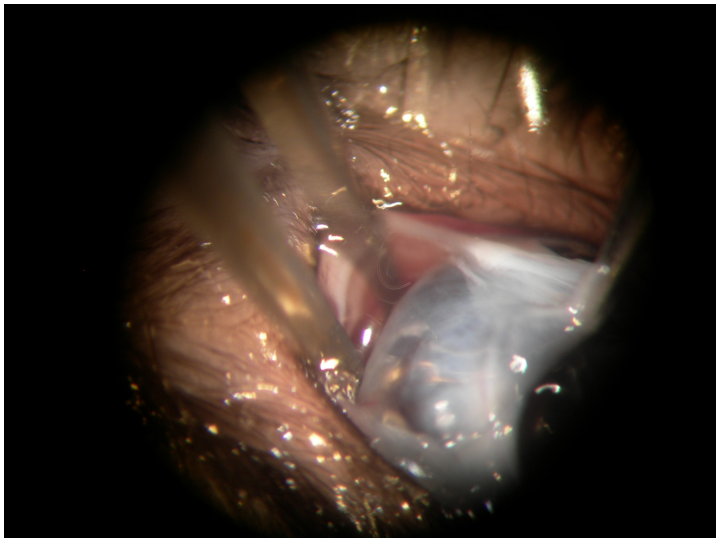

Figure 3.1G

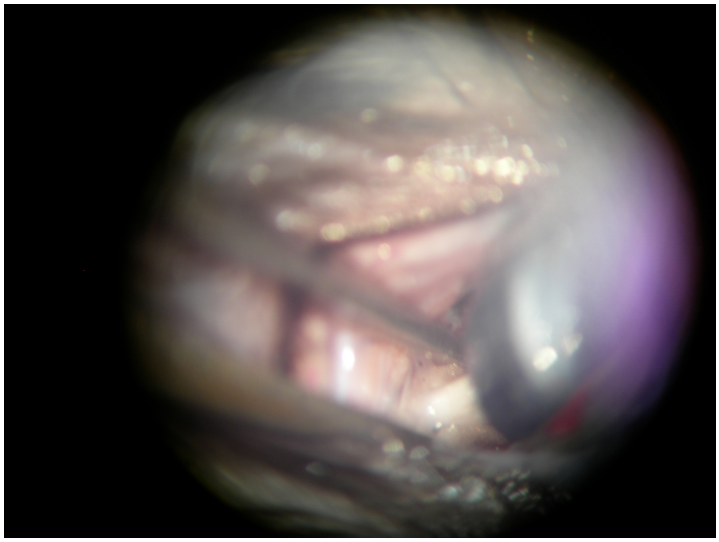

Figure 3.1H

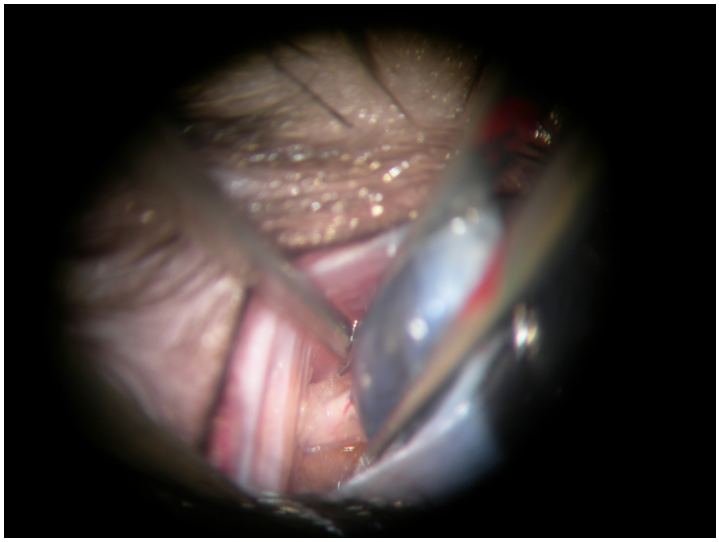

Figure 3.1 I

Using the fine noserrated forceps (Fine surgical Tools, Vancouver, Canada), the optic nerve is crushed for 5 seconds at approximately 3 mm posterior to the globe.

The wound is closed with 5-0 vicryl sutures and bacitracin applied to reduce chances of infection. Animals are observed until recovered from anesthesia. The contralateral optic nerve in each rat serves as a control for each rat and therefore is not operated on.

Optic nerve transection

As already outlined in the preceding chapters, optic nerve transection has been previously demonstrated to induce the production of oxidative species in the *in vivo* model.

Anesthetize the rat (see figure 3.1 A). Check animal is asleep (response to pain, tail manipulation etc). Rodents will be observed for signs of distress in the perioperative period (poor grooming, decreased appetite etc as outlined in standard animal handling protocols) and additional doses of analgesia and anesthetic will be administered as required.

Figure 3.1 A

Put lacrilube ointment in both of the rats eyes to maintain corneal hydration. Shave the lateral side of the right temporal area with electric razor to minimize contamination from animal hairs. Use chlorhexidine to clean the area surrounding the planned incision.

The lateral canthus is clamped with a fine hemostat for 5 seconds and then incised. 9. A lateral conjunctival incision is made using a microscissors (Fine Surgical Tools, Vancouver Canada) and using blunt dissection the lateral aspect of the orbit is exposed until finally the

retrobulbar portion of the optic nerve is visualized.

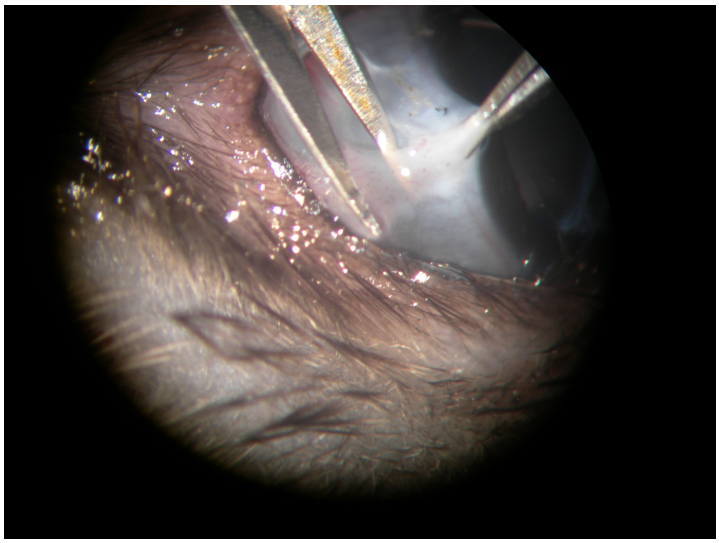

Figure 3.1F

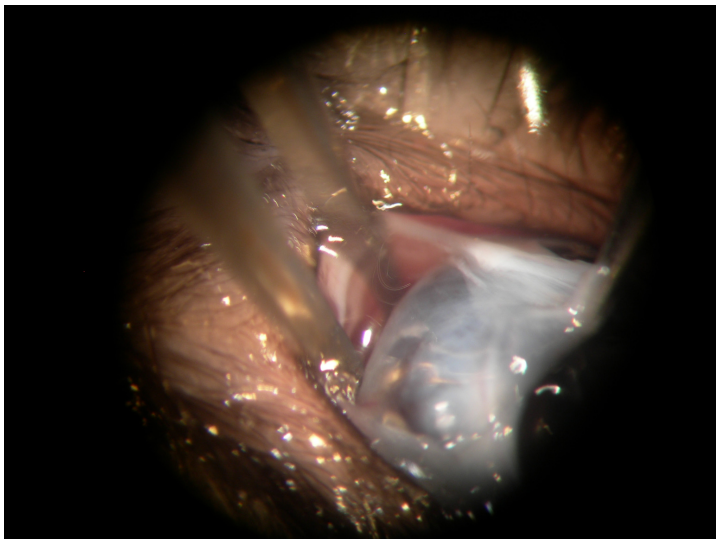

Figure 3.1 G

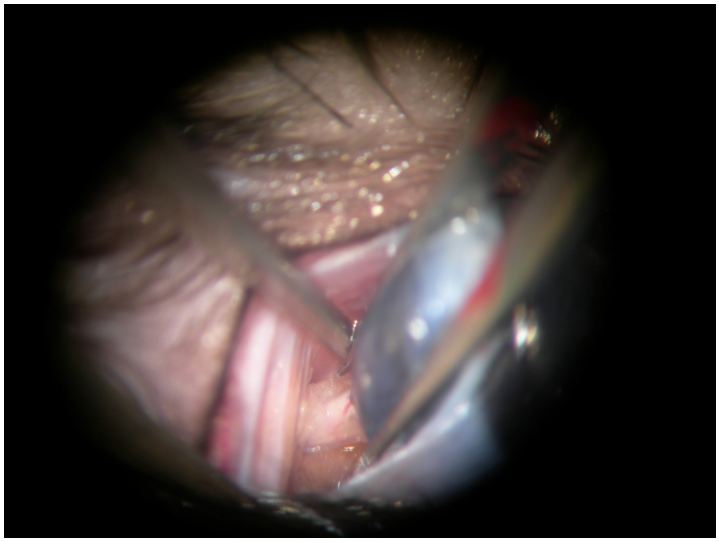

Figure 3.1 H

Using the fine scissors (Fine surgical Tools, Vancouver), the optic nerve is completely transected approximately 3 mm posterior to the globe. The wound is closed with 5-0 vicryl sutures and bacitracin applied. Animals are observed until recovered from anesthesia. The contralateral optic nerve in each rat serves as a control for each rat and therefore is not operated on.

Specific experimental details

Imaging of the retinal nerve fiber layer

3.1 Imaging of the retinal nerve fiber layer using the infra-red and red-free filters.

For this experiment we used ten adult Long-Evans rats which has had no previous ocular injection/manipulation or other interventions previously performed on them. Adult rats were anethetized (see protocol already described) using lidocaine and ketamine in mixed in equal standard concentrations injected intraperitonally at a concentration of 100 microliters per 100g eg a 100g adult rat had 50 microliters of ketamine and 50 microliters of xylocaine

injected intraperitoneally. See table 4.1 A for concentrations of anesthetic stock solution used. Image the retina after the application of balanced salt solution to maintain corneal hydration.

Table 3.1 A

Duration of procedure	**Medication**	**Desired effect**	**Dose**	**Method administration**
15 minutes	Ketamine	Anesthezia	40 – 80 mg/kg	i.p.
15 minutes	Xylazine	Anesthezia	5 -10 mg/kg	i.p.
15 minutes	Buphrenorphine	Analgesia	0.01-0.5mg/kg	s.c.
15 minutes	Isoflurane (if above methods are insufficient)	Anesthezia	3-5 L/minute	Inhalation
5 minutes	Intravitreal hydrogen peroxide	See below	0.2 mM	Intravitreal injection
5 minutes	Intravitreal dihydroethidium (HEt)	See below	3.2 mM or 0.032 mM	Intravitreal injection
5 minutes	Intravenous ethidium bromide	See below	10 microliters of 0.1 % ethidium bromide	Intravenous injection.

3.2 Imaging the retinal nerve fiber layer and determining that the application of balanced salt solution and Saran wrap to the cornea was optimal for preservation of corneal clarity.

We wanted to determine the best method for optimization of corneal clarity.

For this experiment we used three adult Long-Evans rats which has had no previous injection/manipulation or other intervention previously performed on them. Adult rats were anethetized using lidocaine and ketamine in standard concentrations injected intraperitonally at a concentration of 100 microliters per 100g eg a 100g adult rat had 50 microliters of ketamine and 50 microliters of xylocaine injected intraperitoneally. Place BSS alone on one cornea and image through this. Place saran wrap with balanced salt solution interposed between this and the cornea and image through this. Compare this with the contralateral eye which had balanced salt solution alone. Image each cornea at 15 and 30 minutes. Corneal clarity was reduced when the image was taken with saran wrap in situ, with reduction in detail resolution. However, when the saran wrap was removed from the right eye and the retina reimaged without the saran wrap, it was noted that corneal clarity was more preserved in this eye compared with the contralateral one which has balanced salt solution alone placed at 10 second intervals during imaging to maintain corneal hydration.

3.3 Imaging the retinal nerve fiber layer following optic nerve transection

As already outlined in previous chapters, optic nerve crush and transection cause the production of reactive oxygen species.

For this experiment we used two adult Long-Evans rats which has had no previous ocular injection/manipulation or other interventions previously performed on them. Adult rats

were anesthetized using lidocaine and ketamine in mixed in equal standard concentrations injected intraperitonally at a concentration of 100 microliters per 100g eg a 100g adult rat had 50 microliters of ketamine and 50 microliters of xylocaine injected intraperitoneally. See table 4.1 A for the exact concentration of stock solutions of analgesic and anesthesia medications used in our experiments. Check animal is asleep (response to pain, tail manipulation etc). Rodents will be observed for signs of distress in the perioperative period (poor grooming, decreased appetite etc as outlined in standard animal handling protocols) and additional doses of analgesia and anesthetic will be administered as required. The method used to transect the optic nerve was performed as described in the methods section.

3.4 Examining the effect of intravitreal injection of 0.9% sodium chloride

As sodium chloride would be used as the diluent in many experiments, it was important to establish that sodium chloride did not produce any fluorescence.

For this experiment we used three adult Long-Evans rats which has had no previous ocular injection/manipulation or other interventions previously performed on them.

Anesthetize rat using intraperitoneal lidocaine and xylocaine as already outlined.

Inject 4 microliters of normal saline intravitreally into the right eye. Make an incision in lateral aspect of the conjuctiva of the right eye. Use the surgical limbus as your landmak and insert the hamilton 32 gauge syringe needle just posterior to this and inject 4 microliters of normal saline into the vitreal compartment of the eye. Following injection examine the fundus using the direct ophthalmoscope to ensure there is no damage to the

retina of the animal. Left eye will be the control. Maintain corneal hydration using balanced salt solution topical drops applied to the cornea.

Place the anethetized Long-Evans rat (using standard protocol mentioned above already and mantaining corneal hydration as above) on the viewing platform of the HRA2 and image at 15 minute intervals.

HRA2 detection of fluorescent species

3.5 Quantifying the fluorescence of ICG, dihydroethidium and its derivatives using the HRA2

In order to examine the intensity of fluorescence from various dyes used to image either retinal ganglion cells or oxidative species, it was important to explore the intensity of fluorescence of their fluorescence at serial concentrations. The computer software application known as Image J was used to measure fluorescence on each image. This is a program which provides a discrete variable indicating the intensity of the fluorescence in a specific area of the image. We measured the fluorescence in the same part of the cuvette image in every image to ensure a homogenous sample. Samples were placed at approximately the same distance from the HRA2 lens to ensure optimal clarity and homogenous samples. Following acquiring each of the values for the intensity at increasing concentrations we plotted this on a graph. The sensitivity of the HRA2 can also be varied from 100 to 0% and the samples were each imaged at sensitivities from 93% down to 25%. These arbitrary numbers were chosen because above 93% the entire image became distorted and similarly below 25% the same issue occured.

Stock concentrations and then serial dilutions of each of the below solutions up until 1 in

1, 000, 000 dilutions.

- ICG (stock concentration of 25 mg in 1 ml water)
- Oxy-ethidium (Sigma-aldrich, Canada)
- Oxy-ethidium-DNA (Sigma-aldrich, Canada)

The above solutions were placed in polystyrene cuvettes. Polystyrene was used as it minimized the absorption of the infrared waves of laser by the material used to hold the solution. (100 microliter volume per cuvette) Serial dilutions were then done of each solution until 1 in 1, 000, 000 dilutions were reached. In order to standardize the analysis for each particular labeling dye, the cuvettes were placed at a fixed distance from the HRA2 objective lens. This distance was choosen to provide the clearest image possible.
Images were captured and subsequently analysed using the image J program.

Oxy-Et Standardisation curves

In order to minimise variations in distance and focal point when comparing different concentrations of oxy-Et, the intensity of fluorescence calibration curves were measured with all the polystyrene cuvettes containing the oxy-Et-DNA placed at a distance of 3.5 centrimetres from the HRA2 objective lens and using a 47.50 Diopter setting on the HRA2. As previously this distance was choosen to provide the clearest image possible. Quantitative values obtained from image J were then plotted.

Oxy-Et-DNA Standardisation Curves

In order to minimise variations in distance and focal point when comparing different concentrations of oxy-Et-DNA, the intensity of fluorescence calibration curves were

measured with all the polystyrene cuvettes containing the oxy-Et-DNA placed at a distance of 3.5 centrimetres from the HRA2 objective lens and using a 47.50 Diopter setting on the HRA2. As previously this distance was choosen to provide the clearest image possible. Quantitative values obtained from image J were then plotted on the below chart.

ICG standardisation curve

In order to minimise variations in distance and point of focus when comparing different concentrations of ICG, the intensity of fluorescein calibration curves were done with all the polystyrene cuvettes containing the ICG placed at a distance of 3.3 centrimetres from the HRA2 objective lens and using a 46.75 Diopter setting on theHRA2. As previously this distance was choosen to provide the clearest image possible. Quantitative values obtained from image J were then plotted on the below chart.

3.6A Detecting retinal ganglion cells using ICG

Retrograde labeling of retinal ganglion cells was performed using techniques already described and retinas were imaged prior to labeling and then at 24 hours intervals thereafter.

3.7 Examination of fluorescence pattern following injection of ICG into the optic nerve

This experiment allowed us to examine fluorescence patterns following optic nerve injection of a fluorescent dye and examine this as a potential route of administration.

For this experiment we used three adult Long-Evans rats which has had no previous ocular injection/manipulation or other interventions previously performed on them. Lateral canthotomy and orbitotomy were performed on the right side in a 3 month old Long-Evans rat. Injection of 4 uL of ICG (concentration of 25g/10 ml) in retro-orbital area of Optic nerve using the 32 gauge Hamilton syringe. Image at 24 hour intervals from the time of injection up to and including 7 days post injection.

3.8 Examination of fluorescence following injecting the optic nerve with DiO

This experiment allowed us to examine fluorescence patterns following optic nerve injection of a fluorescent dye and examine this as a potential route of administration.

For this experiment we used three adult Long-Evans rats which has had no previous ocular injection/manipulation or other interventions previously performed on them.
Lateral canthotomy and orbitotomy were performed on the right side in a 3 month old Long-Evans adult rat. Exposure of lateral aspect of the optic nerve is described above in detail in experiment 3.3. Injection of 4 uL of DiO (5 mg/100 ul) in retro-orbital optic nerve using the 32 gauge Hamilton syringe shown below. Image at 24 hour intervals from the time of injection up to and including 7 days post injection.

3.9 Examination of fluorescence following intravenous injection of fluorescein

In view of the fact that we had considerable difficulty using fluorescent markers with excitation in the fluorescein range (488 nm) we performed a fluorescein angiogram on an adult live rat to confirm the laser on the HRA2 was functional.

Make up solution of fluorescein (excitiation at 488 nm) at a concentration of 25g in 10 ml diluting medium. Place the anethetized Long-Evans rat (using standard protocol mentioned above already and mantaining corneal hydration as above) on the viewing platform of the HRA2. Inject 1 ml of this solution into the tail vein of an adult Long-Evans rat using the technique described under the methods section. HRA2 settings recorded were as follows: 93 % sensitivity, 12.46 diopters, 4.76 micrometers/pixel.

Markers of oxidative species : Dihydroethidium (HEt)

3.10 A Examination for background fluorescence of HEt in the absence of oxidative factors in the in vivo model and determining the optimum concentration

For this experiment we sought to examine whether there was any fluorescence of one of the markers of oxidative species when there was no source of oxidative species.

We used three adult Long-Evans rats which has had no previous
ocular injection/manipulation or other interventions previously performed on them.
Anethetize rat as already described above. Inject a total volume of 4 uL intravitreally (2 uL of HEt and 2 uL of BSS into each vitreous body). As already explained in previous chapters this has been shown to be the optimal volume which can be injected into the vitreous of adult rats in previous studies.

Right eye: final Dihydroethidium concentration 3.2 mM

Left eye: final Dihydroethidium concentration 0.032 mM

Image at 0, 10, 20, 30, 45, 60 minutes, 2, 4, 6, 12, 24 and 48 hours.

3.10 B Demonstrating that HEt does not react with hydrogen peroxide

In this experiment we wanted to demonstrate that the oxidative species hydrogen peroxide did not react with HEt and therefore show that HEt was more specific to reacting with the superoxide anion.

For this experiment three adult Long-Evans rats which has had no previous ocular injection/manipulation or other interventions previously performed on them.

Adult rats were anesthetized using lidocaine and ketamine in mixed in equal standard concentrations injected intraperitonally at standard concentrations as described previously above. Plan of injections and imaging is outlined in table below.

Table 3.10 B showing time points of injections/manipulations etc

Time point	**Procedure Perfomed**	
	Right Eye	**Left Eye**
0 minutes	Image	Image
0 minutes	Inject Intravenous DCFDA	Inject Intravenous DCFDA
20 minutes	Inject intravitreal hydrogen peroxide (0.2 mM, 4 microliters)	
30 minutes	Image	Image
45 minutes	Image	Image
60 minutes	Image	Image

3.10 C Examination of the fluorescence patten following intravenous injection of ethidium bromide

For this experiment we sought to examine whether there was any fluorescence with ethidium bromide, a substance whose chemical structure bears some resemblance to dihydroethidium. In this way we could verify whether there were false positive results.

For this experiment we used three adult Long-Evans rats which had had no previous ocular injection/manipulation or other interventions previously performed on them.

Adult rats were anesthetized using lidocaine and ketamine in mixed in equal standard concentrations injected intraperitonally at standard concentrations as described previously above. Intravenous injection of ethidium bromide was made and then serial images were taken.

3.11 Examination of fluorescence pattern following intravitreal injection of menadione and intravenous injection of HEt.

As already discussed in previous chapters menadione uncouples the redox reaction in mitochondria and causes an increase in the production of oxidative species *(Nguyen et al 2003)*. Therefore by using this compound with HEt we proposed to demonstrate production of reactive oxygen species and fluorescence. We choose to administer the HEt intravenously to ascertain if this route of administration had any effect on the production of fluorescence.

Adult rats were anesthetized using lidocaine and ketamine in mixed in equal standard

concentrations injected intraperitonally at standard concentrations as described previously above. Intravenous injection of HEt and intravitreal injection of menadione was made (using standard concentrations already described in table 3.1A based on concentrations used in previous studies) and then serial images were taken.

3.12A Examination of fluorescence patterns of a mixture of Menadione and HEt when both are injected intravitreally

As already outlined in the introduction menadione is a known producer of oxidative species. For this reason we wanted to inject it intravitreally and examine whether there was any fluorescence when dihydroethidium was injected both intravenously (4.12 B) and intravitreally (4.12 A).

For this experiment we used three adult Long-Evans rats which has had no previous ocular injection/manipulation or other interventions previously performed on them.

Rat was anethetized using standard methodology already described above.

Right eye: HEt (intravitreal injection to achieve a final concentration of 3.2 mM) and Menadione (intravitreal injection as already described to achieve intravitreal concentration of 10 mM)

Left eye: HEt 3.2 mM

Image at preinjection, 0, 10, 20, 30 45, 60 mins, 1, 2, 4, 6, and 12 hours and every 24 hours thereafter.

Overall summary of results demonstrated a speckled pattern of fluorescence but less marked in the eye which had both menadione and HEt during first 12 hours, with an

absence of this pattern from 24 – 72 hrs.

Poor clarity was found in both eyes when imaged at day following injection. The results are summarized in the below table. Of note there was some fluorescence present prior to injection in both eyes in a diffuse pattern making the results difficult to interpret.

3.12B Examination of fluorescence pattern following intravitreal injection of menadione and intravenous injection of HEt

For this experiment we used three adult Long-Evans rats which has had no previous ocular injection/manipulation or other interventions previously performed on them. The rat was anethetized using standard methodology already described above. Image at preinjection, 0, 10, 20, 30 45, 60 mins, 1, 2, 4, 6, and 12 hours and every 24 hours thereafter.

Table 3.12 B showing time points of injections/manipulations etc

Time point	**Procedure Perfomed**	
	Right Eye	**Left Eye**
0 minutes	Image and then inject intravenous HEt	Image and then inject intravenous HEt
10 minutes	Image and then inject intravitreal menadione	
40 minutes	Image	Image
50 minutes	Image	Image
90 minutes	Image	Image
110 minutes	Image	Image

3.13 Examination of fluorescence pattern following the injection of ferrous sulfate and dihydroethidium intravitreally

Ferrous sulfate is capable of producing the superoxide anion and in this experiment we postulate that its intravitreal injection will produce superoxide anion in vivo (*Rogers et al 2007, Kambayashi et al 2003*).

For this experiment we used three adult Long-Evans rats which has had no previous ocular injection/manipulation or other interventions previously performed on them.

Adult rats were anesthetized using lidocaine and ketamine in mixed in equal standard concentrations injected intraperitonally at standard concentrations as described previously above. As previousy the left eye will act as the control. Intravitreal injection of 0.5 mM ferrous sulphate (Sigma Aldrich, Canada) in the right eye. The rats cornea is protected using lacrilube ointment. Seventy two hours following this injection, intravitreal injection of 0.32 mM dihydroethidium is done in both eyes and 45 minutes following this the retina of both eyes is imaged using all four laser frequencies.

Markers of oxidative species : DCFDA

3.14A Determination of optimal intravitreal concentration of DCFDA

As already explained in the introductory chapters, DCFDA is a marker of oxidative species and therefore we attempted to initially use this to verify the correct concentration using those used by previous studies as a guide.

For this experiment we used three adult Long-Evans rats which has had no previous ocular

injection/manipulation or other interventions previously performed on them. Adult rats were anesthetized using lidocaine and ketamine in mixed in equal standard concentrations injected intraperitonally at standard concentrations as described previously above. As previously the left eye will act as the control. Intravitreal injections of 3.2 mM , 0.32 mM and 0.032 mM DCFDA were performed.

Table 3.14 part 1 and 2 showing plan of experiment and results

Time point	**Procedure Perfomed**	
	Right Eye	**Left Eye**
0 minutes	Image and then inject 3.2 mM DCFDA	Image
10 minutes	Image	Image
40 minutes	Image	Image
50 minutes	Image	Image
90 minutes	Image	Image
110 minutes	Image	Image

3.14B Fluorescence pattern following injection of DCFDA (intravenously) and hydrogen peroxide (intravitreally).

As already explained in the introductory chapters, DCFDA is a marker of oxidative species and therefore we attempted to verify if any fluorescence was produced in the presence of hydrogen peroxide when DCFDA was administered intravenously.

For this experiment we used three adult Long-Evans rats which has had no previous ocular injection/manipulation or other interventions previously performed on them.

Adult rats were anesthetized using lidocaine and ketamine in mixed in equal standard concentrations injected intraperitonally at standard concentrations as described previously above.

Table 3.14 B showing time points of injections/manipulations etc

Time point	**Intervention performed in each eye**	
	OD	**OS**
Preintervention		
0 minutes	**Intravenous injection DCFDA**	**Intravenous injection DCFDA**
20 minutes	**Intravitreal injection hydrogen peroxide**	
30 minutes	**Image**	**Image**
40 minutes	**Image**	**Image**
50 minutes	**Image**	**Image**
60 minutes	**Image**	**Image**

1 hour 10 minutes	**Image**	**Image**
1 hour 20 minutes	**Image**	**Image**
1 hour 40 minutes	**Image**	**Image**

3.14C Demonstrate that DCFDA and hydrogen peroxide do not react when injected intravitreally

This is a further elaboration on the preceding experiment. As already explained in the introductory chapters, DCFDA is a marker of oxidative species and therefore we attempted to verify if any fluorescence was produced in the presence of hydrogen peroxide when DCFDA was administered intravitreally. Here we are attempting to determine if the route of administration has any effect on the production of fluorescence.

For this experiment we used three adult Long-Evans rats which has had no previous ocular injection/manipulation or other interventions previously performed on them.

Adult rats were anesthetized using lidocaine and ketamine in mixed in equal standard concentrations injected intraperitonally at standard concentrations as described previously above.

Table 3.14 C showing time points of injections/manipulations etc

Time point	**Intervention performed in each eye**	
	OD	**OS**
Preintervention	**Image**	**Image**
O minutes	**Inject intravitreal DCFDA**	
25 minutes	**Inject intravitreal**	

	hydrogen peroxide	
30 minutes	**Image**	**Image**
40 minutes	**Image**	**Image**
50 minutes	**Image**	**Image**
60 minutes	**Image**	**Image**
70 minutes	**Image**	**Image**

3.14D Examination of fluorescence following DCFDA intravenously and Menadione intravitreally.

As already explained in the introductory chapters, DCFDA is a marker of oxidative species and therefore we attempted to verify if any fluorescence was produced in the presence of menadione (menadione as explained previously produces oxidative species by uncoupling redox reactions in the mitochondria) when DCFDA was administered intravenously.

For this experiment we used three adult Long-Evans rats which has had no previous ocular injection/manipulation or other interventions previously performed on them. Adult rats were anesthetized using lidocaine and ketamine in mixed in equal standard concentrations injected intraperitonally at standard concentrations as described previously above.

Table 3.14D showing time points of injections/manipulations etc

Time point	Intervention performed in each eye	
	OD	**OS**
Preintervention	**Image**	**Image**
O minutes	**Inject intravenous DCFDA**	**Inject intravenous DCFDA**
15 minutes	**Image**	**Image**
30 minutes	**Inject menadione (10 mM) intravitreally**	
40 minutes	**Image**	**Image**
60 minutes	**Image**	**Image**
80 minutes	**Image**	**Image**
105 minutes	**Image**	**Image**
120 minutes	**Image**	**Image**

Retinal ganglion cells after crush

3.15 Examining the effect of optic nerve crush on retinal ganglion cells labelled with ICG

As the optic nerve and therefore retinal ganglion cell axons will be crushed, it was important to establish what effect this had on the already established retrograde transportation of fluorescent dye to the retinal ganglion cell body fromthe superior colliculus.

For this experiment we used three adult Long-Evans rats which has had no previous ocular injection/manipulation or other interventions previously performed on them.

Retinal ganglion cells are labeled using the established retrograde labeling technique via the superior colliculus already outlined. Image at 24 hour intervals from the time of injection up to and including 7 days post injection.

Table 3.16 showing time points of injections/manipulations etc

Time point	**Intervention performed in each eye**	
	OD	**OS**
Preintervention	**Image**	**Image**
O minutes	**Retrograde labeling with ICG**	**Retrograde labeling with ICG**
24 hours	**Image**	**Image**
24 hours and 10 minutes	**Optic nerve crush**	**Optic nerve crush**
48 hours	**Image**	**Image**
72 hours	**Image**	**Image**
96 hours	**Image**	**Image**
120 hours	**Image**	**Image**
144 hours	**Image**	**Image**

3.16 Imaging superoxide following optic nerve crush using CMH_2DCFDA

This experiment used CMH_2DCFDA (also known as DCFDA) to demonstrate the generation of reactive oxygen species following crush.

For this experiment we used three adult Long-Evans rats which has had no previous ocular injection/manipulation or other interventions previously performed on them. Adult rats were anesthetized using lidocaine and ketamine in mixed in equal standard concentrations injected intraperitonally at standard concentrations as described previously. As previously the left eye will act as the control. Crush right optic nerve on day 0 and image pre and post crush. Inject 3.2 mM intravitreal concentration of CMH_2DCFDA intravitreally at 10 minutes following crush. Image at 10, 30, 60, 120 minutes and 4 hours, 6 hours, 24 hours and 2, 3, 5 and 7 days**.**

3.17 Labeling retinal ganglion cells with ICG and using DCFDA to examine for reactive oxygen species following optic nerve crush

For this experiment we used three adult Long-Evans rats which has had no previous ocular injection/manipulation or other interventions previously performed on them. Adult rats were anesthetized using lidocaine and ketamine in mixed in equal standard concentrations injected intraperitonally at standard concentrations as described previously above. Image using HRA2. Image the retina. Use technique described above already to retrogradely label retinal ganglion cells. using indocyanine green at the superior colliculus. Image at 24 hours later. Crush right optic nerve as already described above taking care to preserve retinal circulation and verifying this using direct ophthalmoscope.

Image immediately afterwards. Inject dihydroethidium intravitreally to achieve a concentration of 0.32 mM. Image at 10 minute intervals and at regular time intervals thereafter (every 24 hours) following this injection. Table 4.17 illustrates the time points and procedures performed.

Table 3.17 showing time points of injections/manipulations etc

Time point from RGC labeling	**Intervention performed in each eye**	
	OD	**OS**
Preintervention	Image	Image
O minutes	Crush optic nerve	
10 minutes	Image	Image
20 minutes	0.32mM CMH_2DCFDA intravitreally	0.32mM CMH_2DCFDA intravitreally
30 minutes	Image	Image
24 hours	Image	Image
48 hours	**Image**	**Image**

Chapter 4 Results

Part one: standardization

HRA2 imaging of retinal nerve fiber layer

4.1 The retinal nerve fiber layer can be imaged using red-free and infrared filters.

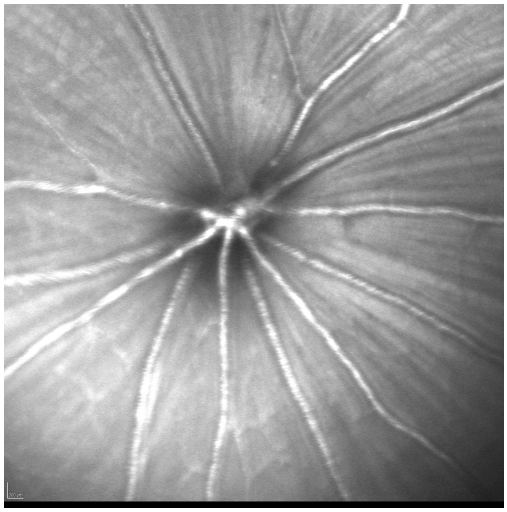

Figure 4.1 A

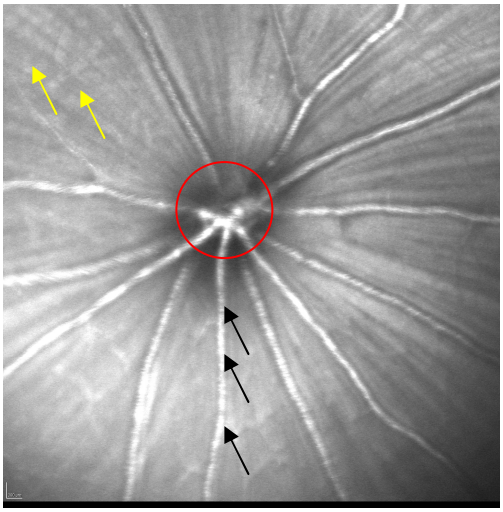

Figure 4.1B

Infrared image

Imaging of the right retina in an adult rat under infra-red laser with annotation of the structures in the identical image on right. The yellow arrows highlight a part of the image in which one can appreciate the the nerve fiber layer striations in greater detail. The red circle highlights the optic disc area. The black arrows follow the path of a vessel from the peripheral area towards the optic disc.

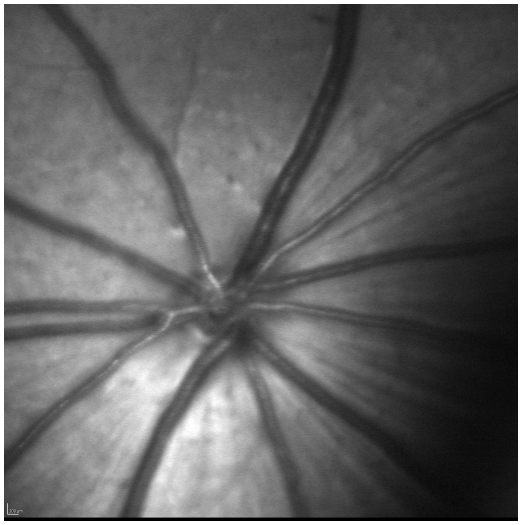

Figure 4.1 C Red-free image

Imaging of the left retina in an adult rat under the red-free laser. One can see a similar shows level of detail to the previous image under infra-red laser, however because the focal point of the red-free laser is at the level of the retinal ganglion cell layer, one can see a greater delineation of detail of this layer using this laser.

4.2 Imaging the retinal nerve fiber layer and determining that the application of balanced salt solution and Saran wrap to the cornea was optimal for preservation of corneal clarity.

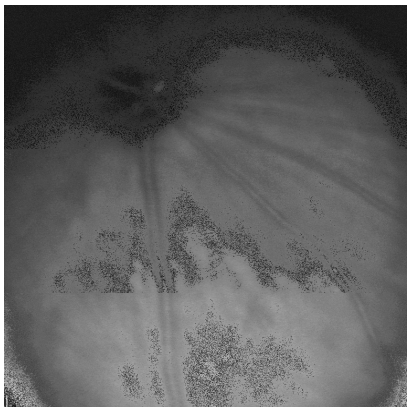

Figure 4.2A 15 minutes
OS IR 488 nm laser
Control (no Saran)

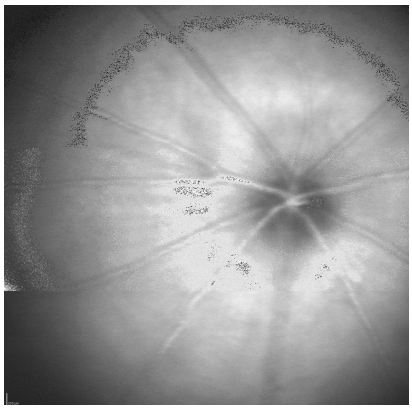

Figure 4.2B 15 minutes
OD IR 488 nm laser
(Saran removed just prior to image)

In summary one can see that corneal clarity was better in those rats which had the saran wrap applied (images on the right side) compared to those which had not (images on the left side) at all time intervals up until 30 minutes.

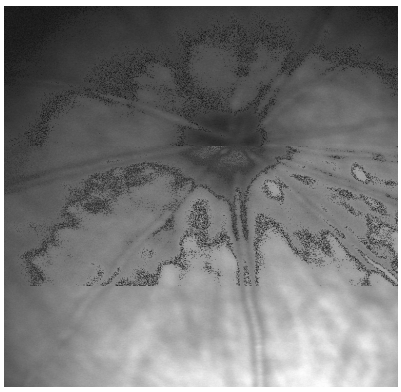

Figure 4.2C 30 minutes
OS IR 488 nm laser
(no Saran) at 30 minutes

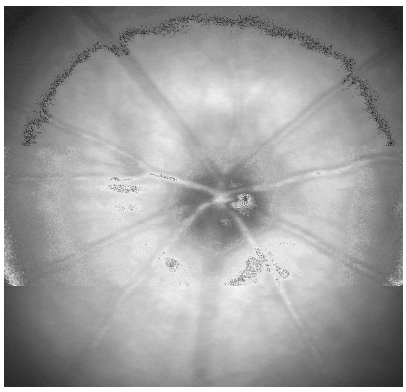

Figure 4.2D (30 minutes)
OD IR 488 nm laser Saran applied
and removed just prior to imaging

4.3 Optic nerve transection reduces corneal clarity significantly and therefore decreases our ability to visualize the retinal nerve fiber layer

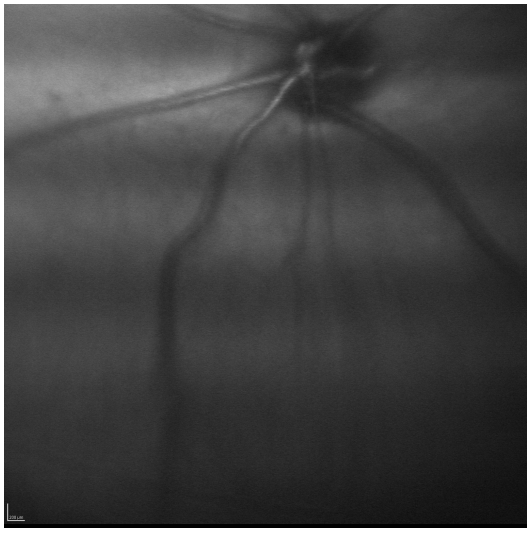

Figure 4.3A
Control OS 48hrs post transection IR filter

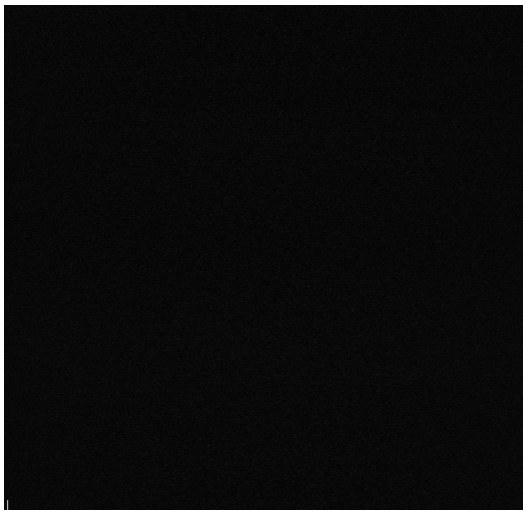

Figure 4.3B- no fluorescence
Control OS at 48hrs fluorescein filter

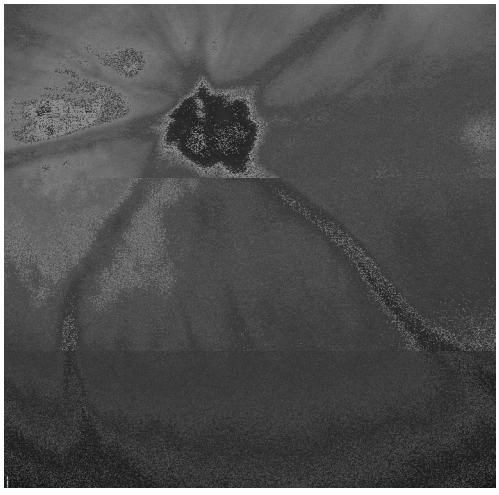

Figure 4.3C
Transected right optic nerve day 2 infrared filter.

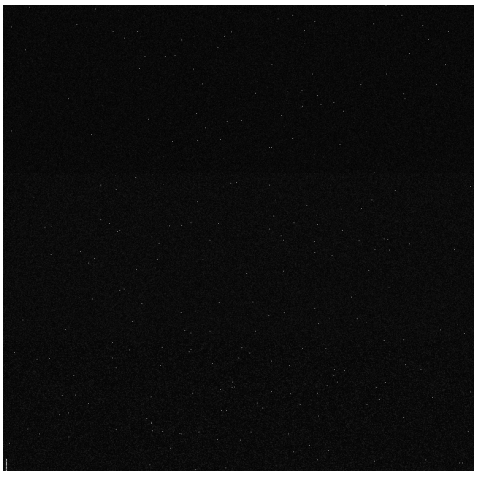

Figure 4.3D- no fluorescence
Right retinal image at 48 hours using the fluorescein filter.

4.4 Compare intravitreal injection 0.9%NaCl OD with no intervention OS

Intravitreal injection of sodium chloride did not cause the production of fluorescence.

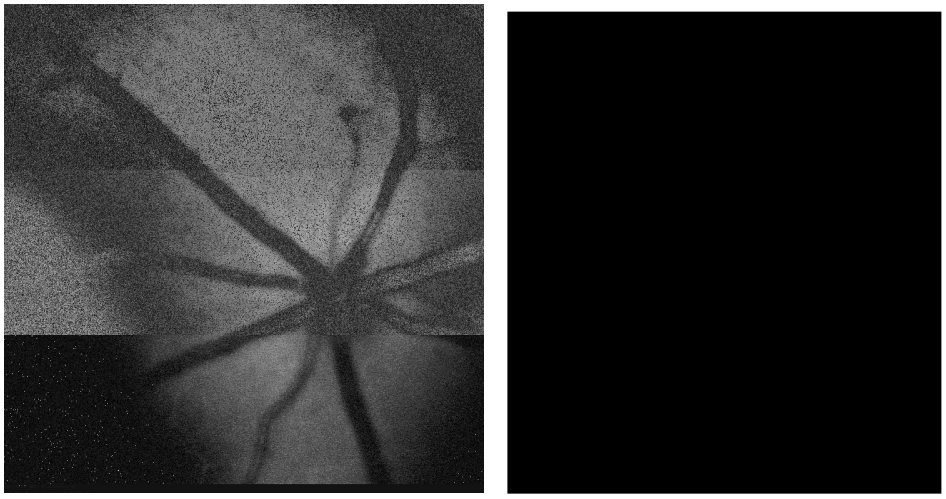

Figure 4.4 Red-free (788 nm) image of retina at 15 minutes post intravitreal injection on the left and under 488 nm filter on the right clearly demonstrating no fluorescence. Similarly there was no fluorescence using the 788 nm filter at any of the time points.

HRA2 detection of fluorescent species

4.5 Quantify the fluorescence of ICG, dihydroethidium and its derivatives using the HRA2

Overall we showed a non-linear reduction in fluorescence intensity as the concentration of the fluorescent dyes is reduced.

Oxy-Et Standardisation curves

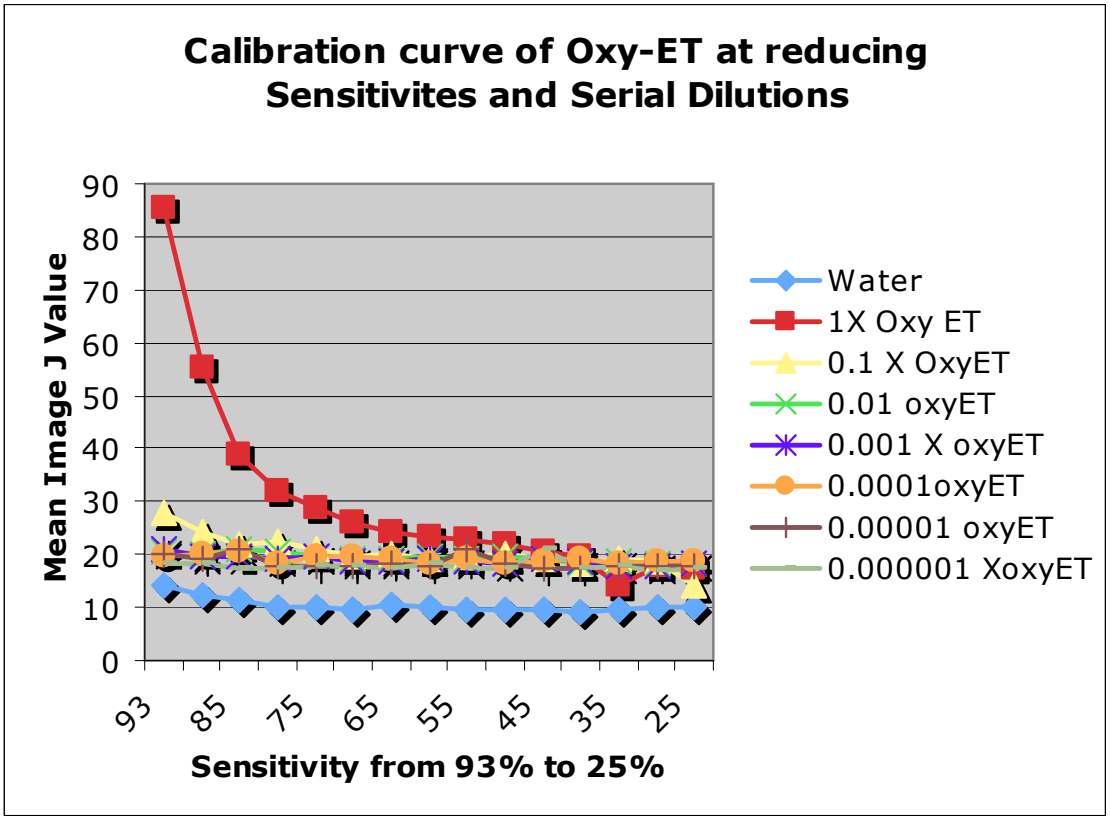

Table 4.5 A

Oxy-Et-DNA Standardisation Curves

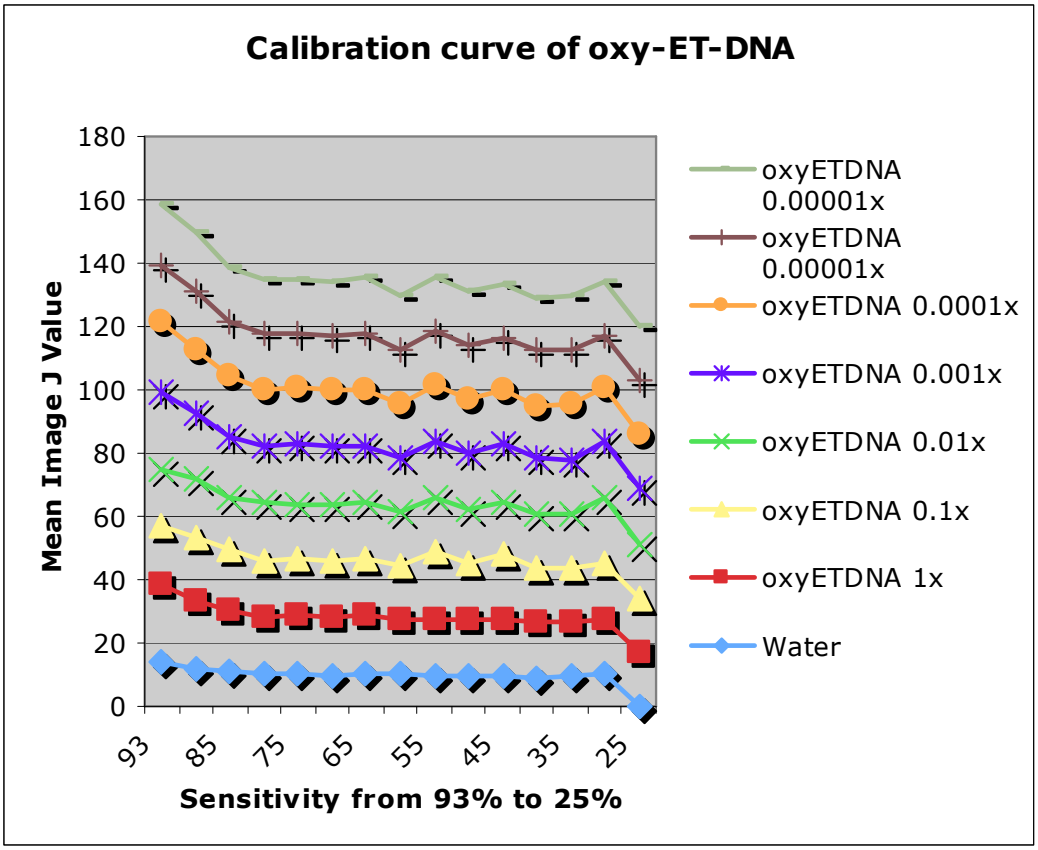

Table 4.5 B

ICG standardisation curve

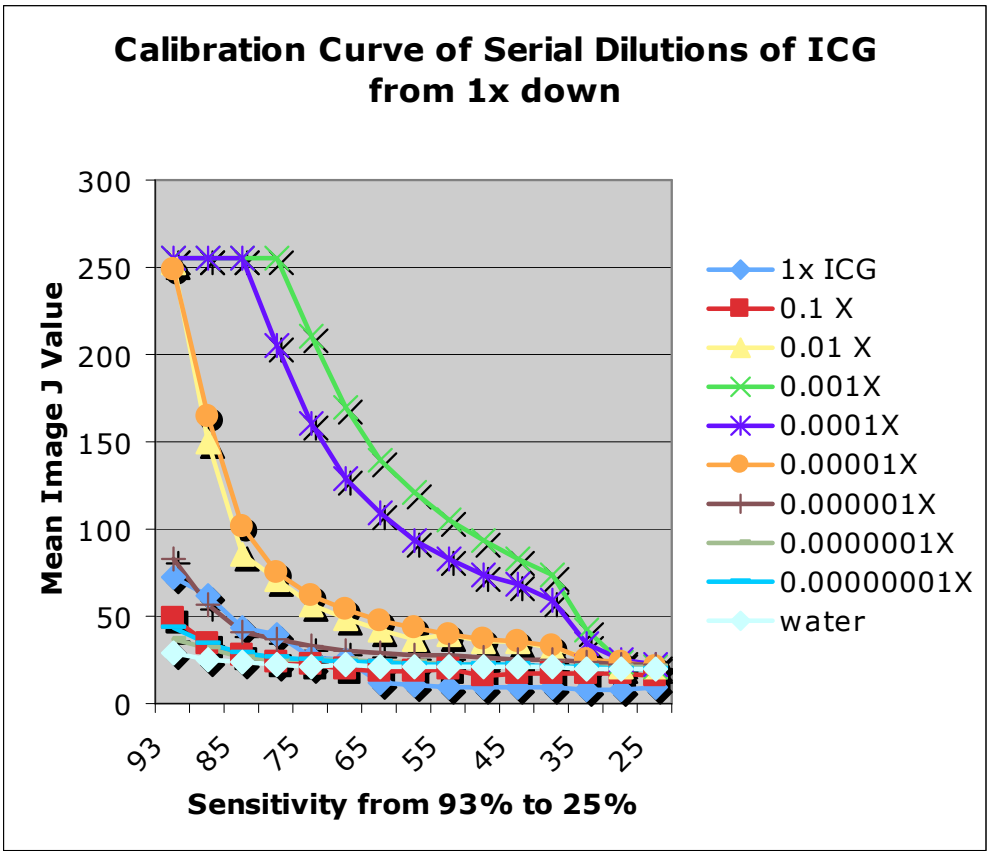

Table 4.5 C

Retrograde labeling of retinal ganglion cells with fluorescent markers.

4.6A HRA2 detection of retinal ganglion cell fluorescent marker indocyanine green (ICG)

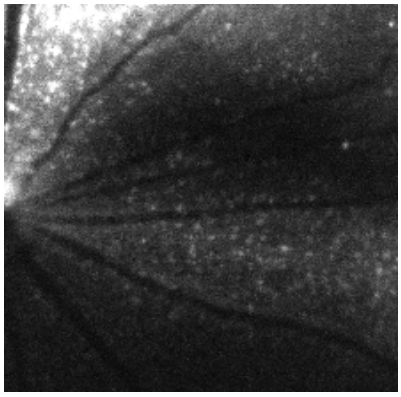

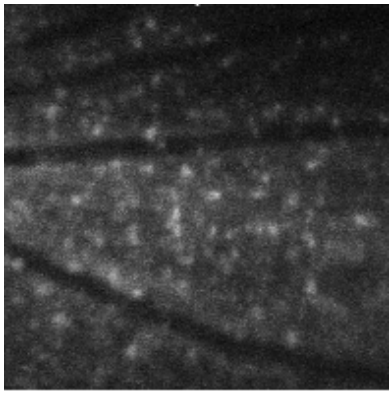

Figure 4.6 A1 (left) and A2 (right)
Left shows retinal image captured using the 30 degree field of view at 72 hours.

Right image shows a part of the same retinal image at 72 hours just lateral to the optic disc but this time using the 15 degrees

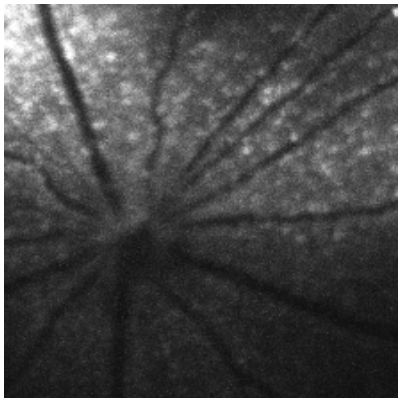

Figure 4.6 A3
Reinal image using 30 degrees field of view captured at 96 hours.

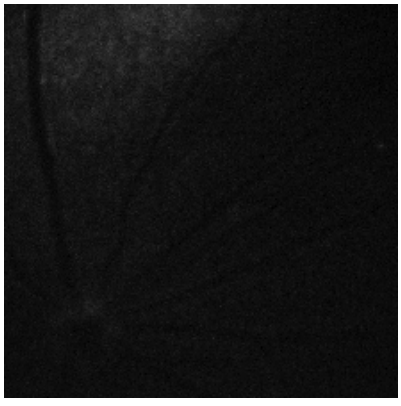

Figure 4.6 A4
Retinal image using 30 degrees field of view at 120 hours.

4.7 Examination of fluorescence pattern following injecting the optic nerve with Indocyanine green

Overall there was no significant fluorescence except optic disc autofluorescence which was likely to be significant.

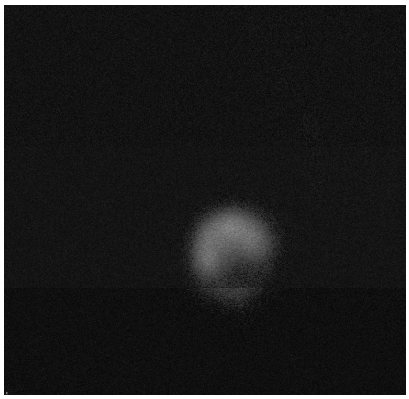

Figure 4.7 A showing retinal image at 24 hours

24hr Optic Disc fluorescence

48hr Optic Disc fluorescence

72hr No view- no images taken

Day 5 corneal clarity suboptimal- hazy view, no fluorescence seen

Day 7 No Fluorescence

4.8 Examination of fluorescence pattern following optic nerve injection with DiO

Overall there was no significant fluorescence except optic disc autofluorescence which was likely to be significant.

24 hours- no fluorescence
Day 2 corneal clarity suboptimal
Day 3 corneal clarity suboptimal
Day 5 corneal clarity suboptimal
Day 7 as above

4.9 Fluorescein injected intravenously causes fluorescence using the 488 nm laser on the HRA2

Figure 4.9 A

Red-free prior to injection of fluorescein.

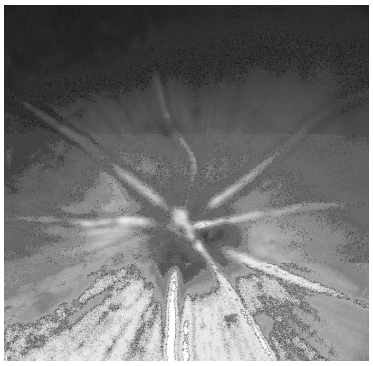

Figure 4.9 B (fluorescein filter)

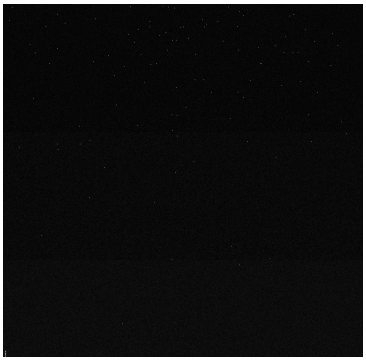

Figure 4.9 C

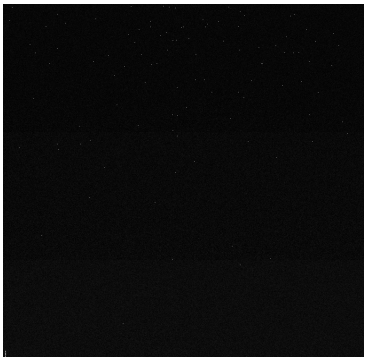

Figure 4.9 D

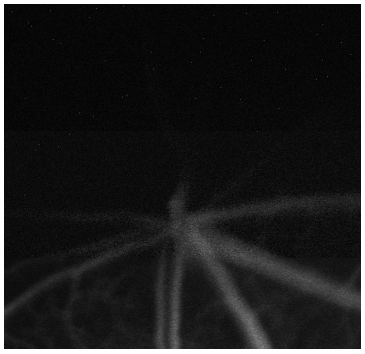

Figure 4.9 E

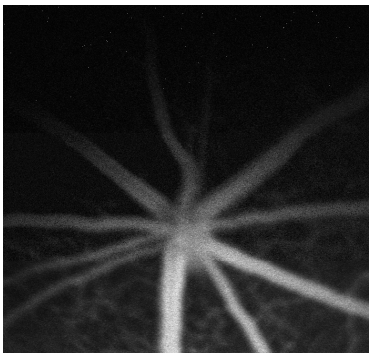

Figure 4.9 F

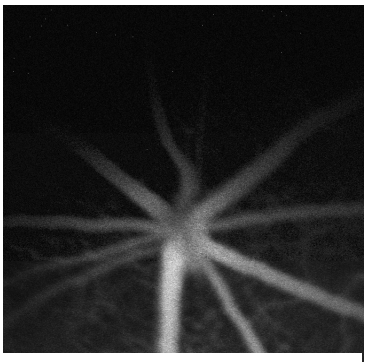

Figure 4.9 G

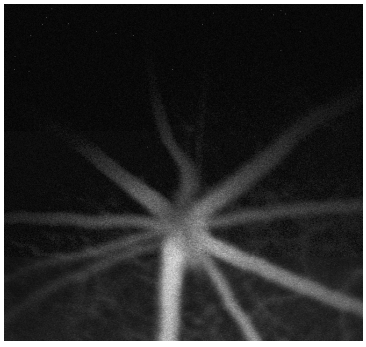

Figure 4.9 H

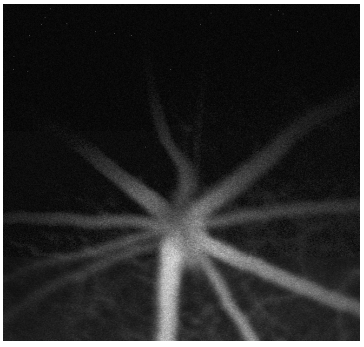

Figure 4.9 I

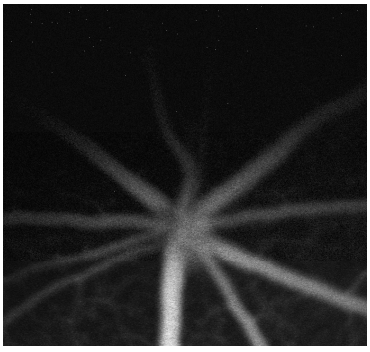

Figure 4.9 J

Figure 4.9 K

Figure 4.9 L

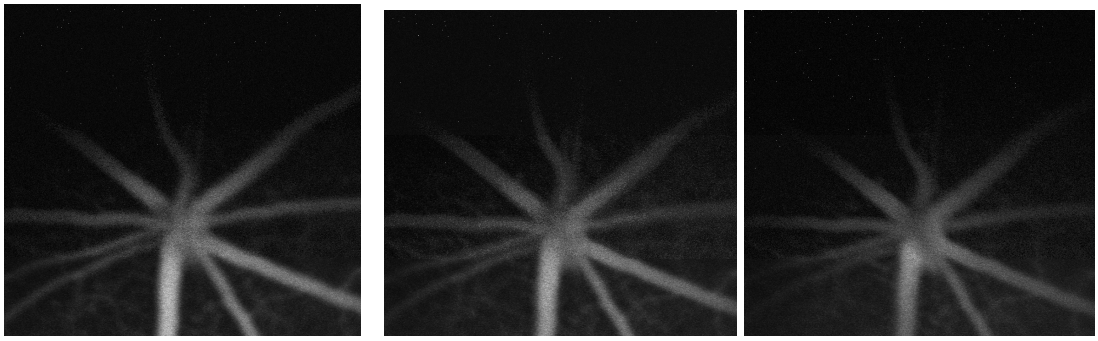

Figures 4.9 A to L: Fluorescein angiogram following intravenous injection of fluorescein at a concentration of 2.5g/ml with each image taken at 30 second intervals. A used infra-red filter and the remainder of the images used a fluorescein filter.

Markers of Oxidative Species

Dihydroethidium and its derivatives

4.10A Examining for background fluorescence of HEt in the absence of oxidative factors in the in vivo model and determining the optimum concentration.

Overall in this experiment we found optimal concentration of HEt was 0.32 mM as higher concentrations produce a profound fluorescence and oversaturation and lower concentrations produced none. We estimated the specific concentrations to use in this experiment by using previous studies as a guide (see introductory chapter).

Red-free laser on left and fluorescein on right

Right eye (OD): final intravitreal HEt concentration 3.2 mM

Left eye (OS): final intravitreal HEt concentration 0.032 mM

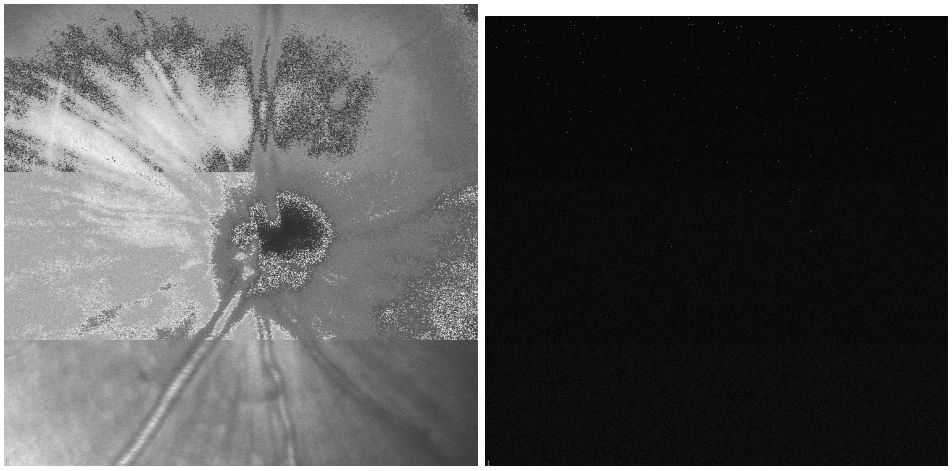

Figure 4.10 A1 Preinjection OD (HEt 3.2 mM) Red-free laser on left and fluorescein on right

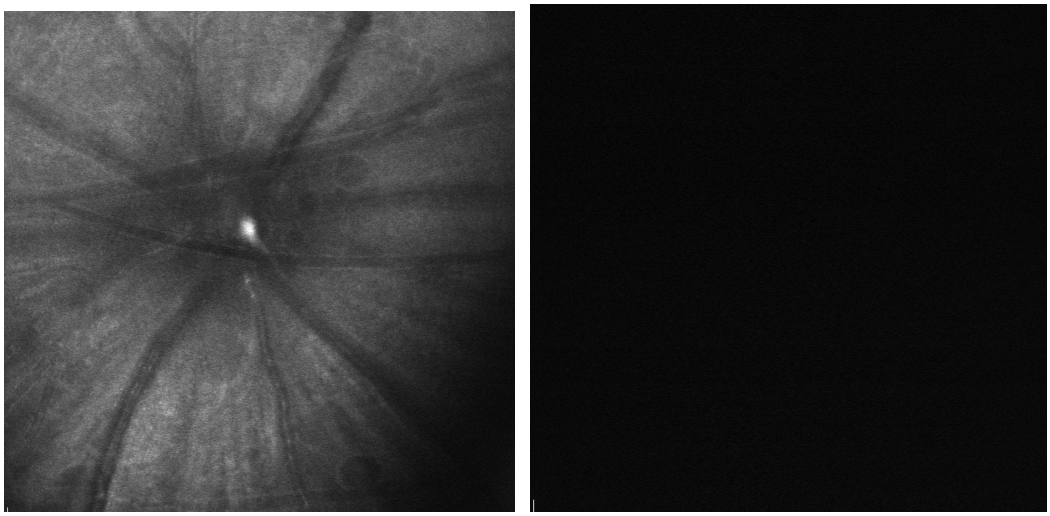

Figure 4.10 A2 Preinjection OS (HEt 3.2 mM) Red-free laser on left and fluorescein on right

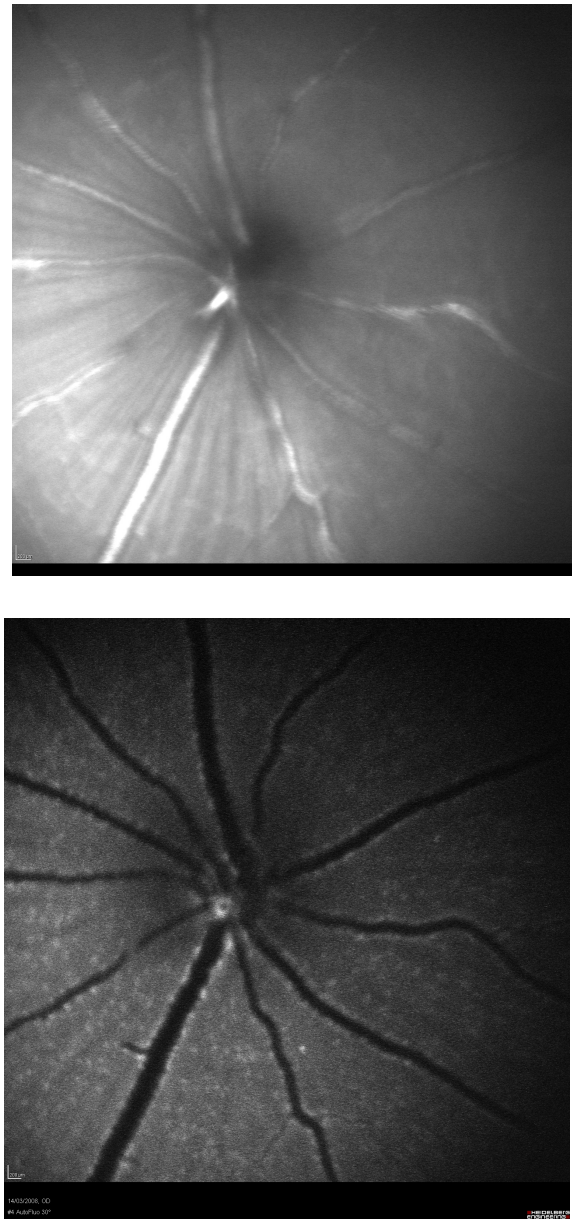

Figure 4.10 A3 at 10 minutes post injection OD (3.2 mM HEt). Red-free laser on left and fluorescein on right clearly demonstrating speckled fluorescence pattern. This speckled fluorescence pattern was continued up until approximately 60 minutes post injection and was not present thereafter in the rats which we imaged. We continued to repeat the imaging up until 48 hours following the initial intravitreal injection.

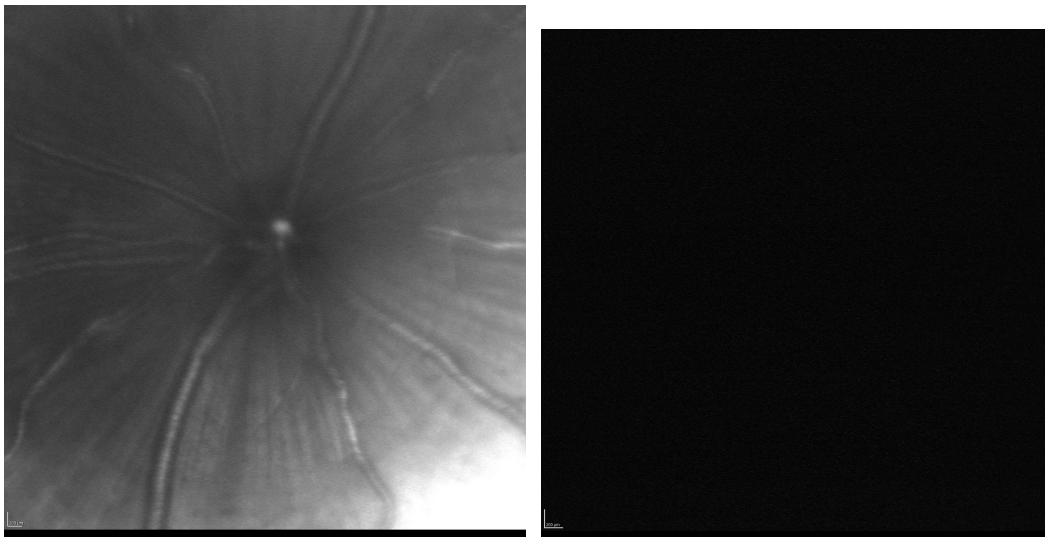

Figure 4.10 A4 at 10 minutes post injection OS (0.032mM HEt). Red-free laser on left and fluorescein on right. We continued to repeat the imaging up until 48 hours following the initial intravitreal injection and saw no fluorescence on this eye in the animals we examined.

4.10B Demonstrating that HEt does not react with Hydrogen peroxide

Overall we found that HEt does not react with hydrogen peroxide and produced no fluorescence.

Figure 4.10 B1 showing left eye (control) pre injection with red-free on left and ICG on right

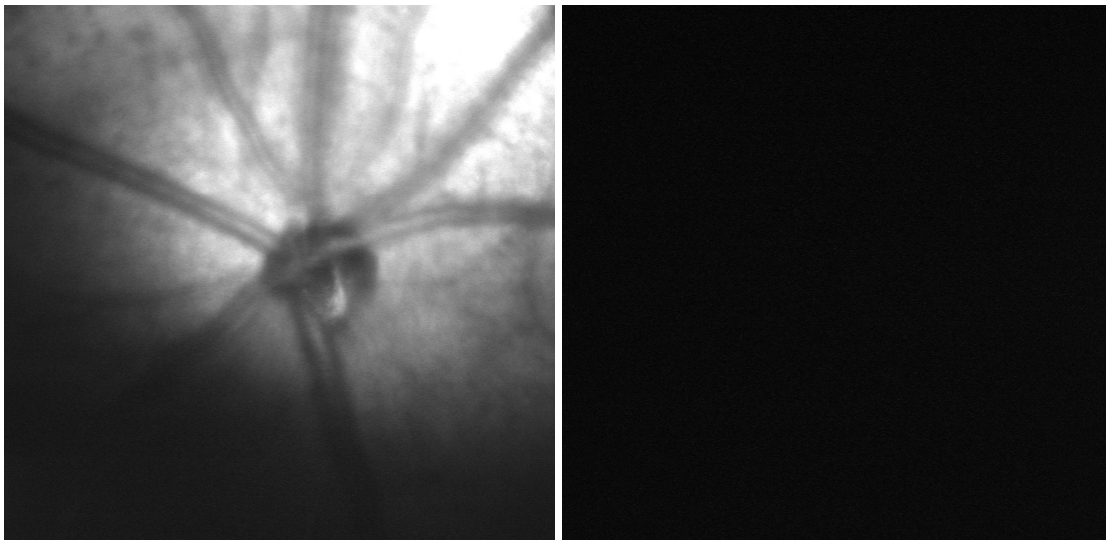

Figure 4.10 B2 showing right eye (which had the hydrogen peroxide injected) pre injection with red-free on left and ICG on right.

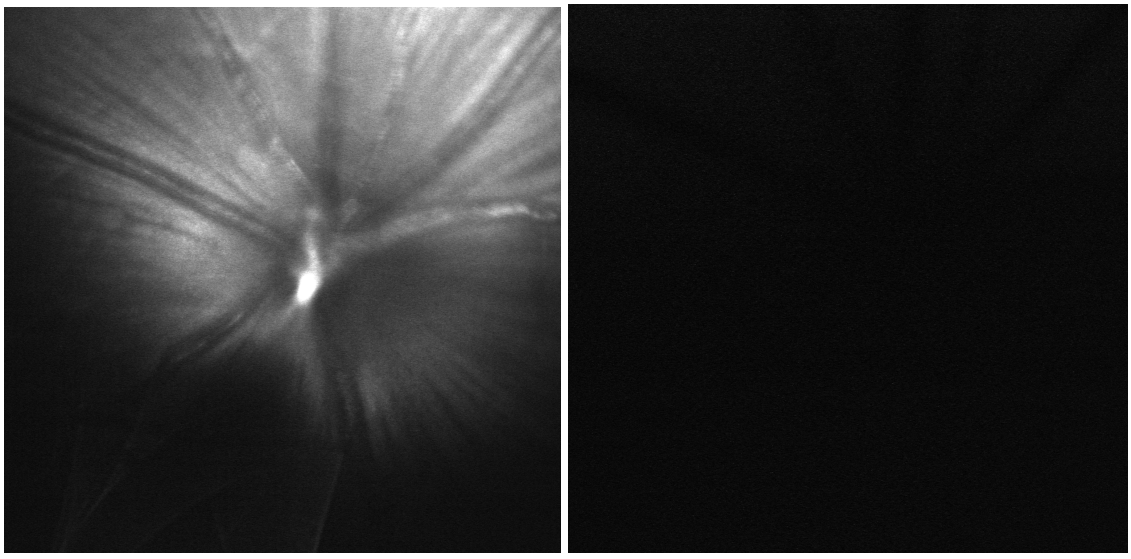

Figure 4.10 B3 showing left eye (control) 30 minutes post injection intravenous DCFDA with red-free on left and ICG on right.

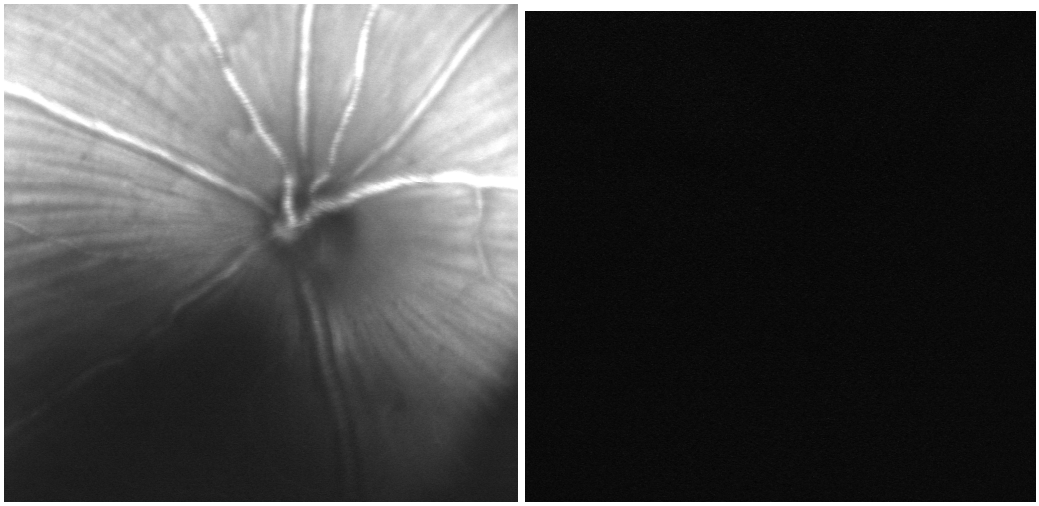

Figure 4.10 B4 showing right eye 30 minutes post injection intravenous DCFDA and 10 minutes following intravitreal injection of hydrogen peroxide with red-free on left and ICG on right

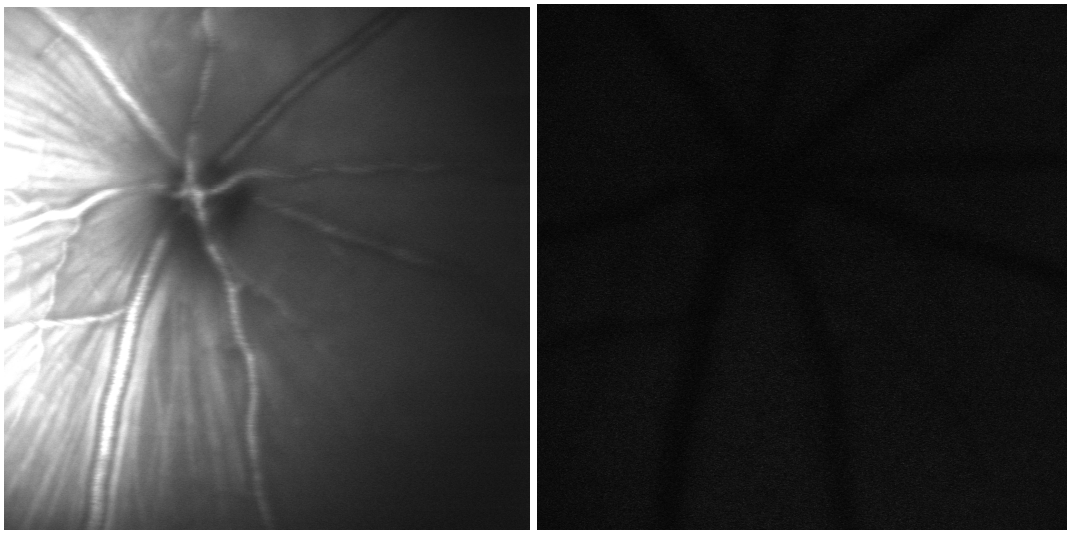

1.10 C Examination of fluorescence pattern following injection of Ethidium Bromide into rats Intravenously

Overall we found no fluorescence when ethidium bromide was injected intravenously.

Figure 4.10 C1 at 45 mins following ethidium bromide injection intravenously OS (Left side shows view under 788 nm filter and right shows view under infrared filter)

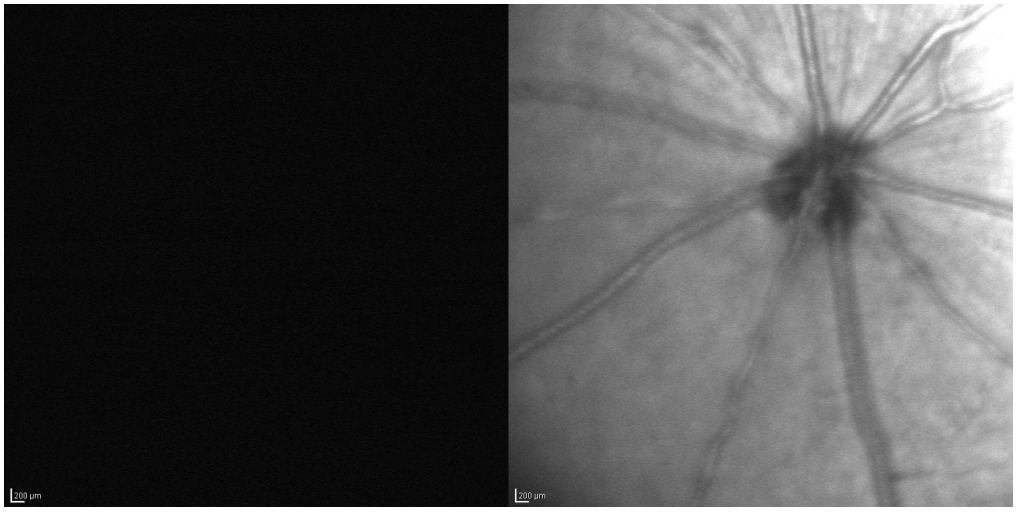

Figure 4.10 C2 at 45 mins following ethidium bromide injection intravenously OS (Left side shows view under 788 nm filter and right shows view under infrared filter)

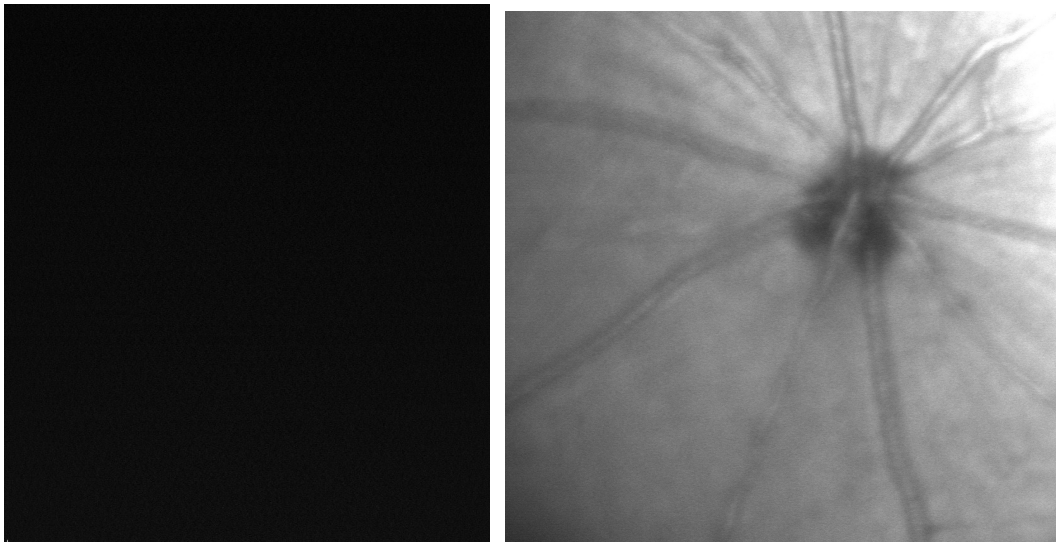

Menadione

4.11 Examination of fluorescence pattern following intravitreal injection of menadione and intravenous injection of HEt.

No fluorescence was demonstrated at the time points examined.

Menadione and HEt

4.12A Examination of fluorescence patterns of mixture of Menadione and HEt when both are injected intravitreally

Overall summary of results demonstrated a speckled pattern of fluorescence but less marked in the eye which had both menadione and HEt during first 12 hours, with an absence of this pattern from 24 – 72 hrs.

Poor clarity was found in both eyes when imaged at day following injection. The results are summarized in the below table. Of note there was some fluorescence present prior to injection in both eyes in a diffuse pattern making the results difficult to interpret.

<table>
<tr><th>Time</th><th>Action</th><th>Result</th><th>Summary</th></tr>
<tr><td>Day 1</td><td>3.2 mM HEt and 10 mM Menadione OD with HEt 3.2 mM HEt OS</td><td>Results (Corneal Clarity excellent):
<table>
<tr><th>Time Point</th><th>OD</th><th>OS</th></tr>
<tr><td>Preinjection</td><td>Positive FA/ ICG</td><td>Positive FA/ ICG</td></tr>
<tr><td>10</td><td>Increasing above</td><td>Positive FA/ ICG</td></tr>
<tr><td>20</td><td>Sustained</td><td>decreased</td></tr>
<tr><td>30</td><td>Reduced both</td><td>Further decreased</td></tr>
<tr><td>45min, 1, 2, 4, 6 hr</td><td>Reduced</td><td>As above</td></tr>
<tr><td>12 hr</td><td>Mild increase in FA</td><td>As above</td></tr>
</table></td><td>Speckled pattern fluorescence OU but less OD (with menadione injection)

Reduced as time went on over</td></tr>
<tr><td>Day 2</td><td>Imaged</td><td>None OU</td><td>None at 24hrs</td></tr>
<tr><td>Day 3</td><td>Imaged</td><td>None OU</td><td>None at 48 hrs</td></tr>
<tr><td>Day 4</td><td>Imaged</td><td>None OU</td><td>None at 72 hrs</td></tr>
<tr><td>Day 5</td><td>0.32 mM HEt OD and 0. 032 mM OS</td><td>Poor clarity
Increased OS at 10 and 30 mins
Poor clarity at 45 mins.</td><td>Poor clarity</td></tr>
</table>

Table 4.12 A

4.12B Examination of fluorescence pattern following intravitreal injection of menadione and intravenous injection of Het.

Overall there was mild diffuse fluorescence at all timepoints with no demonstrable pattern.

Table 4.12C

Time point	**Imaging Perfomed under both 788 nm and 488 nm**	
	Right Eye	**Left Eye**
0 minutes	Mild diffuse fluorescence	Mild diffuse fluorescence
10 minutes	Mild diffuse fluorescence	Mild diffuse fluorescence
40 minutes	Mild diffuse fluorescence	Mild diffuse fluorescence
50 minutes	Mild diffuse fluorescence	Mild diffuse fluorescence
90 minutes	Mild diffuse fluorescence	Mild diffuse fluorescence
110 minutes	Mild diffuse fluorescence	Mild diffuse fluorescence

4.13 Examination of fluorescence pattern following the injection of ferrous sulfate and dihydroethidium intravitreally shows discrete areas of fluorescence.

Figure 4.13 A
Examination of retina in the in vivo model at 3 days following the intravitreal injection of 0.5 mM FeSO4 and subsequent injection of 0.32 mM dihydroethidium at 45 minutes prior to the image being taken on day 3.

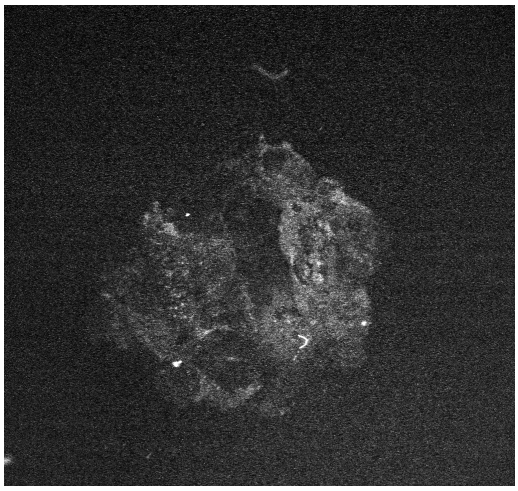

Figure 4.13 B
Retinal wholemount following removal from the eye. The wholemount was held up to the HRA2 objective lens on the slide and one can see fluorescence on the retinal specimen.

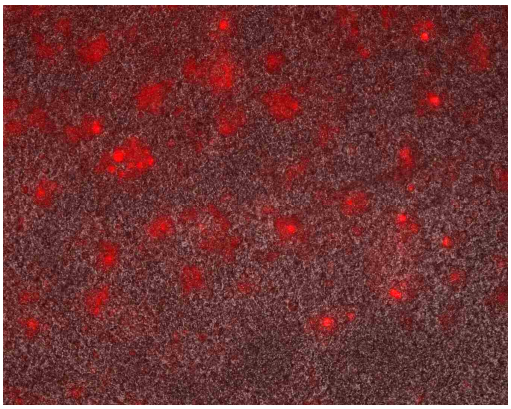

Figure 4.13 C
Retinal wholemount following removal from the eye and examination under the axiocam microscope showing bright fluorescent areas corresponding to the oxidation of dihydroethidium to oxyethidium-DNA caused by superoxide production.

Markers of Oxidative species: DCFDA

4.14A Determination of optimal intravitreal concentration of DCFDA

Overall we found the optimal concentration for DCFDA to be 0.32 mM.

4.14B Fluorescence pattern following injection of DCFDA (intravenously) and hydrogen peroxide (intravitreally)

Overall we demonstrated no fluorescence at any of the time points up to and including 100 minutes. Corneal clarity limited further imaging.

4.14C

To demonstrate that DCFDA and hydrogen peroxide do not react when injected intravitreally

Overall we demonstrated no fluorescence at any of the time points up to and including 70 minutes. Corneal clarity limited further imaging.

4.14D

Examination of fluorescence following DCFDA intravenously and Menadione intravitreally

Overall we demonstrated no fluorescence at any of the time points up to and including 80 minutes. Corneal clarity limited further imaging.

Part 2 Retinal ganglion cells after crush

4.15 Examining the effect of optic nerve crush on retinal ganglion cells labelled with ICG

24 hours following labeling (ICG filter on left and red-free on right)

Figure 4.15 a **Figure 4.15 b**

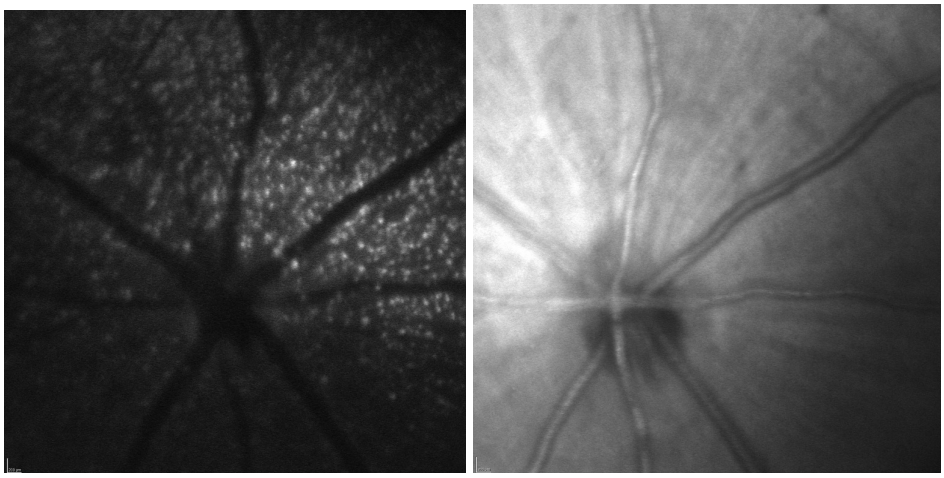

48 hours following labeling (ICG filter on left and red-free on right)

Figure 4.15 c **Figure 4.15 d**

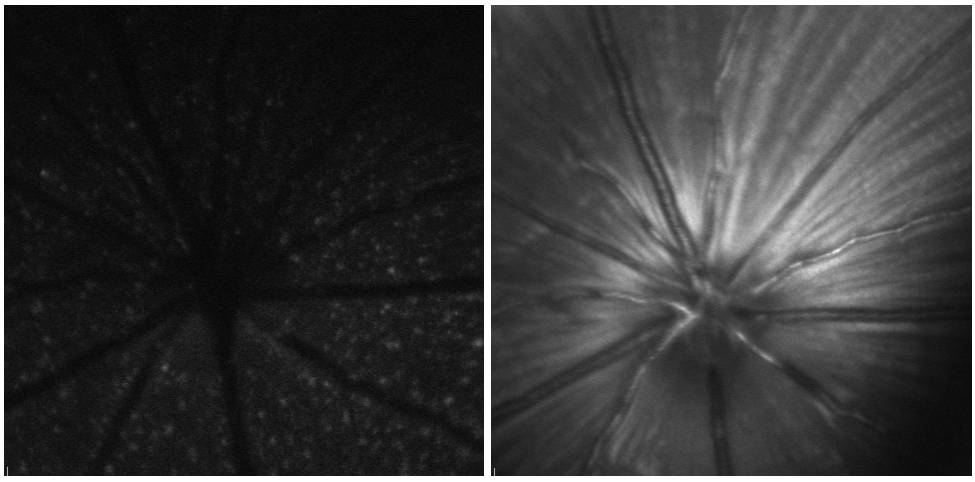

48 hours following labeling (ICG filter on left and red-free on right)

Figure 4.15 e **Figure 4.15 f**

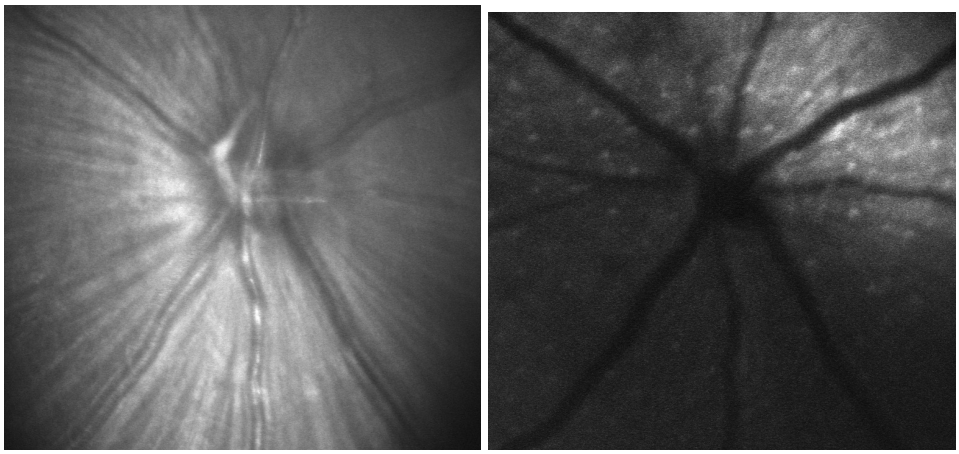

72 hours following labeling (ICG filter on left and red-free on right)

Figure 4.15 g **Figure 4.15 h**

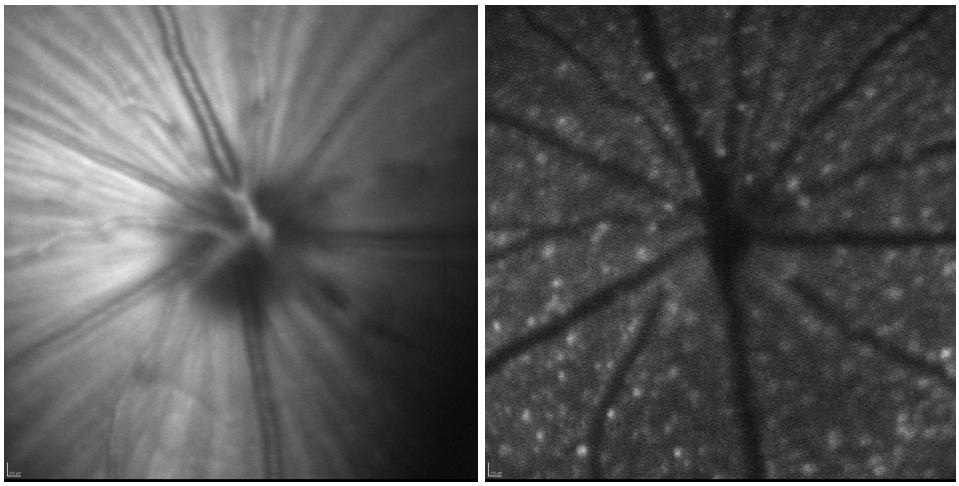

96 hours following labeling (ICG filter on left and red-free on right)

Figure 4.15 i **Figure 4.15 j**

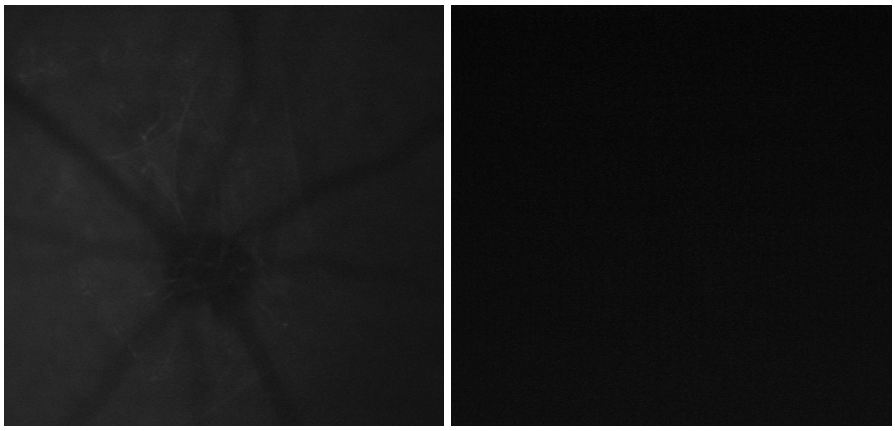

120 hours following labeling (ICG filter on left and red-free on right)

Figure 4.15 k Figure 4.15

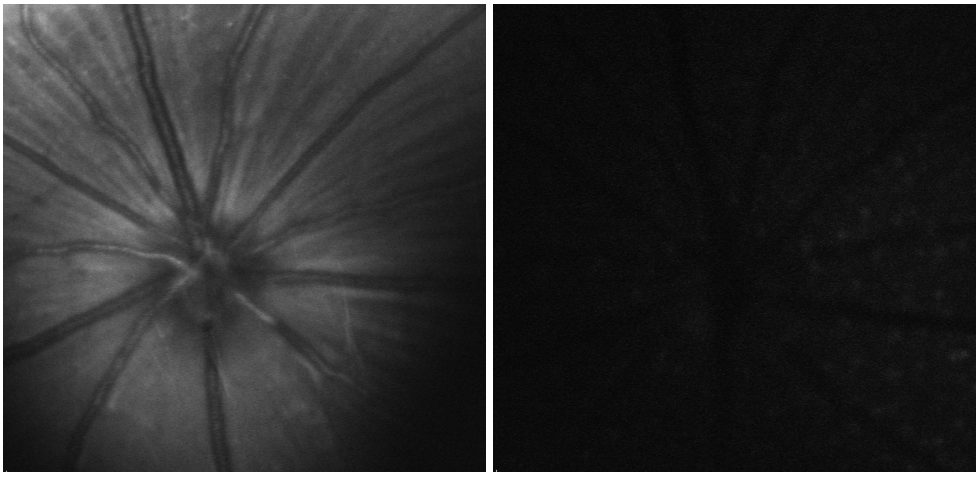

4.16 Imaging Superoxide Following Optic Nerve Crush using CMH_2DCFDA

Figure 4.16 a

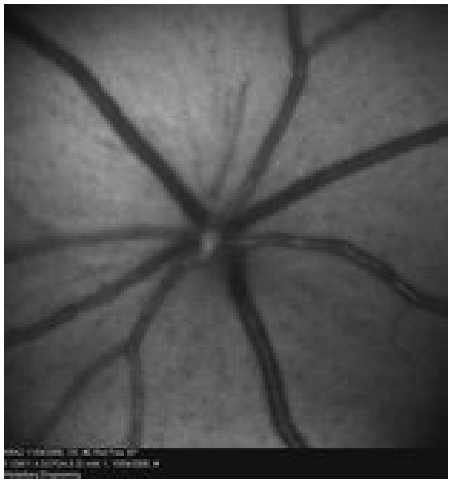

Figure 4.16 b

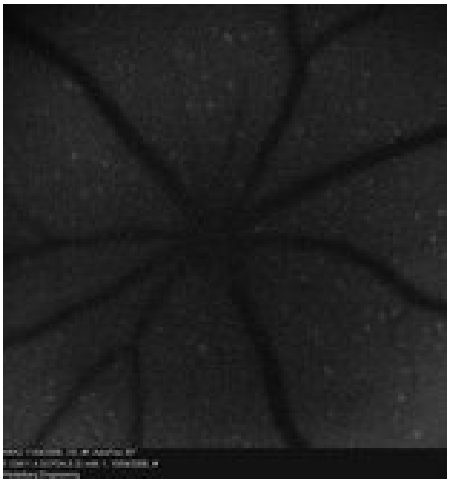

Above two images showing the side with the crushed optic nerves at 24 hours following optic nerve crush. Left side shows the image captured using the red-free filter and image on the right shows the image captured using the 488 nm filter. There is no fluorescence visible in the latter image unlike the crushed side. We were unable to re-examine the fundi at later intervals because of impaired clarity due to cataract formation.

Below images (4.16 c and d) showing the control side with the uncrushed optic nerves at 24 hours following optic nerve crush. Left side shows the image captured using the red-free filter and image on the right shows the image captured using the 488 nm filter. There is no fluorescence visible in the latter image unlike the crushed side. The experiment was repeated three times and yielded the same results.

Figure 4.16 c

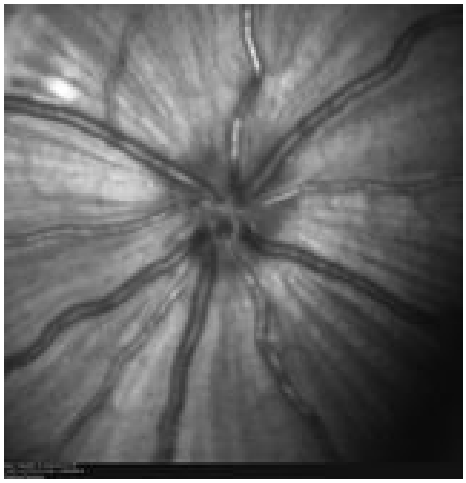

Figure 4.16 d

4.17 Labeling retinal ganglion cells with ICG and using DCFDA to examine for reactive oxygen species following optic nerve crush

Overall this experiment showed retinal ganglion cells did indeed label with ICG well within the first 48 hours however fluorescence rapidly decreased after this. There was no fluorescence of oxidative species. I have included all the images so one can appreciate the clarity issues encountered.

Figure 4.17 A Right eye preinjection showing red-free (above), 788 nm (below left) 488 nm (below right)

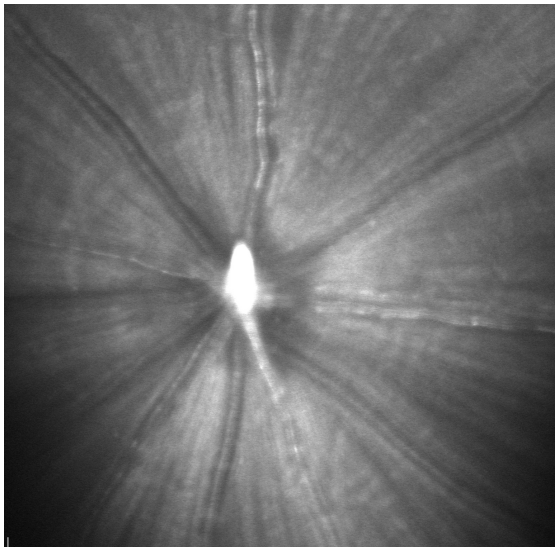

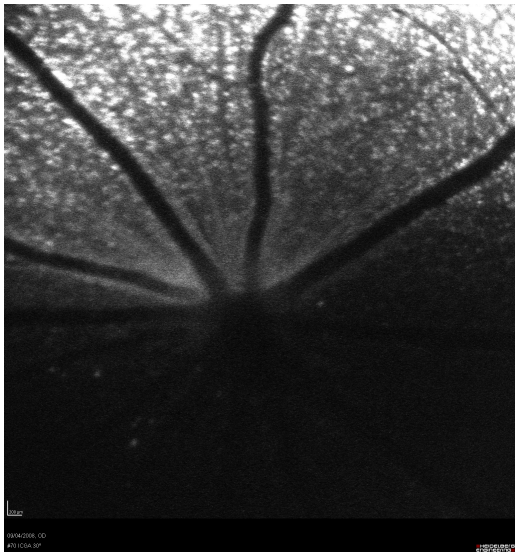

Images taken within the first 24 hours showed no significant changes from the initial ones taken. Therefore we are showing those taken at 24 hour intervals thereafter.

Figure 4.17 B Right eye at 24 hours post optic nerve crush showing red-free (above), 788 nm (below left) 488 nm (below right)

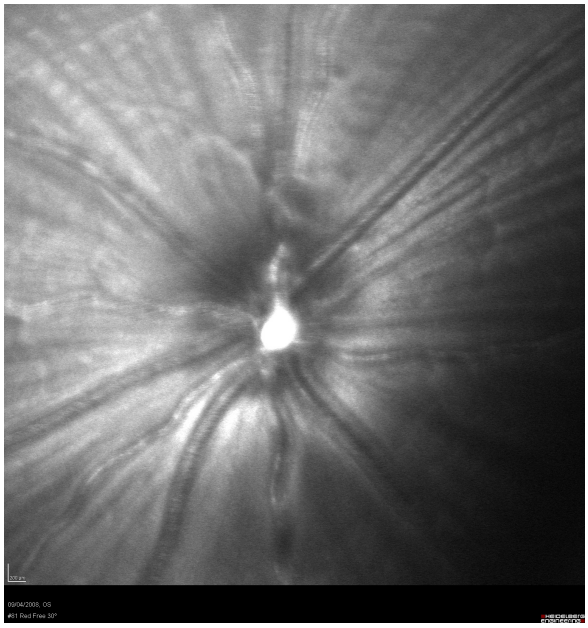

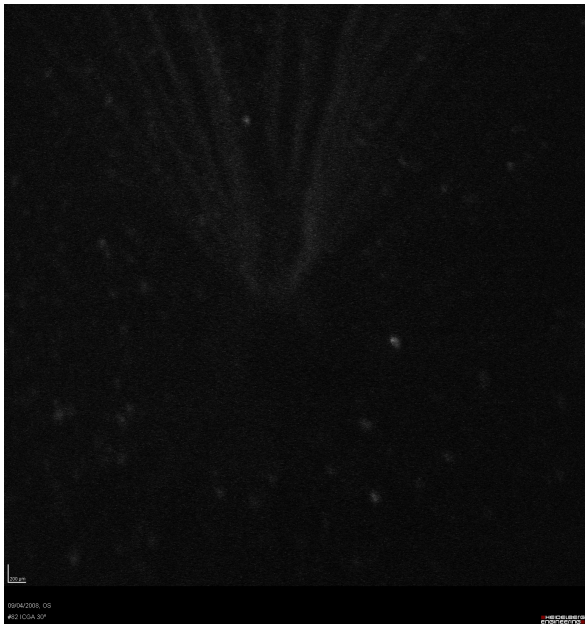

Figure 4.17 C Left eye (control) at 24 hours post optic nerve crush showing red-free (above), 788 nm (below left) 488 nm (below right)

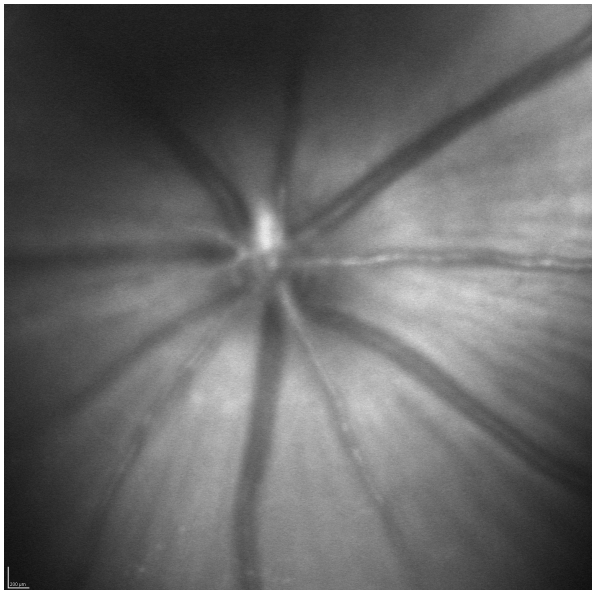

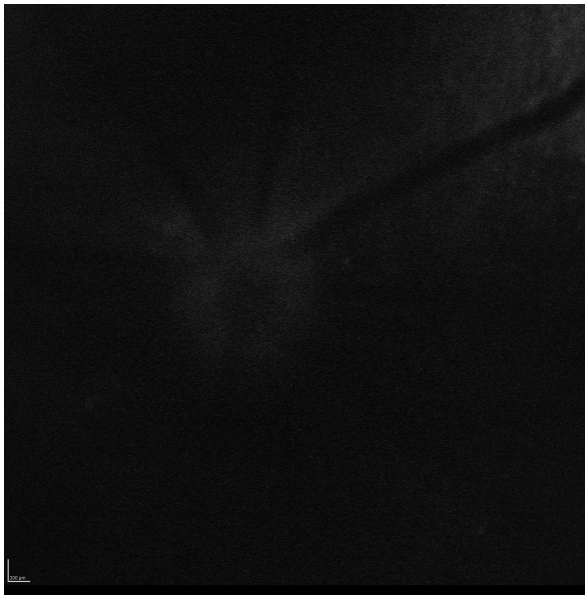

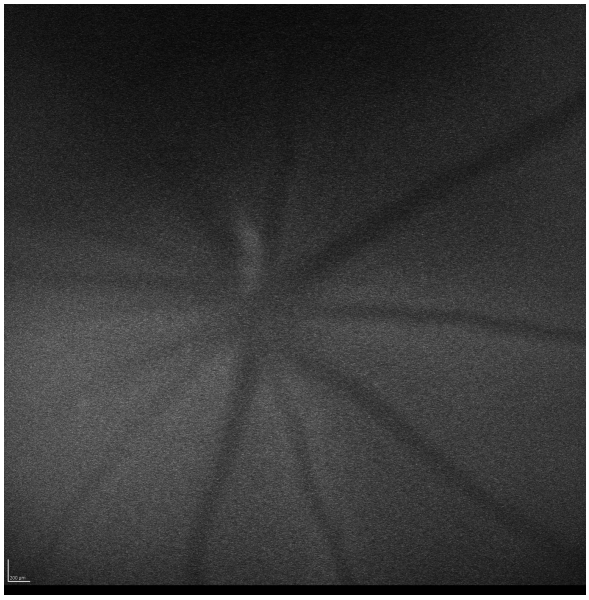

Figure 4.17 D Right eye at 48 hours post optic nerve crush showing red-free (above), 788 nm (below left). Image at 488 nm is omitted because of poor corneal clarity.

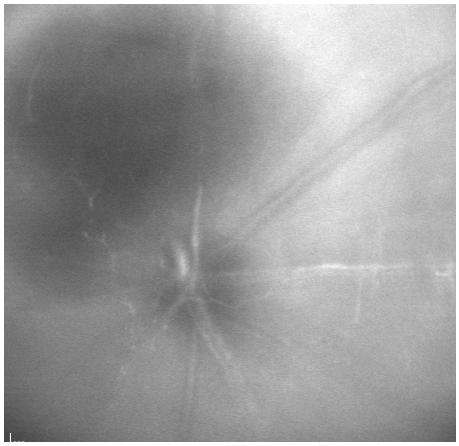

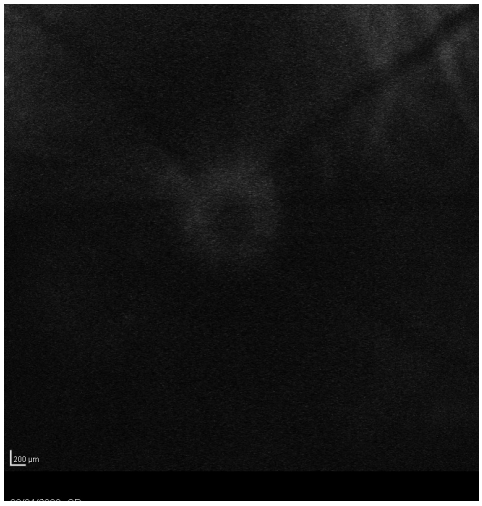

Figure 4.17 E Left eye at 48 hours post optic nerve crush of right optic nerve showing red-free (above), 788 nm (below left) and 488 nm (below right) with much better corneal clarity than the crushed side and therefore much more visible diffuse pattern of fluorescence.

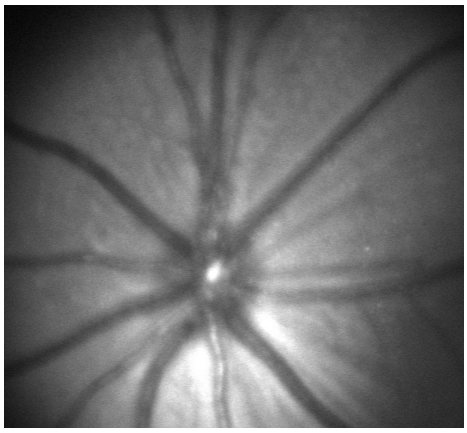

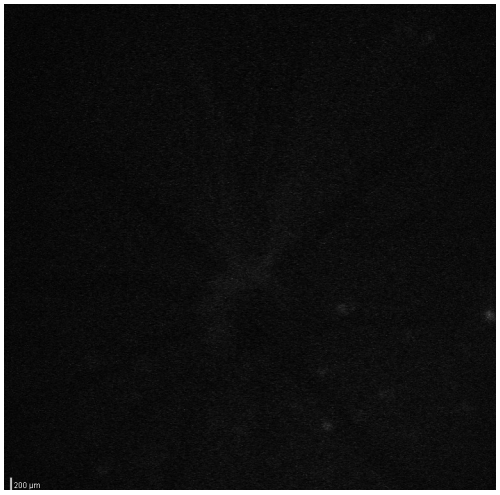

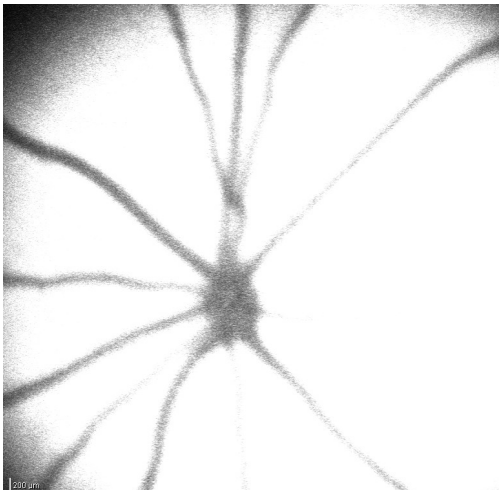

Figure 4.17 F Right eye at 72 hours post optic nerve crush showing red-free (above), 788 nm (below left) 488 nm (below right)

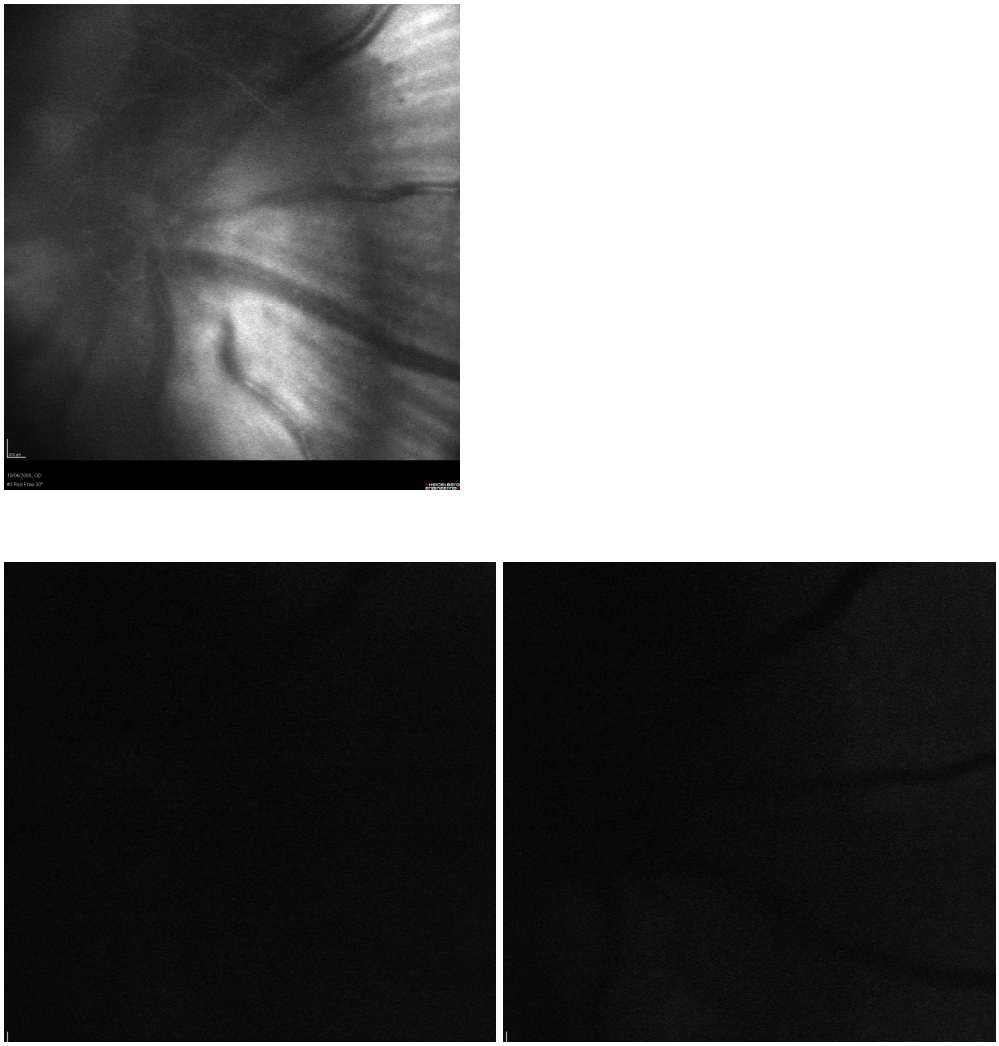

Figure 4.17 G Left eye (control) at 72 hours post right optic nerve crush showing red-free (above), 788 nm (below left) 488 nm (below right)

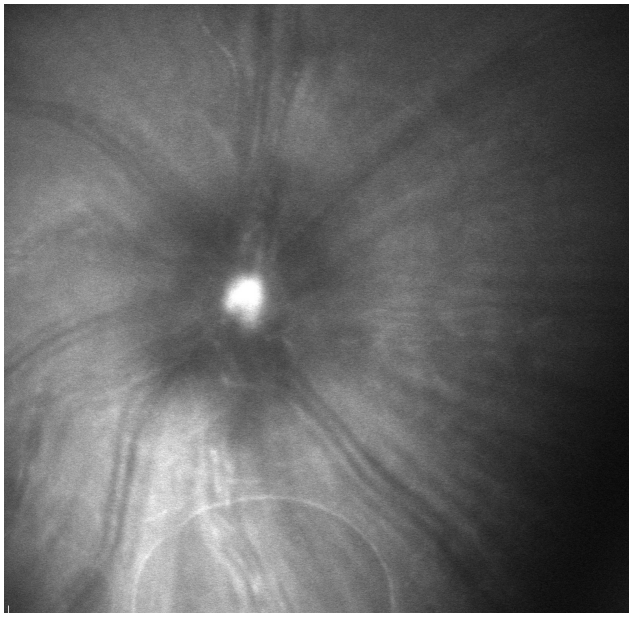

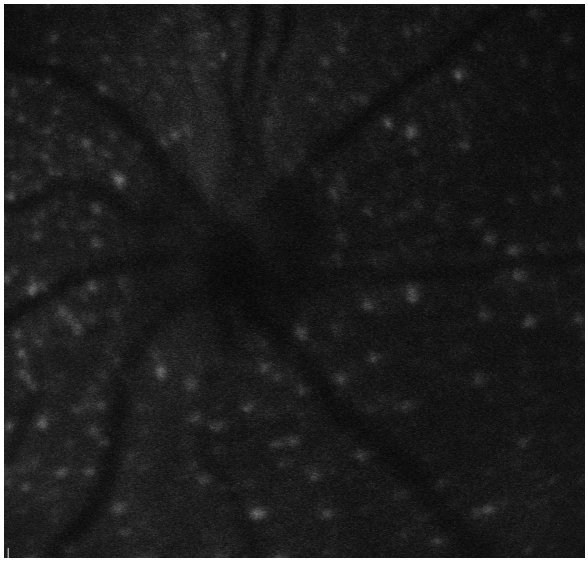

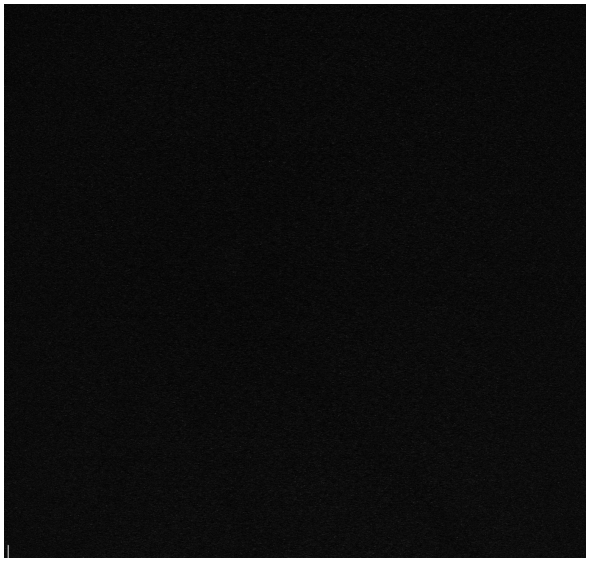

Chapter 5 Discussion

Firstly I will give a brief outline of the results in the next few paragraphs. Following this I will compare these results to those from other studies and highlight the strengths and weaknesses of our study compared with previous work in the same area.

Our results demonstrated that retinal nerve fiber layer as well as retinal ganglion cells can indeed be imaged in the *in vivo* rat model using the HRA2 apparatus as a convenient and alternate method of imaging. We showed that image quality can vary and was highly dependant on corneal lubrication, manipulation and duration of each experiment with a tendancy to become reduced after 72 hours, optic nerve transection and optic nerve crush. Intravitreal injection of normal saline (0.9% sodium chloride) caused no increase in fluorescence compared with rats which had no intervention.

When we standardized the various fluorescent markers, there was a variation in the fluorescence of markers at different concentrations (4.5). We showed that retinal ganglion cells can be imaged in the in vivo rat model using the retrograde labeling technique of the superior colliculus which used ICG as the fluorescent marker. Injecting a fluorescent probe into the optic nerve directly did not produce fluorescence. Fluorescein injected intravenously did produce fluorescence (4.9). Dihydroethidium did show some background, speckled fluorescence in the absence of oxidative stress in the live animal (4.10), although of note we were unable to reproduce this in more than one animal. When both dihydroethidium and hydrogen peroxide were injected intravitreally, there was no fluorescence, which would confirm previous studies which showed that dihydroethidium was a more specific marker for superoxide and not hydrogen peroxide *(Fink et al 2004,*

Zhao et al 2003, Zhao et al 2005). We wanted to demonstrate the fluorescence patterns (if any) of the markers of oxidative stress in our study (eg dihydroethidium) when it was delivered to the rat model in different ways eg intravenously, intravitreally in order to decide on the optimal method of administration. Intravenous injection of eithidium bromide (a closely related compound of hydroethidium) showed no fluorescence.

As already outlined in the introduction and methods, menadione is a known producer of oxidative species in the in vitro models. For this reason we wanted to inject it intravitreally and examine whether there was fluorescence when dihydroethidium was injected both intravenously and intravitreally. We found diffuse fluorescence with intravitreal menadione and intravenous dihydroethidium, however it was difficult to ascertain whether this was due to diffuse fluorescence because of too high a concentration of the dye.

As already explained ferrous sulfate dissociates into Fe^{2+} causing the formation of oxidative species. When ferrous sulfate was injected intravitreally there was a definite reproducible pattern of speckled discrete areas of fluorescence.

When hydrogen peroxide was injected intravitreally we did not show any fluorescence both when dihydroethidium was injected intravitreally and intravenously.

Retinal ganglion cells labeled with ICG whose optic nerve was subsequently crushed showed decreasing fluorescence with time. Intravitreal injection of dihydroethidium in rats whose optic nerve was crushed showed definite discrete areas of fluorescence at 24 hours following optic nerve crush. In rats whose retinal ganglion cells were simultaneously labeled with ICG and crushed, RGCs were identified using ICG but clarity decreased dramatically after 24 hours and clarity made any fluorescence from oxidized

dihydroethidium very challenging to visualize.

There were many stages involved in the planning and eventual experimental path taken in this study. One of these was choosing the appropriate marker for retinal ganglion cells and oxidative species. Other groups have outlined the use of ICG, which is a tricarbocyanine dye and can be used as a a RGC marker in the rat model using the well-described retrograde labeling technique. This dye has an axonal transport rate of 2 mm per hour and persistence of this for between 7 to 14 day and its appearance in the RGCs seen within 4 hours of injection into the lateral geniculate nucleus (*Paques et al 2003*). These features make it an important novel method of marking RGCs and was important in our eventual choice of marking agent. Additionally the peak excitation and absorbance is also optimal for the 788 nm laser of the HRA2.

The dialkylcarbocyanines fluorescence is easily detected when incorporated into membranes. There are several in existence including DiI, DiO, DiA and DiR *(Levin et al 2006*). It was for this reason that we considered the dialkylcarbocyanines as an alternate retinal ganglion cell marker, even injecting one of them (DiO) directly into the optic nerve at one point to investigate its potential. This had obvious pitfalls in terms of optic nerve damage and therefore was not utilized.

In an attempt to seek a less invasive method of labeling RGCs, several researchers have published techniques using members of the fluorescent protein family to label RGCs. The family of fluorescent proteins encompasses several proteins having the distinctive B-pleated sheet structure of fluorescent proteins. The cell surface glycoprotein known as Thy-

1 is expressed by projection neurons in many parts of the nervous system and in the retina is largely expressed in RGCs. In the transgenic mouse model developed by Feng (*Feng et al 2000*), the fluorescent protein is under the control of the Thy-1 promoter construct protein. One paper examined mice in which cyan fluorescent protein was expressed in RGCs and used DiI as the confirmatory marker for RGCs. This represented a less invasive mechanism for labeling RGCs in the live animal and utilised the confocal scanning laser ophthalmoscope to image the RGCs (*Leung et al 2008*). Another more recent paper utilized a similar technique except this time used mice which had yellow fluorescent protein expression (*Walsh et al 2008*). This is a method which could certainly be used in future studies

Use of reagents/cell markers which were within the therapeutic/effective range but not within the toxic range for live animals was a challenge during the experiments.

While in the introductory planning of the experiments, we had considered the many approaches to labeling retinal ganglion cells in the live animals and the myriad of techniques available to label the various oxidative radicals, we did encounter some difficulty with regard to using sufficient concentrations of the cell marking agents such as indocyanine green to label retinal ganglion cells and dimethsulfoxide (DMSO) as one of the diluents of dihydroethidium (*Paques et al 2003, Schulman et al 1989*). Previous studies had reported transient electroretinogram depression after an intravitreal injection of 0.1 ml of DMSO at concentrations of 10%, 50% and 100% (*Silverman et al 1983*). In all of these subjects animals had demonstrated a 50% decrease in the amplitude of the scotopic response after injection with DMSO one week after the injection. While in our study it

would have been technically difficult to perform and confirm absence of electroretinogram depression in live rats, we used the minimal concentration of DMSO (less than 1.5 %) which had previously not been shown to produce any toxic retinal effects. Once we had decided on appropriate labeling agents (e.g. ICG, DiI, HEt etc), we had some difficulty getting fluorescence using the 488 nm laser on the HRA2. It was because of this that we decided to perform a fluorescein angiogram on an adult rat as described. As fluorescein has similar excitation and emission spectra as oxy-ethidium-DNA we were therefore able to confirm that this part of our apparatus was indeed functional and subsequently were able to demonstrate fluorescence.

Preserving retinal circulation in the crush technique may have been a factor which made our experiment more challenging than expected. While we do not wish to dwell on this, it is important to examine this aspect of our study as its correction could dramatically advance the progress in imaging retinal ganglion cells. Transection of the optic nerve allows us to study the effects of oxidative stress on the retinal ganglion cell, however it also is not without its drawbacks. During and following crushing of the optic nerve, we made consistent direct visual examination of the retinal vasculature immediately afterwards and prior to each imaging session in order to ensure it was preserved. As already outlined in the introductary anatomy, the retinal circulation runs along the outside of the optic nerve and therefore leaves it prone to injury during crush.

We did have a lot of difficulty with cataract formation and corneal haziness. We attributed loss of corneal clarity in many of our animals to either loss of innervation to the cornea caused by the crushing mechanism and resultant loss of the corneal blink reflex and the

vital mechanisms which maintain corneal hydration and clarity. During our experiment we directly observed loss of the blink reflex in animals which developed this problem. This was despite our best efforts to mantain clarity by frequent application of lubricants, both during and after the experiments. We attributed the cataract formation to an ischemic process, probably once again related to crushing of the optic nerve and resultant anterior segment ischemic changes in the lens secondary to this. This slowed our progress considerably and stimulated us to examine improvements which could be made in technical aspects of optic nerve crush surgery, which we outline below.

Other studies which used a similar imaging modality did not mention corneal clarity as a challenge, however this could be related to the fact that these experiments involved much less manipulation of the cornea and intraoperative procedures such as intravitreal injections etc (*Weinreb et al 2008*).

A complete transection of the optic nerve will also transect the meningeal sheath. When this is done in the rat, then the blood supply to the retina will also be affected. This happens because the vessels destined for the retina travel in the meninges, unlike the human central retinal artery, which enters the optic nerve within the orbit and continues anteriorly until the globe. Strategies to transect the optic nerve within the meningeal sheath have been devised, involving making a slit in the sheath and using an instrument to transect the fibers within and therefore avoiding damaging the retinal blood suppy and innervation to the cornea.

Intravascular injections of reagents using the rats tail veins has been previously examined

and literature search of tehnical aspects of this proved helpful and assisted in improving delivery techniques (*Staszck et al 1993, Philip et al 1997, Kranzlin et al 2001*).

Our images which we displayed demonstrated clear images and while this was a challenge to achieve, it was possible once technical aspects of our procedures were improved (frequent applications of lubricant, improved crushing technique, etc). While we did demonstrate Saran wrap applied to the cornea improved clarity over time periods because of improved corneal hydration, imaging through this was difficult and imaging was always done with Saran wrap removed.

Retinal ganglion cells were successfully identified using already established retrograde labeling techniques via the superior colliculus and peak fluorescence was achieved at between 48 to 72 hours following labelling (see 4.6). Following crush of labelled retinal ganglion cells, a decrease in fluorescence was seen from 24 hours onwards. We postulate that this was due to decrease in retrograde transport of the labelling dye used after the optic nerve wass crushed, although the precise reason underlying this finding remains unknown.

When we intially started to use the HRA2 apparatus, we had success in labelling with ICG and imaging in vivo using the 788 nm laser, however we had difficulty in getting any fluorescence when we used the 488 nm laser. We attempted to use this when we labelled cells using DiI (a carbocyanine outlined in the introduction, the excitation of which at 488 nm and emission at 550 nm made it ideal for our experiment). However we consistently had difficulty with getting any fluorescence and therefore decided to prove that we could image with the 488 nm laser on the HRA2. We did this by performing a fluorescein angiogram in which fluorescein is injected intravenously. Fluorescein, outlined in the

introductory chapter, is a compound used in human subjects intravenously which excites at 488 nm.

We were able to establish that there was no fluorescence following intravitreal injection of normal saline which was used as a diluent in some of our intravitreal injections later on in the experiments. This was an important point to establish before proceeding.

In the absence of oxidative species, experiments with intravitreal dihydroethidium showed an intense speckled pattern of fluorescence when 3.2 mM dihydroethidium alone was injected intravitreally and no fluorescence when 0.032 mM was injected. Therefore we used a concentration intermediate between these two values in our experiments to quantify reactive oxygen species. We also attempted to investigate whether intravenous delivery of one of the oxidation products of dihydroethidium, ethidium, could elicit any fluorescence in the absence of oxidative stress. However, no fluorescence was produced. This may have been because of inability of the dye to cross into the retinal and/or into retinal cells.

As menadione has already been shown to induces the production of reactive oxygen species via redox cycling in other models and ex vivo cultures (*Levin et al, 2006*), we attempted to show this could produce reactive oxygen species in the retina *in vivo*.

When both 10 mM menadione and 3.2 mM dihydroethidium were injected intravitreally, a similar speckled pattern of fluorescence to the previous experiment was produced. This was perhaps not surprising, indicating the concentration of the dihydroethidium was again too high. However we failed to elicit any fluorescence even at a 10-fold lower concentration of dihydroethidium, indicating that perhaps menadione did not produce sufficient reactive

oxygen species to be detected in this in vivo model.

Ferrous sulfate is capable of producing superoxide anion (*Rogers et al 2007, Kambayashi et al 2003*), and therefore its intravitreal injection in experiment 4.13, should have produced fluorescence with dihydroethidium. Surprisingly, although we had no fluorescence with in vivo imaging, when we did a retinal wholemount (4.13 B) and held the wholemount slide up to the HRA2 imaging device, there was fluorescence. When viewed under the appropriate filters using a fluorescent microscope, we also had abundant fluorescence in multiple discrete patterns, as one would expect from retinal ganglion cells with superoxide anion production. The failure to visualise any fluorescence in the live in vivo model despite having a clear fundus view (4.13A) may have been because of insufficient intensity, although it is difficult to be certain. In view of the many difficulties we had with dihydroethidium, i.e. finding an appropriate intravitreal concentration and obtaining no fluorescence in the live animal imaging despite having fluorescence in the same retina when examined as a wholemout, we decided to use an alternate mechanism to demonstrate the production of reactive oxygen species and this was why we then started to use DCFDA.

DCFDA is a nonspecific indicator of reactive oxygen species. As outlined in the introductory chapter it fluoresces when exposed to a wide variety of reactive oxygen species including superoxide anion. As we found 0.32 mM to be the optimal concentration of DCFDA for indicating the production of reactive oxygen species, we proceded to use this following optic nerve crush. We noted discrete patterns of fluorescence in the crushed optic nerve at 24 hours following crush with no fluoresence produced in the contralateral

(control) eye. This indicated the production of reactive oxygen species. DCFDA is a nonspecific marker of reactive oxygen species (ROS) and therefore fluoresces when multiple ROS subtypes are present. On the contrary dihydroethidium is specific for the superoxide anion. One possible reason for why we did not get fluorescence at the same time points with dihydroethdium as with DCFDA could be this difference in specificity. There also could not be enough superoxide anion produced to elicit sufficient fluorescence to be visualized through the ocular media with in vivo imaging. This would explain the absence of fluorescence despite clear media. With DCFDA, there may have been several reactive oxygen species and presumably a high enough concentration of one or more of these to elicit enough fluorescence to be visualized through the ocular media.

Simultaneously identifying RGCs with ICG while using DCFDA to image ROS production following crush was attempted in 3.15. This had some challenges. Following labeling with ICG, the optic nerve in one eye was crushed and unfortunately the intensity of ICG fluorescence decreased markedly thereafter making it very difficult to identify any specific retinal ganglion cells which produced fluoresence. Despite repeating this several times, the multiple surgeries and interventions caused a loss of corneal clarity, hazy imaging and difficulty obtaining clear images.

Chapter 5 Conclusions

We conclude that retinal ganglion cells can be identified in vivo using retrograde labeling techniques. Reactive oxygen species can be imaged in the in vivo rat model using DCFDA, however we were unable to show the production of the superoxide anion using HEt as a marker. This may have been due to insufficient production, low sensitivity of detection with the filters on the HRA2, or other reasons. Simultaneous labeling of retinal ganglion cells and reactive oxygen species was not possible in our model because of issues with corneal clarity after optic nerve crush. This may be resolved by future studies where the optic nerve is transected but a modified technique is used, e.g. optic nerve sheath splitting for optimal preservation of corneal innervation and the retinal vasculature.

Future work should focus on optimal methods of preservation of corneal clarity following repeated manipulations (intravitreal injections, imaging, general anesthesia and subsequent loss of corneal reflex, optic nerve crush). In addition to this, multiple fluorescent probes for several reactive oxygen species could be used in a similar model to image ROS production at serial intervals following crushing the optic nerve, including the interesting model already shown to work invivo (*Leung et al 2008*). In this way a better understanding of the temporal aspects of ROS production as well as strategies to protect retinal ganglion cells from their harmful effects could be addressed.

Bibliographie

Alexander GE, DeLong MR, Strick PL. Parallel organization of functionally segregated circuits linking basal ganglia and cortex. Annu Rev Neurosci. 1986 ; 9: 357-81

Barres BA, Silverstein BE, Corey DP, et al. Immunological, morphological, and electrophysiological variation among retinal ganglion cells purified by panning. Neuron. 1988;1:791-803.

Bartsch DU, Weinreb RN, Sinzer G, Freeman WR. Confocal scanning laser infrared laser ophthalmoscopy for indocyanine green angiography. Am H Ophthalmol. 1995; 120 :642-651

Bartsch DU, Weinreb RN, Sinzer G, Freeman WR. Confocal scanning infrared laser angiography using indocyanine green. Invest Ophthalmol Vis Sci. 1994 ; 35 : S1634

Baynes J.W, Role of oxidative stress in development of complications in diabetes, Diabetes 40 (1991), pp. 405–412.

Bellman C, Kabanarou SA, Sahel JA, et al. Age-related macular disease :how to assess the retina using scanning laser techniques?. Aging Clin Exp Res. 2005; 17 (6) : 435-444

Berkelaar M, Clarke DB, Wang YC, Bray GM, Aguayo AJ. Axotomy results in delayed death and apoptosis of retinal ganglion cells in adult rats. J Neurosci 1994;14:4368-74.

Bertrand J, Di Polo A, McKerracher L. Enhanced survival and regeneration of axotomized retinal neurons by repeated delivery of cell-permeable C3-like Rho antagonists. Neurobiol dis 2007 Jan;25(1):65-72.

Berkowitz BA, Lukaszew RA, Mullins CM, Penn JS.Impaired hyaloidal circulation function and uncoordinated ocular growth patterns in experimental retinopathy of prematurity. Invest Ophthalmol Vis Sci. 1998 Feb;39(2):391-6

Bharathi Laxman, Daniel E. Hall, Mahaveer Swaroop Bhojani, Daniel A. Hamstra, Thomas L. Chenevert, Brian D. Ross, and Alnawaz Rehemtulla. Noninvasive Real-time Imaging of Apoptosis. Proc Natl Sci USA 2002 ;99 : 16551 -16555

Bilski P, Belanger AG, Chignell CF. Photosensitized oxidation of 2',7'-dichlorofluorescin: singlet oxygen does not contribute to the formation of fluorescent oxidation product 2',7'-dichlorofluorescein. Free Radic Biol Med. 2002 Oct 1;33(7):938-46.

Bondan EF, Lallo MA, Trigueiro AH, Ribeiro P, Sinhorini L, Graca DL. Delayed Schwan cell and oligodendrocyte remyelination after ethidium bromide injection in the brainstem of wistar rats submitted to streptozotocin diabetogenic treatment. Brazilian journal of medical and biological research 2006, vol. 39; 5, pp. 637-646

Bosking WH, Zhang Y, Schofield B, Fitzpatrick D. Orientation selectivity and the arrangement of horizontal connections in tree shrew striate cortex. J Neurosci. 1997 Mar 15;17 (6):2112-27.

Brown A. Axonal transport of membranou and nonmembranou cargoes : a unified perspective. J Cell Biol. 2003. Mar 17 ;160 (6) : 817-21

Brown LA, Key BJ, Lovick TA. Bio-imaging of nitric oxide-producing neurones in slices of rat brain using 4,5-diaminofluorescein. J Neurosci Methods 1999; 92(1-2):101-110

Brownlee M, The pathobiology of diabetic complications: a unifying mechanism, Diabetes 54 (2005), pp. 1615–1625.

Buxser SE, Sawada G, Raub TJ. Analytical and numerical techniques for evaluation of free radical damage in cultured cells using imaging cytometry and fluorescent indicators. Methods Enzymol. 1999;300:256-75.

Caldwell R.B , M. Bartoli, M.A. Behzadian, A.E. El-Remessy, M. Al-Shabrawey, D.H. Platt, G.I. Liou and R.W. Caldwell, Vascular endothelial growth factor and diabetic retinopathy: role of oxidative stress, Curr. Drug Targets 6 (2005), pp. 511–524

Chalupa LM. Developing dendrites demonstrate unexpected specificity. Neuron 2006;52 (4) : 567-8

Chen JY, Taranath DA, Chappell AJ, Brophy BP, Craig JE. Objective monitoring of papilloedema using confocal scanning laser ophthalmoscopy.Clin Experiment Ophthalmol. 2007 Dec;35(9):863-5.

Chen CS, Johnson MA, Flower RA, Slater BJ, Miller NR, Bernstein SL. A primate model of nonarteritic anterior ischemic optic neuropathy. Invest OphthalmVis Sci. 2008 Jul; 49 (7):2985- 92.

Cioffi GA, Orgul S, Onda E, et al. An in vivo model of chronic optic nerve ischemia: the dose-dependent effects of endothelin-1 on the optic nerve microvasculature. Curr Eye Res. 1995;14:1147-1153.

Cordeiro Francesca M., Guo Li, Luong Vy , Harding Glen , Wang Wei, Jones Helen E., Moss Stephen E., Sillito Adam M., and Fitzke Frederick W. Real-time imaging of single nerve cell apoptosis in retinal neurodegeneration. Proc Nat Acad sci USA, 2004, vol. 101; no. 36 : 13352-13356

Crow JP. Dihydrofluorescein and dihydrorhodamine 123 are sensitive indicators of peroxynitrite in vitro:implications for intracellular measurements of reactive nitrogen and oxygen species. Nitric Oxide 1:145- 157;1997

Deshmukh M, Johnson EM Jr. Staurosporine-induced neuronal death: multiple mechanisms and methodological implications. Cell Death Differ. March 2000, Volume 7, Number 3, Pages 250-2

Deshpande, S., Thompson, M., Parker, J.A. and Abrahamson, E.W., 1992. Study of retinal dystrophy in RCS rats: a comparison of Mg-ATP dependent light scattering activity and ERG b-wave. Vision Res. 32, pp. 425–432

Engelmann R, Sabel BA. In vivo imaging of mammalian central nervous system neurons with the in vivo confocal neuroimaging (ICON) method. Methods Enzymol. 1999;307:563-70.

Ebirt KK, Bonkovsky HL. Heme oxygenase: recent advances in understanding its regulation role. Proc Assoc Am Physicians. 1999;111: 438-447

Eter N, Engel D, Meyer L, Helb HM, Roth F, Maurer J, Holz FG, Kurts C. In vivo visualization of dendritic cells, macrophages and microglial cells responding to laser-induced damage in the fundus of the eye. Invest Ophthalmol Vis Sci. 2008 Aug;49(8):3649-58. Epub 2008 Mar 3.

Faulkner K, Fridovich I. Luminol and lucigenin as detectors for $O2^{\cdot-}$. Free radical biol med 15:447-451:19

Feldmen E.L, Oxidative stress and diabetic neuropathy: a new understanding of an old problem, J. Clin. Invest. 111 (2003), pp. 431–433.

Feng G, Mellor RH, Bernstein M, Keller-Peck C, Nguyen QT, Wallace M, Nerbonne JM, Lichtman JW, Sanes JR. Imaging neuronal subsets in transgenic mice expressing multiple spectral variants of GFP. Neuron. 2000 Oct;28(1):41-51.

Fink B, Laude K, McCann L, Doughan A, Harrison DG, Dikalov S. Detection of intracellular superoxide formation in endothelial cells and intact tissues using dihydroethidium and an HPLC- based assay. American Journal of Cell Physiology 2004, Vol 56, 4, 895-902.

Flower RW, Csaky KG, Murphy RP. Disparity between fundus camera and scanning laser ophthalmoscope. Invest Ophthalmol Vis Sci. 1999;40 :S123

Foissner I, Wendehenne D, Langebartels C, Durner J. In vivo imaging of an elicitor-induced nitric oxide burst in tobacco. Plant J 2000; 23(6):817-824

Freeman EE, Grosskreutz CL. The effects of FK506 on retinal ganglion cells after optic nerve crush. Invest Ophthalmol Vis Sci 2000;41:1111-5.

Gaasterland D, Tanishima T, Kuwabaa T. Axonoplasmic flow during chronic experimental glaucoma. Light and electron microscope studies of the monkey optic nerve head during development of glaucomatous glaucomatous cupping. Invest Ophthalmol Vis Sci. 1978;17:838-846.

Garcia-Valenzuela E, Shareef S, Walsh J, et al. Programmed cell death of retinal ganglion cells during experimental glaucoma. Exp Eye Res. 1995;61:33-44.

Gellrich NC, Schimming R, Zerfowski M, Eysel UT. Quantification of histological changes after calibrated crush of the intraorbital optic nerve in rats. Br J Ophthalmol. 2002 Feb;86(2):233-7

Godement P, Wang L-C, Mason CA Retinal axon divergence in the optic chiasm: dynamics of growth cone behavior at the midline. J Neurosci 14:7024 –7039 1994.

Gray DC, Wolfe R, Gee BP, Scoles D, Geng Y, Masella BD, Dubra A, Luque S, Williams DR, Merigan WH In vivo imaging of the fine structure of rhodamine-labeled macaque retinal ganglion cells. Invest Ophthalmol Vis Sci. 2008 Jan;49(1):467-73.

Greenfield DS, Weinreb RN. Role of Optic Nerve Imaging in Glaucoma Clinical Practice and Clinical Trials. Am J Ophthalmol. 2008 Feb 22 [Epub ahead of print]

Grutzendler J, Kasthuri N, Gan WB. Long-term dendritic spine stability in the adult cortex. Nature. 2002 Dec 19-26;420(6917):812-6.

Grzelak A, Balcerczyk A, Mateja A, Bartosz G. Hemoglobin can nitrate itself and other proteins. Biochim Biophys Acta 2001; 1528(2-3):97-100

Guillery RW, Mason CA, Taylor JSH (1995) Developmental determinants at the mammalian optic chiasm. J Neurosci 15:4727– 4737.

Halder G, Callaerts P, Gehring W J. New perspectives on eye evolution. Curr Opin Genet Dev. 1995 Oct ;5 (5):602-9

Hendrikus H. Boersma, Bas L.J.H. Kietselaer, Leo M.L. Stolk, Abdelkader Bennaghmouch, Leonard Hofstra, Jagat Narula, Guido A.K. Heidendal and Chris P.M. Reutelingsperger. Past, Present, and Future of Annexin A5: From Protein Discovery to Clinical Applications. Journal of Nuclear Medicine Vol. 46 No. 12 2035-2050

Herrera, A A., Banner, L. R. & Nagaya, N. (1990) Repeated, in vivo observation of frog neuromuscular junctions: Remodelling involves concurrent growth and retraction. J. Neurocytol. 19, 85–99

Hubel D H, Wiesel T N. Ferrier lecture. Functional architecture of macaque monkey visual cortex. Proc R Soc Lond B Biol Sci. 1977 Jul 28;198 (1130):1-59 20635 (P,S,E,B)

Kanwar M, P.S. Chan, T.S. Kern and R.A. Kowluru, Oxidative damage in the retinal mitochondria of diabetic mice: possible protection by superoxide dismutase, Investig. Ophthalmol. Vis. Sci. 48 (2007), pp. 3805–3811.

Kowluru R.A, V. Kowluru, Y.S. Ho and Y. Xiong, Overexpression of mitochondrial superoxide dismutase in mice protects the retina from diabetes-induced oxidative stress, Free Radic. Biol. Med. Sci. 41 (2006), pp. 1191–1196.

Kowluru R.A., T.S. Kern and R.L. Engerman, Abnormalities of retinal metabolism in diabetes or experimental galactosemia. IV. Antioxidant defense system, Free Radic. Biol. Med. 22 (1991), pp. 587–592.

Kowluru R.A., J. Tang and T.S. Kern, Abnormalities of retinal metabolism in diabetes and experimental galactosemia. VII. Effect of long-term administration of antioxidants on the development of retinopathy, Diabetes 50 (2001), pp. 1938–1942.

Kowluru R.A. and S.N. Abbas, Diabetes-induced mitochondrial dysfunction in the retina, Investig. Ophthalmol. Vis. Sci. 44 (2003), pp. 5327–5334.

Kranzlin B, Schwartz M, Grotz N. Contribution of the Course of Arterial and Venous Vessels in the Mouse Tail, 39. Jahrestagung der Gersellschaft fur Versuchtierkunde, Ulm Tagumgsband, p75 (2001)

Tomomi Higashide, Ichiro Kawaguchi, Shinji Ohkubo, Hisashi Takeda, and Kazuhisa Sugiyama. In Vivo Imaging and Counting of Rat Retinal Ganglion Cells Using a Scanning Laser Ophthalmoscope. Investigative Ophthalmology and Visual Science. 2006;47:2943-2950

Ischiropoulos H, Gow A, Thom SR, Kooy NW, Royall JA, Crow JP. Detection of reactive nitrogen species using 2,7-dichlorodihydrofluorescein and dihydrorhodamine 123. Methods Enzymol. 1999;301:367-73.

John SW, Smith RS, Savinova OV, et al. Essential iris atrophy, pigment dispersion, and glaucoma in DBA/2J mice. Invest Ophthalmol Vis Sci. 1998;39:951-962.

LaVail, M.M., 1981. Photoreceptor characteristics in congenic strains of RCS rats. Invest. Ophthalmol. Vision Sci. 20, pp. 671–675. View Record in Scopus | Cited By in Scopus (25)

LeBel CP, Ischiropoulos H, Bondy SC. Evaluation of the probe 2',7'-dichlorofluorescin as an indicator of reactive oxygen species formation and oxidative stress. Chem Res Toxicol. 1992 Mar-Apr;5(2):227-31.

Lebrun-Julien F, Morquette B, Douillette A, Saragovi HU, Di Polo A. Inhibition of p75(NTR) in glia potentiates TrkA-mediated survival of injured retinal ganglion cells. Mol Cell Neurosci. 2009 Apr;40(4):410-20.

Leung CK, Lindsey JD, Crowston JG, Ju WK, Liu Q, Bartsch DU, Weinreb RN. In vivo imaging of murine retinal ganglion cells. J Neurosci Methods. 2008 Mar 15;168(2):475-8.Epub2007Nov7.

Levy NS. The effect of interruption of the short posterior ciliary arteries on slow axoplasmic transport and histology within the optic nerve of the rhesus monkey. Invest Ophthal. 1976 Jun ;15 (6):495 -9

Li Y, Schlamp CL, Nickells RW. Experimental induction of retinal ganglion cell death in adult mice. Invest Ophthalmol Vis Sci 1999;40:1004-8.

Lichtman JW, Fraser SE. The neuronal naturalist: watching neurons in their native habitat. Nat Neurosci 2001;4(Suppl):1215–20.

Lichtman JW, Sanes JR. Watching the neuromuscular junction. J Neurocytol 2003;32(5–8):767–75.

Livingstone M, Hubel D. Segregation of form, color, movement, and depth: anatomy, physiology, and perception. Science. 1988 May 6;240 (4853):740-9

Lü LQ, Zhu AH, Lou MQ, Cai RJ, Dong Y, Lu YC. Establishment of animal model of chronic optic nerve injury and pathological changes thereof: experiment with cats. August 22 2006. 86 (31):2177-81.

Karp G. 2005. Cell and Molecular Biology : Concepts and Experiments, Fourth ed344 JohnWiley and sons, Hoboken, NJ. ISBN 0471465801

Kato Y, Kawakishi S, Aoki T, Itakura K, Osawa T. Oxidative modification of tryptophan residues exposed to peroxynitrite. Biochem Biophys Res Commun 1997; 234(1):82-84

Kawaguchi I, Higashide T, Ohkubo S, Takeda H, Sugiyama K. In vivo imaging and quantitative evaluation of the rat retinal nerve fiber layer using scanning laser ophthalmoscopy. Invest Ophthalmol Vis Sci. 2006 Jul;47(7):2911-6.

Ken-ichi Setsukinai, Yasuteru Urano, Katsuko Katinuma, Hideyuki J. Majima, Tersuo Nagano. Development of Novel Fluorescence probes that can reliably detect reactive species and distinguish specific species. The Journal of Biological Chemistry. January 31 2003. Vol 278, 5, 3170-3175.

Kerrigan LA, Zack DJ, Quigley HA, et al. TUNEL-positive ganglion cells in human primary open-angle glaucoma. Archives of Ophthalmology 1997;115:1031-5.

Kilinc K, Kilinc A, Wolf RE, Grisham MB. Myoglobin-catalyzed tyrosine nitration: no need for peroxynitrite. Biochem Biophys Res Commun 2001; 285(2):273-276

Kojima H, Nakatsubo N, Kikuchi K, Kawahara S, Kirino Y, Nagoshi H, Hirata Y, Nagano T. Detection and imaging of nitric oxide with novel fluorescent indicators: diaminofluoresceins. Anal Chem 1998; 70(13):2446-2453

Kojima H, Sakurai K, Kikuchi K, Kawahara S, Kirino Y, Nagoshi H, Hirata Y, Nagano T. Development of a fluorescent indicator for nitric oxide based on the fluorescein chromophore. Chem Pharm Bull (Tokyo) 1998; 46(2):373-375

Kortuem K, Geiger L, Levin LA. Differential Susceptibility of Retinal Ganglion Cells to Reactive Oxygen Species. Invest. Ophthalmol. Vis. Sci. 2000 41: 3176-3182.

LeVay S, Wiesel TN, Hubel DH. The development of ocular dominance columns in normal and visually deprived monkeys. J Comp Neurol. 1980 May 1;191 (1):1-51

Levin LA. Mechanisms of optic neuropathy. Curr Opin Ophthalmol 1997;8:9-15.

Lieven CI, Hoegger MJ, Schlieve CR, Levin LA. Retinal ganglion cell axotomy induces an increase in intracellular superoxide anion. Invest Ophthalmol Vis Sci. 2006 Apr;47(4):1477-85

Lichtman, J. W., Magrassi, L. & Purves, D. (1987) Visualization of neuromuscular junctions over periods of several months in living mice. Journal of Neuroscience 7, 1215–1222.

Lichtman, J. W., & Wilkinson, R. S. (1987) Properties of motor units in the transversus abdominis muscle of the garter snake. J. Physiol. 393, 355–374.

Lin SC, Singh K, Jampel HD, et al. Optic disc nerve head and retinal nerve fiber analysis. A report by the American Academy of Ophthalmology. 2007; 114: 1937-1949.

Liu Q, Raina AK, Smith MA, Sayre LM, Perry G. Hydroxynonenal toxic carbonyls and Alzheimer disease. Mol aspects Med. 2003;24:305-313

Liu Q, Won-Kyu J, Crowston G, Xie F, Perry G, Smith MA, Lindsey JD, Weinreib RN. Oxidative stress is an early event in hydrostatic pressure-induced retinal ganglion cell damage. Invest Ophthalmol Vis Sci. 2007;48:4580-4589.

López-Figueroa MO, Caamaño C, Morano MI, Rønn LC, Akil H, Watson SJ. Direct

evidence of nitric oxide presence within mitochondria. Biochem Biophys Res Commun 2000; 272(1):129-133

López-Figueroa MO, Day HE, Lee S, Rivier C, Akil H, Watson SJ. Temporal and anatomical distribution of nitric oxide synthase mRNA expression and nitric oxide production during central nervous system inflammation. Brain Res 2000; 852(1):239-246

Maass A , Lundh von Leithner P, Luong V , Guo Li, Salt T, Fitzke FW, Cordeiro F. Assessment of Rat and Mouse RGC Apoptosis Imaging in Vivo with Different Scanning Laser Ophthalmoscopes. Current Eye Research, Volume 32, Issue 10 October 2007 , pages 851 – 861

MacMillan-Crow LA, Crow JP, Kerby JD, Beckman JS, Thompson JA
Nitration and inactivation of manganese superoxide dismutase in chronic rejection of human renal allografts. Proc Natl Acad Sci U S A 1996; 93(21):11853-11858

Maskiewicz R, Sogah D, Bruice TC. Chemiluminescence reactions of lucingenin. 1. Reactions of lucingenin with hydrogen proxide. J Am Chem Soc. 101;534: 75354;1978

Maskiewicz R, Sogah D, Bruice TC. Chemiluminescence reactions of lucingenin. 2. Reactions of lucingenin with hydroxide ion and nucleophiles. J Am Chem Soc. 101;535-5364;1978

Morgan J, Huckfeldt R, Wong RO. Imaging techniques in retinal research. Exp Eye Res. 2005 Mar;80(3):297-306.

Morrison JC Fraunfelder FW, Milne ST, Moore CG. Limbal microvasculature of the rat eye. Invest Ophthalmol Vis Sci. (1995)

Morrison JC, Moore CG, Deppmeier LM, et al. A rat model of chronic pressure-induced optic nerve damage. Exp Eye Res. 1997;64:85-96.

Mulholland DA, Craig JJ, Rankin SJ. Use of scanning laser ophthalmoscopy to monitor papilloedema in idiopathic intracranial hypertension. Br J Ophthalmol. 1998 Nov;82(11):1301-5.

Mumm JS, Williams PR, Godinho L, Koerber A, Pittman AJ, Roeser T, Chien CB, Baier H, Wong RO. In vivo imaging reveals dendritic targeting of laminated afferents by zebrafish retinal ganglion cells. Neuron. 2006 Nov 22;52(4):567-8.

Murphy TH, Miyamoto M, Sastre A, Schaar RL, Coyle JT. Glutamate toxicity in a neuronal cell line involve inhibition of cystine transport leading to oxidative stress. Neuron. 1989;2:1547-1558.

Murray TG, Burton TC, Rajani C, et al. Methanol poisoning. A rodent model with structural and functional evidence for retinal involvement. Arch Ophthalmol. 1991;109:1012-1016.

Myhre O, Andersen JM, Aarnes H, Fonnum F. Evaluation of the probes 2',7'-dichlorofluorescin diacetate, luminol, and lucigenin as indicators of reactive species formation. Biochem Pharmacol. 2003 May 15;65(10):1575-82.

Nickells RW. Retinal ganglion cell death in glaucoma: the how, the why, and the maybe. Journal of Glaucoma 1996;5:345-56.

Nickells RW, Zack DJ. Apoptosis in ocular disease: a molecular overview. Ophthalmic Genetics 1996;17:145-65.

O' Connor N, Aphinyanaphongs Y, Zinser G et al. Computational resolving power improvement for the scanning laser ophthalmoscope. Invest Ophthalmol Vis Sci. 1999; 40 :

Ohashi T, Mizutani A, Murakami A, Kojo S, Ishii T, Taketani S. Rapid oxidation of dichlorodihydrofluorescin with heme and hemoproteins: formation of the fluorescein is independent of the generation of reactive oxygen species. FEBS Lett. 2002 Jan 30;511(1-3):21-7.

Osborne NN, Ugarte M, Chao M, et al. Neuroprotection in relation to retinal ischemia and relevance to glaucoma. Surv Ophthalmol 1999; 43: S102 – S128.

Paques M, Genevois O, Régnier A, Tadayoni R, Sercombe R, Gaudric A, Vicaut E. Axon-tracing properties of indocyanine green. Arch Ophthalmol. 2003 Mar;121(3):367-70.

Patel DV, Sherwin T, McGhee CN. Laser scanning in vivo confocal microscopy of the normal human corneoscleral limbus. Invest Ophthalmol Vis Sci. 2006 Jul;47(7):2823-7.

Philip M. Saphenous vein injection in the rat : a simple and time efficient technique. Plastic and Reconstructive Surgery. Vol 100 (7) ; December 1997, 1935-1936.

Quigley HA, Nickells RW, Kerrigan LA, et al. Retinal ganglion cell death in experimental glaucoma and after axotomy occurs by apoptosis. Investigative Ophthalmology & Visual Science 1995;36:774-86.

Renu A. Kowluru, Mamta Kanwar. Oxidative stress and the development of diabetic retinopathy: Contributory role of matrix metalloproteinase-2. Free Radical Biology and Medicine, Volume 46, Issue 12, 15 June 2009, Pages 1677-1685

Rothman SM. The neurotoxicity of excitatory amino acids is produced by passive chloride influx. J Neurosci. 1985;5:1483-1489.

Rothman SM, Olney JW. Glutamate and the pathoophysiology of hypoxic-ischemic brain damage. Ann Neurol 1986; 19: 105-111.

Roy S et al 2007. Rapid and intermittent cotransport of slow component-b proteins. J Neurosci. 2007 Mar 21 ;27 (12) : 3131-8

Sabel BA, Engelmann R, Humphrey MF. In vivo confocal neuroimaging (ICON) of CNS neurons. Nat Med. 1997 Feb;3(2):244-7.

Sabry J, O'Connor TP and Kirschner M. 1995. Axonal transport of tubulinin Ti1 pioneer Neurons in Situ. Neuron. 14(6) :1247-1256. PMID 7541635. January 25 2007

Sadowsky AE, Leavenworth N, Wirtschafter JD. Compressive optic neuropathy induced by intranasal balloon catheter. Am J Ophthalmol, 1985 Apr 15; 99 (4):487-9

Satre LM, Zelasko DA, Harris PL, Perry G. 4- Hydroxynonenal-derived advanced lipid peroxidation end products are increased in Alzheimers disease. J Neurochem. 1997;68:2092-2097

Schori H, Kipnis J, Yoles E, et al. Vaccination for protection of retinal ganglion cells against death from glutamate cytotoxicity and ocular hypertension: Implications for glaucoma. Proc Natl Acad Sci U S A. 2001;98:3398-3403.

Schipper HM. Heme oxygenase-1: transducer of pathological brain iron sequestration under oxidative stress. Ann NY Acad Sci. 2004;1012:84-93

Schlamp CL, Johnson EC, Li Y, Morrison JC, Nickells RW. Changes in Thy1 gene expression associated with damaged retinal ganglion cells. Mol Vis 2001;7:192-201.

Schwartz M, Belkin M, Yoles E, Solomon A. Potential treatment modalities for glaucomatous neuropathy: neuroprotection and neuroregeneration. J Glaucoma 1996;5:427-32.

Schori H, Kipnis J, Yoles E, WoldeMussie E, Ruiz G, Wheeler LA, Schwartz M. Vaccination for protection of retinal ganglion cells against death from glutamate cytotoxicity and ocular hypertension: implications for glaucoma. Proc Natl Acad Sci U S A. 2001 Mar 13;98(6):3398-403. Epub 2001 Mar 6.

Schmitz-Valckenberg S, Guo L, Maass A, Cheung W, Vugler A, Moss SE, Munro PM, Fitzke FW, Cordeiro MF. Real-time in-vivo imaging of retinal cell apoptosis after laser exposure. Invest Ophthalmol Vis Sci. 2008 Feb 15 [Epub ahead of print]

Schulman Joel A., Peyman Gholam A., Dietlein Jon, Fiscella Richard. Toxicity of intravitreal oxiconazole. International Ophthalmology 13 : 201-203, 1989.

Swanson KI, Schlieve CR, Lieven CJ, Levin LA. Neuroprotective effect of sulfhydryl reduction in a rat optic nerve crush model. Invest Ophthalmol Vis Sci 2005;46:3737-41.

Seeliger MW, Beck SC, Pereyra-Muñoz N, Dangel S, Tsai JY, Luhmann UF, van de Pavert SA, Wijnholds J, Samardzija M, Wenzel A, Zrenner E, Narfström K, Fahl E, Tanimoto N, Acar N, Tonagel F. In vivo confocal imaging of the retina in animal models using scanning laser ophthalmoscopy. Vision Res. 2005 Dec;45(28):3512-9.

Shernab S M, Spear P D. Organization of visual pathways in normal and visually deprived cats. Physiol Rev. 1982 Apr ;62 (2):738-855.

Silverman C.A., Yoshizumi M.O., Ocular Toxicity of Experimental Intravitreal DMSO. Cutaneous and Ocular Toxicology, Volume 2, Issue 2 & 3 1983 , pages 193 – 200.

Smith MA, Kutty RK, Richey PL et al. Heme oxygenase -1 is associated with the neurofibrillary pathology of Alzheimers disease. Am J Pathol. 1994;145:42-47.

Solomon AS, Lavie V, Hauben U, et al. Complete transection of rat optic nerve while sparing the meninges and the vasculature: an experimental model for optic nerve neuropathy and trauma. J Neurosci Methods. 1996;70:21-25.

Staszyk C, Bohnet W, Gassse H, Hackbarth H. Blood vessels of the rat tail : a histological re-examination with respect to blood vessel puncture methods. Laboratory animals 2003. 37, (121- 125)

Tan S, Schubert D, Maher P. Oxytosis: a novel form of programmed cell death. Curr Top

Med Chem. 2001;1:497-506

Uchida K. 4-Hydroxy-2-nonenal: a product and mediator of oxidative stress. Prog Lipid res. 2003;42:318-343

Tezel G, Wax MB. Increased production of tumor necrosis factor-alpha by glial cells exposed to simulated ischemia or elevated hydrostatic pressure induces apoptosis in cocultured retinal ganglion cells. J Neurosci. 2000;20:8693-8700

Thanos S, Indorf L, Naskar R. In vivo FM: using conventional fluorescence microscopy to monitor retinal neuronal death in vivo. Trends Neurosci. 2002 Sep;25(9):441-4.

Trachtenberg JT, Chen BE, Knott GW, Feng G, Sanes JR, Welker E, Svoboda K. Long-term in vivo imaging of experience-dependent synaptic plasticity in adult cortex.
Nature. 2002 Dec 19-26;420(6917):788-94.

Ts'o DY, Gilbert CD, Wiesel TN. Relationships between horizontal interactions and functional architecture in cat striate cortex as revealed by cross-correlation analysis. J Neurosci. 1986 Apr ;6 (4):1160-70.

Uchida K. 4-Hydroxy-2-nonenal: a product and mediator of oxidative stress. Prog Lipid res. 2003;42:318-343

Van Essen DC, Anderson CH, Fellema DJ. Information processing in the primate visual system: an integrated systems perspective. Science. 1992 Jan 24;255:419-23.

Vercelli, Repici M, Garbossa D., and Grimaldi A. Recent techniques for tracing pathways in the central nervous system of developing and adult mammals. Brain Research Bulletin, Vol. 51, No. 1, pp. 11–28, 2000

Vidal-Sanz M, Lafuente MP, Mayor S, et al. Retinal ganglion cell death induced by retinal ischemia. neuroprotective effects of two alpha-2 agonists. Surv Ophthalmol. 2001;45:S261-267.

Vytautas P. Bindokas, Joaquin JordBn, Chong C. Lee, and Richard J. Miller. Superoxide Production in Rat Hippocampal Neurons: Selective Imaging with Hydroethidine. The Journal of Neuroscience, February 15, 1996, 76(4):1324-1336

Walsh MK, Quigley HA. In vivo time-lapse fluorescence imaging of individual retinal ganglion cells in mice. J Neurosci Methods. 2008 Mar 30;169(1):214-21. Epub 2007 Dec 8.

Walsh MK, Lichtman JW. In vivo time-lapse imaging of synaptic takeover associated with naturally occurring synapse elimination. Neuron. 2003 Jan 9;37(1):67-73.

Wardman P. Fluorescent and luminescent probes for measurement of oxidative and nitrosative species in cells and tissues: progress, pitfalls, and prospects. Free Radic Biol Med. 2007 Oct 1;43(7):995-1022. Epub 2007 Jul 10.

Weinreb RN, Greve EL. Glaucoma diagnosis. Amesterdam: Kugler Publications, 2004; 155-157.

Wigston, D. J. (1990) Repeated in vivo visualization of neuromuscular junctions in adult mouse lateral gastrocnemius. J. Neurosci. 10, 1753–1761.

WoldeMussie E, Yoles E, Schwartz M, Ruiz G, Wheeler LA. Neuroprotective effect of memantine in different retinal injury models in rats. J Glaucoma, 2002 Dec;1196): 474

Wrona M, Patel KB, Wardman P. Reactivity of 2, 7- dichlorodihydrofluorescein and dihydrorhodamine 123 and their oxidized forms towards carbonate, nitrogen dioxide and hydroxyl radicals. Free Radic Biol Med. 38:262-270; 2005

Xu Dong Zhang, Susan K. Gillespie and Peter Hersey. Staurosporine induces apoptosis of melanoma by both caspase-dependent and -independent apoptotic pathways. Mol Cancer Ther. 2004;3;187-197

Yoles E, Muller S, Schwartz M. NMDA-receptor antagonist protects neurons from secondary degeneration after partial optic nerve crush. J Neurotrauma. 1997;14:665-675.

Clifford-Jones RE, McDonald WI, Landon DN. Chronic optic nerve compression. An experimental study. Brain. 1985;108:241-262.

Yoles E, Schwartz M. Potential neuroprotective therapy for glaucomatous optic neuropathy. Survey of Ophthalmology 1998;42:367-72

Clifford-Jones RE, McDonald WI, Landon DN. Chronic optic nerve compression. An experimental study. Brain. 1985;108:241-262.

Zhao H, Joseph J, Fales HM, Sokoloski EA, Levine RL, Vasquez-Vivar J, Kalyanaraman B. Detection and characterization of the product of hydroethidine and intracellular superoxide by HPLC and limitations of fluorescence. Proc Natl Acad Sci U S A. 2005 Apr 19;102(16):5727-32.1

Zhao H, Kalivendi S, Zhang H, Joseph J, Nithipatikom K,ásquez-Vivar J, Kalyanaraman B. Superoxide reacts with hydroethidine but forms a fluorescent product that is distinctly different from ethidium: potential implications in intracellular fluorescence detection of superoxide. Free Radic Biol Med. 2003 Jun 1;34(11):1359-68

Zhou X-R, Yuan H-P, Qu W, Ma C-Y, Li H-Y, Wang Y. The Study of Retinal Ganglion Cell Apoptosis Induced by Different Intensities of Microwave Irradiation. Ophthalmologica 2008; 222: 6-10

Zolessi FR, Poggi L, Wilkinson CJ, Chien CB, Harris WA. Polarization and orientation of retinal ganglion cells in vivo. Neural Develop. 2006 Oct 13;1:2.